Hydrologic and Hydrochemical Processes on Mine Spoil Fills

by

Elyse Virginia Clark

Dissertation submitted to the faculty of the Virginia Polytechnic Institute and State University in partial fulfillment of the requirements for the degree of

DOCTOR OF PHILOSOPHY

In

CROP AND SOIL ENVIRONMENTAL SCIENCES

Carl. E. Zipper, Chair
W. Lee Daniels
Kevin J. McGuire
Matthew J. Eick

(March 23, 2017)
Blacksburg, Virginia

Keywords: coal mining, reclamation, disturbance hydrology, total dissolved solids

Hydrologic and Hydrochemical Processes on Mine Spoil Fills

by

Elyse Virginia Clark

ABSTRACT (ACADEMIC)

Appalachian surface coal mining operations fracture rocks (termed "mine spoils"), resulting in the weathering of minerals and release of water-soluble ions to streams. Collectively, the concentration of water-soluble ions in streams is called total dissolved solids (TDS) and streams with elevated TDS often have altered biota. The surficial, subsurface, and discharge properties of mine spoils influence TDS discharge concentrations. This study aimed to improve understanding of how hydrologic and hydrochemical processes occur and function in coal mining areas. These processes were characterized by infiltration and dye staining tests, mine spoil leaching experiments and modeling, and mining-influenced stream discharge monitoring. Results indicate that many factors influence hydrologic and hydrochemical processes in Appalachian coal mining areas, but these processes evolve over time as subsurface flow paths develop, mine rocks weather, and TDS is released from mine spoils. Fourteen years after placement, mean infiltration rates of mine soils reclaimed with trees were statistically greater than areas reclaimed with grasses, and different subsurface flow types were evident, indicating vegetation type influenced hydrologic processes. Specific conductance (SC) leaching patterns from mine spoils conformed to an exponential decay and linear segmented regression model. Maximum SC values (1108 ± 161 µS cm^{-1}) occurred initially during leaching, exponentially decayed, then exhibited linear SC releases (276 ± 25 µS cm^{-1}) that were elevated relative to natural background levels at the end of leaching. Major element (S, Ca, Mg, K, Na) leaching patterns resembled those of SC, whereas trace elements (As, Cd, Cu, Ni, Pb, Se) transitioned to linear release earlier in the leaching period. Mining-influenced stream SC discharge patterns varied by season and by precipitation amounts during storm events. Storm responses were characterized by either infiltration-excess overland flow or delayed SC releases due to internal flow through the VF. Given these results, mining companies wishing to control TDS discharges may be selective and pre-test mine spoils for total S and paste SC to determine TDS-generation potential. Isolation of spoils with high-TDS release potentials (i.e. unweathered sandstones and mudstones) from water-rock contact may help improve TDS discharges.

Hydrologic and Hydrochemical Processes on Mine Spoil Fills

by

Elyse Virginia Clark

ABSTRACT (GENERAL AUDIENCE)

The Appalachian surface coal mining process removes rock from above a coal seam by fracturing it with explosives. The fractured rock is then used to reconstruct the original shape of the mountain, and any rock left over after that reconstruction is often placed adjacent to the mining area in landforms constructed to direct water from the mine site to a natural stream. During the mining process, the minerals in the rocks rapidly break down, and when rainwater causes the weathering products (e.g. elements such as calcium, magnesium, sulfur, selenium, and arsenic) to discharge to a stream, the aquatic ecosystem of that stream is usually affected. The objective of this study was to characterize the processes occurring in coal mining areas that ultimately influence the water quality discharged by the mine. Results indicate that many factors influence how rainwater travels through coal mining rocks and the eventual quality of waters discharged from mine rocks, and that these factors evolve over time. A study of 14-year-old mine soils indicated that the type of vegetation (i.e. trees vs. grass) planted after mining influences how water infiltrates into soils and the pathways water travels through once infiltrated. Laboratory studies of mine rocks found that many of those rocks conformed to a single mathematical model that described their elemental release patterns. The model indicated that the quality of waters discharged from mining areas is elevated above natural conditions in the initial phase after mining. Those levels appear to decline over time, but may still have long-term effects on aquatic ecosystems. Field studies of five mining-influenced streams also found that the water quality in those streams was above levels which are detrimental to aquatic ecosystems at all flow levels. It may be helpful to mining companies to test mine rocks prior to mining to determine the best location to place the rocks after mining for mitigation of water quality issues. Isolating mine rocks with the highest potentials to impact water quality may improve post-mining water quality effects.

ACKNOWLEDGEMENTS

I would like to thank everyone who assisted me along the way during the entirety of my doctoral research. First and foremost, thank you to Dr. Carl Zipper for not only providing me with the opportunity to pursue a doctorate degree, but also for his endless support and guidance. Thank you to both Drs. Carl Zipper and Lee Daniels for seeing the potential in me and recommending that I apply for the ICTAS Doctoral Scholar Fellowship, an award I deeply appreciate. My committee members Drs. Lee Daniels, Kevin McGuire, and Matt Eick deserve recognition for their dedicated support and effort in providing thoughtful feedback about my dissertation research.

There are many others to thank for their assistance with my research. Thank you to Breeyn Greer and Dr. Erich Hester for their efforts in our collaborative research on mine hydrology. Thank you to Dan Evans, Dr. Trip Krenz, and Joe Buckwalter for assisting with field work, collecting and maintaining our hydrologic datasets, and for memorable times traveling to and from the field. Dr. Zenah Orndorff and Julia Burger, I thank you both for your support in the laboratory and with analysis of the mine spoil samples. Thank you to Chris Stanley, Eddie Clapp, and Jackie Ball for their assistance with site access and data collection at their associated mine sites.

Lastly, I owe a very special thank you to my family for their never-ending encouragement in this endeavor. Mom and Dad, you have believed in me from the start and encouraged me to keep pushing myself to be the best I can be. Wesley, you are my rock and have been there for me from the start, and I will be ever-grateful for your unconditional support and encouragement.

ATTRIBUTION

Several colleagues aided in the writing and research behind Chapters 2-5 as presented as part of this dissertation. Brief descriptions of their contributions are included here.

Chapter III: Vegetation Influences Near-Surface Hydrological Characteristics on a Surface Coal Mine in Eastern USA

This manuscript, published in *Catena* in 2016, is co-authored by Dr. Carl Zipper. As chair of my committee, Dr. Zipper helped to design the experiment and prepare the manuscript for publication.

Chapter IV: Modeling Patterns of Total Dissolved Solids Release from Central Appalachia, USA Mine Spoils

This manuscript, published in *Journal of Environmental Quality* in 2017, is co-authored by my colleagues Dr. Carl Zipper, Dr. W. Lee Daniels, Dr. Zenah W. Orndorff, and Matthew J. Keefe.

Dr. Carl Zipper assisted with developing project goals and objectives, as well as with co-authoring the manuscript.

Dr. W. Lee Daniels, a professor in the Department of Crop and Soil Sciences at Virginia Tech and member on my committee, supervised the experimental procedure, and assisted with development of project goals and writing the manuscript.

Dr. Zenah W. Orndorff, a Senior Research Associate in the Department of Crop and Soil Sciences at Virginia Tech, conducted the experimental procedures and data collection, and assisted with data analysis and writing the manuscript.

Matthew J. Keefe, a doctoral student in the Department of Statistics at Virginia Tech, assisted with model development and coding, statistical analyses, and writing the manuscript.

Chapter V: Appalachian Coal Mine Spoil Elemental Release Patterns and Depletion

This manuscript, which will be submitted to *Applied Geochemistry* in 2017, is co-authored by my colleagues Dr. Carl Zipper, Dr. W. Lee Daniels, Dr. Zenah W. Orndorff, and Matthew J. Keefe.

Dr. Carl Zipper assisted with developing project goals and objectives, as well as with co-authoring the manuscript.

Dr. W. Lee Daniels, a professor in the Department of Crop and Soil Sciences at Virginia Tech and member on my committee, supervised the experimental procedure, and assisted with development of project goals and writing the manuscript.

Dr. Zenah W. Orndorff, a Senior Research Associate in the Department of Crop and Soil Sciences at Virginia Tech, conducted the experimental procedures and data collection, and assisted with data analysis and writing the manuscript.

Matthew J. Keefe, a doctoral student in the Department of Statistics at Virginia Tech, assisted with model development and coding, statistical analyses, and writing the manuscript.

Chapter VI: Specific Conductance-Stage Relationships in Appalachian Valley Fill Streams

This manuscript, published in *Environmental Earth Sciences* in 2016, is co-authored by Ms. Breeyn Greer, Dr. Carl Zipper, and Dr. Erich Hester.

Ms. Breeyn Greer, currently a stormwater engineer at Kapur & Associates, Milwaukee, WI, collected data from three of the five study sites, helped determine project goals and objectives, and assisted with writing the manuscript.

Dr. Carl Zipper assisted with developing project objectives and methodologies, as well as with writing the manuscript.

Dr. Erich Hester, a professor in the Department of Civil and Environmental Engineering at Virginia Tech, supervised Ms. Greer's data collection, assisted with developing project objectives and methodologies, as well as assisted with writing the manuscript.

TABLE OF CONTENTS

I. Introduction

1.1 Background

Appalachian surface coal mining is extensive, with over 600,000 ha of land mined since the 1970's and thousands of additional ha being mined each year (Zipper et al. 2011). The mining process removes rock strata (termed "overburden") from above a coal seam after fracturing the rock with explosives, producing materials called "mine spoils". After mining, the mined area is reconstructed into a new landform using mine spoils. Some mine spoils may also be placed in non-mined areas for disposal as necessary in landforms termed "mine spoil fills".

During mining, the fractured rock materials expand in volume. Material in excess of what is needed to rebuild pre-mining contours as required by the Surface Mining Control and Reclamation Act (SMCRA) of 1977 is called excess spoil and is used to construct landforms called valley fills. A valley fill (VF) is a type of mine spoil fill which has a V-shaped structure comprised of excess spoils that have been dumped into a valley adjacent to the mining pit. Because VFs are typically located below and adjacent to coal surface mines, groundwater and surface waters from the surface mine often flow through VFs prior to discharge into a stream channel.

Newly constructed VFs generally have little vegetative cover and soil development, but vegetation is typically established shortly after construction as required by SMCRA. As precipitation falls on mine spoils, water-rock interaction is initiated, leading to primary mineral weathering and the generation and subsequent transport of water-soluble ions (White et al. 1996; Jin and Brantley 2011) through the spoil materials to the stream draining the VF. Streams draining newly constructed VFs tend to have

elevated concentrations of total dissolved solids (TDS). The TDS concentration influences the electrical conductivity (EC) of the water and EC is often used as an easily measured proxy for TDS in stream water. Specific conductance (SC) is typically reported for TDS monitoring and research reports, and is a measure of the EC corrected to 25° C. Elevated TDS in Appalachian streams is a major concern due to linkages to aquatic community effects including losses of *Ephemeroptera* (mayflies) and other taxa (Pond et al. 2008; Cormier et al. 2013).

As VFs age, vegetative growth and spoil weathering aid the development of mine soils, and such processes create subsurface flow paths and enhance rainwater infiltration. Similarly, the hydrochemistry of waters draining from aging VFs changes temporally as the rapid weathering of freshly-fractured and abraded mineral surfaces in the mine spoils results in the release of ions to streams. That release slows over time (Evans et al. 2014; Daniels et al. 2016) as the weathering front moves deeper into the mine spoil mass and into the internal portion of individual mineral grains. Collectively, vegetative establishment, soil development, and spoil weathering influence the hydrologic and hydrochemical processes occurring on and in mine spoil fills. These processes have been documented in prior studies (e.g. Jorgensen and Gardner 1987; Ritter and Gardner 1993; Hawkins 2004), but more research is needed to further characterize and understand the processes.

1.2 Research Objectives

The research described in this dissertation was conducted to improve scientific understanding of the hydrologic and hydrochemical processes occurring on Appalachian coal mine sites. Specific objectives were to:

i. Compare surficial and near-surface hydrologic properties and processes on reclaimed landforms with differing vegetative covers;
ii. Develop a model of SC release patterns from mine spoils and examine predictive relationships between model parameters and rapid spoil assessment tests;
iii. Determine the bulk chemistry, leaching patterns and degree of depletion of individual elements from mine spoils, and infer the geochemical factors influencing those values and patterns; and
iv. Compare the baseflow and stormflow hydrochemistry as well as SC-Stage relationships among streams discharged from valley fills.

Research findings can inform scientists about the effects of extreme land disturbances on various soil, geochemical, and hydrologic processes and how those processes may differ in areas reclaimed at different times and with different geologic materials and/or vegetation types. Research findings can also assist mining companies with development of water management strategies.

1.3 Document Structure

The structure of this document is as follows: Chapter II provides a description of relevant prior research and concepts, and Chapter III addresses how rainwater infiltrates into mine soils and flows through the subsurface. Such flow paths, which transport water and oxygen through mine spoil fills, influence how mine spoils weather and release soluble ions. Chapters IV and V address how mine spoils release TDS and individual elements via weathering and leaching. Chapter VI addresses the physical hydrology and TDS discharge patterns from field-based studies of Appalachian VFs, as these patterns

are influenced by the infiltration characteristics and flow paths within the mine soils, as well as the chemical weathering processes occurring within VFs. Lastly, Chapter VII provides a summary of the results from prior chapters and draws conclusions about the overall implications of this research.

1.4 REFERENCES

Cormier SM, Suter GW, Zheng L, Pond GJ (2013) Assessing causation of the extirpation of stream macroinvertebrates by a mixture of ions. *Environ. Toxicol. Chem.* 32:277-287.

Daniels WL, Zipper CE, Orndorff ZW, Skousen JG, Barton CD, McDonald L, Beck M (2016) Predicting total dissolved solids release from central Appalachian coal mine spoils. *Environ. Pollut.* 216:371-379.

Evans DM, Zipper CE, Donovan PF, Daniels WL (2014) Long-term trends of specific conductance in waters discharged by coal mine VFs in Central Appalachia, USA. *J. Am. Wat. Res. Assoc.* 50(6): 1449-1460.

Hawkins JW (2004) Predictability of surface mine spoil hydrologic properties in the Appalachian plateau. *Ground Water* 42: 119-125.

Jin L, Brantley SL (2011) Soil chemistry and shale weathering on a hillslope influenced by convergent hydrologic flow regime at the Susquehanna/Shale Hills Critical Zone Observatory. *Appl. Geochem. 26: S51–S56.*

Jorgensen D, Gardner TW (1987) Infiltration capacity of disturbed soils: Temporal change and lithologic control. *Water Resour. Bull.* 23: 1161-1172.

Pond GJ, Passmore ME, Borsuk FE, Reynolds L, Rose CJ (2008) Downstream effects of mountaintop coal mining: comparing biological conditions using family- and genus-level macroinvertebrate bioassessment tools. *J. North Am. Benthol. Soc.* 27:717–737.

Ritter JB, Gardner TW (1993) Hydrologic evolution of drainage basins disturbed by surface mining, Central Pennsylvania. *Geol. Soc. Am. Bull.* 105: 101-115.

Zipper CE, Burger JA, Skousen JG, Angel PN, Barton CD, Davis V, Franklin J (2011) Restoring forests and associated ecosystem services on Appalachian coal surface mines. *Environ Manage* 47: 751-765.

II. Literature Review

2.1 Mine Spoil Lithology and Weathering

In Central Appalachia, the dominant geology is comprised of Pennsylvanian-aged sedimentary rocks including sandstones, siltstones, mudstones, and shales. In the context of mine reclamation, these rocks tend to be classified by their pre-mining weathering extents (Orndorff et al. 2015; Daniels et al. 2016). Weathered (WX) spoils are generally derived from near-surface strata that have brown coloration due to Fe-oxidation. Comparatively, unweathered (UW) spoils are typically derived from deeper in the geologic strata, have been subjected to less influence by surficial weathering relative to WX spoils, and are usually gray in coloration. The primary and secondary minerals occurring in Central Appalachian coal-bearing strata include silicates (quartz, feldspars, muscovite), carbonates (calcite, dolomite, siderite), clay minerals (kaolinite, illite), and sulfides such as pyrite (Howard et al. 1988; Harlow and LeCain 1993; Miller et al. 2012).

Surface coal mining is initiated by removing soil and rocks from the land surface, then the previously-intact geologic strata above a coal seam is fractured with explosives until the coal seam can be mined. The freshly-fractured rocks originating from above the coal seam are removed from the mining pit and placed into mine spoil fills. Within these fills, rainwater and O_2 begin to interact with the mine spoils, resulting in the weathering of the minerals within the rocks. Physical weathering can occur as the solid rock fragments produced by blasting break down into smaller particles via abrasion or freeze-thaw cycles.

Chemical weathering of mine spoils occurs via multiple mechanisms. The sulfide mineral pyrite (FeS_2) oxidizes in the following acid-forming equation:

$$FeS_2 + 3.75\ O_2 + 3.5\ H_2O = Fe(OH)_3 + 2\ SO_4^{2-} + 4\ H^+ \quad [2.3]$$

to release SO_4^{2-} and H^+ ions (Singer and Stumm 1970). Carbonate mineral ($CaCO_3$; $MgCO_3$; $FeCO_3$) dissolution occurs in the acid-consuming reaction as follows:

$$CaCO_3 + H^+ = Ca^{2+} + HCO_3^- \quad [2.2]$$

and results in releases of HCO_3^- and other cations associated with carbonate minerals in these rocks such as Ca^{2+}, Mg^{2+}, Mn^{2+}, and Fe^{2+} (Rose and Cravotta 1998). Also, aluminosilicate hydrolysis, exemplified by the following acid-consuming K-feldspar hydrolysis reaction:

$$KAlSi_3O_8\ (\text{K-feldspar}) + H^+ + H_2O = K^+ + Al_2Si_2O_5(OH)_4\ (\text{kaolinite}) + H_4SiO_4 \quad [2.3]$$

displaces ions that occur in aluminosilicates commonly found in Appalachian mine spoils such as K-feldspar, albite ($NaAlSi_3O_8$), anorthite ($CaAl_2Si_2O_8$), muscovite ($KAl_3Si_3O_{10}(OH)_2$) and chlorite ($Mg_2Al_2SiO_5(OH)_4$) (Rose and Cravotta 1998; Blowes et al. 2014; Johnson 2016).

2.2 Mine Soil Pedogenesis

A mine soil is a soil that has developed from the physical and chemical weathering and biological processes within the mine rocks and/or soil materials from which it is derived. Most mine soils are currently classified as Entisols, which are newly formed soils with little structure and properties including bridging voids between large fragments that have little or no orientation (Grossman 1983; Haering et al. 2005). As mine soils develop, A horizons may begin to form within 2-3 years, followed by weak subsoil structure development, generally within 10 or fewer years (Grossman 1983; Roberts et al. 1988; Haering et al. 1993). A study on the soil textural changes in southwestern Virginia mine spoils showed that within 2 years an A horizon had

developed, sand content had decreased and silt content increased. These soil changes were attributed to dissolution of carbonates, oxidation of Fe^{2+}, and physical weathering mechanisms such as freeze-thaw and shrink-swell cycles (Roberts et al. 1988). After 8 years, the same soils had developed C horizons at the 20-100 cm depth that contained coarse fragments and a few plant roots (Haering et al. 1993). In Pennsylvania, mine soils ranging from 1-24 years after placement had A horizons containing 40-60% coarse fragments, and > 70% coarse fragments deeper in the profile. These profiles were estimated to be developing at a rate of 1.6 cm yr^{-1} and exhibited evidence of illuviation in the form of patchy subsoil clay films (Ciolkosz et al. 1985). Sencindiver and Ammons (2000) claimed that mine soil development from mine spoils may be accelerated when comprised of large voids between spoil fragments, which allow for more air, water and plant roots to penetrate the soil.

2.3 Mine Soil Infiltration

Infiltration characteristics of mine spoil fills influence the partitioning of rain water between subsurface and overland flow, and infiltration-excess overland flow is often the dominant runoff mechanism on mine spoil fills (Jorgensen and Gardner 1987; Ritter and Gardner 1993; Miller and Zégre 2014). In studies of surface hydrology on reclaimed Pennsylvania surface mines, Ritter and Gardner (1993) found that the infiltration rate in a surface mined area was initially ~1 cm hr^{-1}, and increased to ~2.5 cm hr^{-1} after 11 years. Negley and Eshleman (2006) also reported an infiltration rate of < 1 cm hr^{-1} on a surface mine, which was attributed to highly compacted soils with low organic matter contents and high bulk densities. Another study found that new mine soils

in Pennsylvania had infiltration rates of 1-2 cm hr^{-1}, which increased to pre-mining values of 8 cm hr^{-1} within four years after reclamation (Guebert and Gardner 2001).

Ritter and Gardner (1993) demonstrated that young mine soils may have low infiltration capacities that are not characteristic of a natural landform, but other studies have shown that some mine soil infiltration rates can recover to pre-mining values (Guebert and Gardner 2001). These studies demonstrated that macropore and flow path development in the subsurface were linked to the recovery of surface infiltration rates in mine soils. In addition to time, factors such as slope, vegetation, rock content, and soil texture may influence the recovery of infiltration capacity on coal surface mines (Jorgensen and Gardner 1987). The passage of time, however, may not lead to restored infiltration capacities if mine soils have been heavily compacted by mining equipment (Negley and Eshleman 2006; Simmons et al. 2008).

2.4 Flow Pathways through Mine Spoil Fills

2.4.1 Mechanisms of Flow into a Valley Fill

Conceptual models of water flow into VFs include the following mechanisms: precipitation waters transported to a VF via infiltration-excess runoff from compacted upslope locations (Figure 2.1a), groundwater flow through upslope and regional flow paths that intersect the VF (Figure 2.1b), or direct rainfall on the VF surface that may travel along the contact boundary between the VF and original pre-filled slope (Figure 2.1c). A prior study of an Appalachian VF found that artificial rainfall applied directly on the VF surface tended to pond until it was able to infiltrate into the materials via narrow preferential flow paths; this infiltration pattern was attributed to the presence of fine materials at the VF surface inhibiting infiltration (Greer 2015). Since Greer (2015)

presented results for a single VF, more research is necessary to better understand the mechanisms of water transport into VFs.

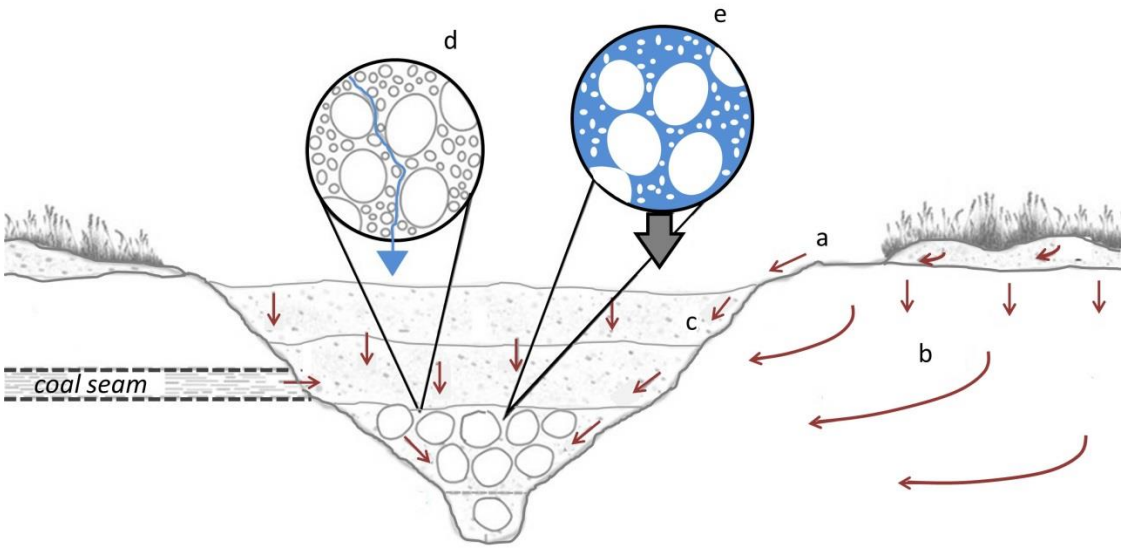

Figure 2.1 Mechanisms of flow into a VF. Red arrows indicate flow paths. **a.** Infiltration-excess overland flow from upslope locations. **b.** Groundwater flow from upslope areas and regional groundwater flow pathways. **c.** Direct rainfall onto the VF surface and flow along the original pre-filled hillslope surface. **d.** Matrix flow through the VF. **e**. Connected saturated pores and voids during storm events. Figure adapted from Miller and Zégre (2014).

2.4.2 Mechanisms of Flow through Valley Fills

When rain water infiltrates a mine spoil fill, the water will flow through the material either as matrix flow or along preferential flow paths. Matrix flow in mine spoil fills likely involves the movement of water through the pores and voids in the fill material (d in Figure 2.1) in response to gravitational forces, H_2O potential gradients (hydraulic head) and differing hydraulic conductivities. Spoil matrix water may be stored in the fill material for long periods of time until a large enough storm event causes the stored water to discharge (Murphy et al. 2014) in a process similar to that of natural hillslopes (McDonnell 1990). Preferential flow paths, which develop along voids in the fill material as well as along pathways created by plant roots and burrowing organisms near the surface (Scherrer and Naef 2003), are influenced by antecedent moisture

conditions, precipitation intensities and amounts of precipitation (Anderson et al. 2009). Preferential flow paths may interconnect when soil moisture increases (Figure 2.1e) (Sidle et al. 2001), and during storm events, preferential flow paths may quickly direct and discharge water out of a VF to the stream below (Miller and Zégre 2014). A prior study of an Appalachian VF subjected to an artificial rainfall event showed that water transport to the interior of the VF (> 15 m depth) via preferential flow paths was rapid and occurred in < 80 minutes (Greer 2015).

After mine spoil fill construction, mine soils begin to develop both matrix and preferential flow pathways in the shallow subsurface (Guebert and Gardner 2001), but it is also possible that flowpaths may develop in deeper materials (Hawkins 1998; Miller and Zégre 2014). Deeper in the fill, the mechanisms of flow through the material are not influenced by soil development processes; therefore, the dominant mechanism of flow appears to be heterogeneous flow through voids between large rocks (Greer 2015). In a study of Pennsylvania mine spoils, Hawkins (1998) demonstrated that hydraulic conductivity (K) values ranged from 4.45×10^{-9} m s^{-1} to upwards of 7.58×10^{-2} m s^{-1} within a mine spoil fill, with the large K values attributed to large voids in the spoil materials. Other studies have also shown that mine spoil fill materials have a wide range of hydraulic conductivities (Bonta et al. 1992; Hawkins 2004), indicating that a variety of transport pathways exist within mine spoil fills.

2.5 Physical Hydrology of Mine Spoil Fills

Mine spoil fill discharges often constitute permanent streams, although intermittent streams have also been observed (Dickens et al. 1989; Wiley et al. 2001; Merricks et al. 2007). Typical hydrographs of mine spoil fills in the early years after

placement have varying patterns ranging from rapid stormflow responses with large peak flows and short falling limbs to hydrographs with decreased peak flows and increased baseflows (Bonta et al. 1997; Wiley et al. 2001; Negley and Eshleman 2006). Studies have shown that relative to forested reference streams, reclaimed surface coal mined lands can produce higher peak flows and greater runoff due to soil compaction and reduced infiltration (Ritter and Gardner 1993; Bonta et al. 1997; Negley and Eshleman 2006; McCormick et al. 2009). In contrast, in their study on streams draining Appalachian coal mining sites, Wiley et al. (2001) hypothesized that VFs act like a sponge during a storm event by storing large amounts of water, thus decreasing the peak flow and resulting in a slow release of baseflow after a storm event. Such slow release patterns indicate the presence of a "pseudokarst" flow regime in which infiltrated waters are stored in the large voids deep in VFs and slowly discharge over time (Caruccio and Geidel 1995; Miller and Zegre 2014).

2.6 Mine Spoil and Discharge Water Chemistry

Mining stream discharge SCs and TDS concentrations are influenced by the composition of the mine spoils infiltrated waters come into contact with as well as the flowpaths along which infiltrated waters travel. Agouridis et al. (2012) compared the EC of waters draining three types of loose-dumped mine spoils in Kentucky over a two-year period. Their study showed that UW spoils had discharge ECs of 1,032 µS cm^{-1} on average, whereas WX spoils had a lower average discharge EC of 829 µS cm^{-1} over the same two-year period. Nine years after spoil placement for the same experiment, the EC of the UW spoils was still greater than the WX spoils, with average values of 564 and 421 µS cm^{-1}, respectively (Sena et al. 2014). In other studies of Appalachian mining-

influenced streams, the ECs vary widely in response to differing geologic materials. For example, the ECs in mining-influenced Central Appalachian streams studied by Bryant et al. (2002) and Hartman et al. (2005) ranged from 502-1,540 µS cm^{-1}, whereas reference streams in the same vicinity had ECs ranging from 13-253 µS cm^{-1}.

Column leaching studies by Orndorff et al. (2015) showed that mine spoil leachate dissolved ion concentrations are generally high initially, but rapidly decline and stabilize at much lower levels after repeated leaching events. The number of leaches it took for dissolved ion release to stabilize (if stabilization occurred) varied among spoil types; thus predicting the time frame for EC stabilization for any given mine spoil type is challenging, especially in field settings. Field experiments have shown similar decreases in SC with time, but over extended time frames. Evans et al. (2014) showed that the SC in streams draining Appalachian VFs decreased as the spoils weathered and the generation of soluble ions slowed, but these processes required decades. Agouridis et al. (2012) showed that EC was very high (>1,000 µS cm^{-1}) initially in the waters draining field plots of 0.5 to 1.5 m thick loose-dumped mine spoils in Kentucky, but eventually stabilized at an EC of ~500 µS cm^{-1} within two years. In a later study of the same Kentucky loose-dumped mine spoil field plots, Sena et al. (2014) found that the ECs of mine spoil discharges remained at similar levels after nine years of field leaching. Daniels et al. (2016) found that the laboratory leaching column results had a general correspondence to the Agouridis et al. (2012) and Sena et al. (2014) field leaching results. Collectively, these studies suggest that Appalachian mine spoil EC release patterns are high initially, decline over a period of time, then stabilize in release at levels typically elevated above background EC levels. However, in a study of 15 Central Appalachian VF

streams ranging from 11-33 years after placement, Pond et al. (2014) found EC levels were ~700 µS cm^{-1} on average, which is well above the 300-500 µS cm^{-1} range of EC stabilization for most mine spoils reported by Orndorff et al. (2015) and Daniels et al. (2016).

Prior research has shown that ions released in the highest concentrations from mine spoil fill discharges generally include SO_4^{2-}, HCO_3^-, Ca^{2+}, and Mg^{2+} (Hartman et al. 2005; Pond et al. 2008; Agouridis et al. 2012). The geochemical composition and weathering extent of the mine spoil influences the concentration of ion release, as shown by the decrease in dissolved ion concentrations in the following pattern: shales > UW sandstone > WX sandstone (Agouridis et al. 2012; Orndorff et al. 2015). Other major and minor ions (e.g. K^+, Na^+, Cl^-, Mn^{2+}, Al^{3+}, Fe^{3+}) that commonly occur in Appalachian mining discharges have also been reported in prior studies (e.g. Pond et al. 2008, 2014; Fritz et al. 2010; Agouridis et al. 2012). Many trace ions are present in mining-influenced stream discharges as well (Bryant et al. 2002; Hartman et al. 2005; Pond et al. 2008), including some which have potential ecotoxicological impacts (e.g. As, Cd, Cu, Ni, Pb, Se).

Waters receiving elevated TDS from Appalachian coal mining discharges are generally associated with biological conditions that are altered relative to reference conditions (Pond et al. 2008, 2014). Benthic macroinvertebrate communities typically have lower taxonomic richness and altered distributions of individuals among taxonomic classes in high-TDS streams compared to reference streams in similar environments. Several studies have been conducted in an effort to define SC thresholds for biological communities downstream of surface mining activity. For example, Gerritsen et al. (2010)

identified 250 µS cm^{-1} as an effect threshold, whereas Timpano et al. (2010) identified an effect threshold of 630 µS cm^{-1} using a different set of biological metrics. Due to the wide range of aquatic-community effect measures utilized by such studies, results have consequently varied. Two widely cited thresholds for toxicity effects, however, are 300 µS cm^{-1} (US EPA 2011; Cormier et al. 2013) and 500 µS cm^{-1} (Pond et al. 2008). The Cormier et al. (2013) effect threshold is a chronic toxicity threshold above which 5% of aquatic genera are extirpated, and the Pond et al. (2008) threshold is associated with altered assemblages of aquatic organisms and losses of taxonomic groups.

2.7 Summary

Prior research on mine spoil fills identified some of the mechanisms influencing how mine soils develop, how water infiltrates into and flows through mine soils, the leaching patterns and geochemistry of mine spoils, and the TDS discharge patterns of VFs; however, more research is needed to better understand these processes, the factors that influence these processes, and how these processes may change or evolve over time. In the following text, four separate studies are presented that fill some of the knowledge gaps about hydrologic and hydrochemical processes occurring on mine spoil fills.

2.8 REFERENCES

Agouridis CT, Angel PN, Taylor TJ, Barton CD, Warner RC, Yu X, Wood C (2012) Water quality characteristics of discharge from reforested loose-dumped mine spoil in eastern Kentucky. *J. Environ. Qual.* 41: 454-468.

Anderson AE, Weiler M, Alila Y, Hudson RD (2009) Dye staining and excavation of a lateral preferential flow network. *Hydrol. Earth Syst. Sc.* 13: 935-944.

Blowes DW, Ptacek CJ, Jambor JL, Weisener CG, Paktunc D, Gould WD, Johnson DB (2014). The geochemistry of acid mine drainage. Holland HD, Turekian KK (Eds.), Treatise on Geochemistry, 2nd Edition, Elsevier, p 131-190.

Bonta J V, Amerman CR, Dick WA, Haghiri FA, Hall GF, Hamon WA, Harlukowicz TJ, Razem AC, Smeck NE (1992) Impact of Coal Surface Mining on Hydrology and Water Quality of Three Ohio Watersheds — Physical Conditions and Ground-Water Hydrology. *Water Resour. Bull.* 28:577-596.

Bonta JV, Amerman CR, Harlokowicz TJ, Dick WA (1997) Impact of coal surface mining on three Ohio watersheds: surface-water hydrology. *J. Am. Water Resour. Assoc.* 33:907-917.

Bryant G, McPhilliamy S, Childers H (2002) A survey of the water quality of streams in the primary region of mountaintop/valley fill coal mining. Mountaintop Mining/Valley Fills in Appalachia Programmatic Environmental Impact Statement. US Environmental Protection Agency, Philadelphia. EPA 9-03-R-00013.

Caruccio FT, Geidel G (1995) Status Report: Long-Term Effects of Alkaline Trenches and Funnels at the Mercer Site. West Virginia Surface Mine Drainage Task Force Symposium: Morgantown, WV, USA.

Ciolkosz EJ, Cronce RC, Cunningham RL, Peterson GW (1985) Characteristics, genesis, and classification of Pennsylvania minesoils. *Soil Science* 139:232-238.

Cormier SM, Suter GW, Zheng L (2013) Derivation of a benchmark for freshwater ionic strength. *Environ. Toxicol. Chem*. 32:263-271.

Daniels WL, Zipper CE, Orndorff ZW, Skousen JG, Barton CD, McDonald L, Beck M (2016) Predicting total dissolved solids release from central Appalachian coal mine spoils. *Environ. Pollut.* 216:371-379.

Dickens PS, Minear RA, Tschantz BA (1989) Hydrologic alteration of mountain watersheds from surface mining. *Water Environment Federation* 61 (7) 1249-1260.

Evans DM, Zipper CE, Donovan PF, Daniels WL (2014) Long-term trends of specific conductance in waters discharged by coal mine VFs in Central Appalachia, USA. *J. Am. Wat. Res. Assoc.* 50(6): 1449-1460.

Fritz JM, Fulton S, Johnson BR, Barton CD, Jack JD, Word DA, Burke RA (2010) Structural and functional characteristics of natural and constructed channels draining a reclaimed mountaintop removal and valley fill coal mine. *J. North Am. Benthol. Soc.* 29:673-689.

Gerritsen J, Zheng L, Burton J, Boschen C, Wilkes S, Ludwig J, Cormier S (2010) Inferring Causes of Biological Impairment in the Clear Fork Watershed, West Virginia. EPA600-R-08-146. U.S. Environmental Protection Agency, Office of

Research and Development, National Center for Environmental Assessment, Cincinnati, OH.

Greer BM (2015) Electrical Resistivity Imaging of Preferential Flow through Surface Mine Valley Fills with Comparison to Other Land Forms. M.S. Thesis, Virginia Tech.

Grossman RB (1983) Entisols. p.55-90. In L.P. Wilding et al. (ed.) *Pedogenesis and soil taxonomy. II. The soil orders.* Elsevier Sci. Publ., Amsterdam.

Guebert MD, Gardner TW (2001) Macropore flow on reclaimed surface mines: infiltration and hillslope hydrology. *Geomorphology* 39: 151-169.

Haering KC, Daniels WL, Galbraith JM (2005) Mapping and classification of southwest Virginia mine soils. *Soil Sci. Soc. Am. J.* 69(2): 463-472.

Haering KC, Daniels WL, Roberts JA (1993) Changes in mine soil properties resulting from overburden weathering. *J. Environ. Qual.* 22: 194-200.

Harlow GE, LeCain GD (1993) Hydraulic characteristics of, and ground-water flow in, coal-bearing rocks of southwestern Virginia. U.S. Geological Survey Water Supply Paper 2388.

Hartman KJ, Kaller MD, Howell JW, Sweka JA (2005) How much do valley fills influence headwater streams? *Hydrobiologia* 532: 91–102.

Hawkins JW (1998) Hydrologic characteristics of surface-mine spoil. In Coal Mine Drainage Prediction and Pollution Prevention in Pennsylvania, ed. K.B.C. Brady, MW. Smith, and J. Schueck, 3.1-3.11. Harrisburg, Pennsylvania: The Pennsylvania Department of Environmental Protection.

Hawkins JW (2004) Predictability of surface mine spoil hydrologic properties in the Appalachian plateau. *Ground Water* 42: 119-125.

Howard JL, Amos DF, Daniels WL (1988) Phosphorus and potassium relationships in southwestern Virginia coal-mine spoils. *J. Environ. Qual.* 17: 695-700.

Johnson D (2016) Geochemical Properties of Soils and Associated Overburden of the Pottsville Group in Central Appalachia. Virginia Polytechnic Institute and State University. Ph.D. Dissertation.

Jorgensen DW, Gardner TW (1987) Infiltration capacity of disturbed soils: temporal change and lithologic control. *Water Resour. Bull.* 23: 1161-1172.

McCormick BC, Eshleman KN, Griffith JL, Townsend PA (2009) Detection of flooding responses at the river basin scale enhanced by land use change. *Water Resour. Res.* 45: W08401.

McDonnell J (1990) A rationale for old water discharge through macropores in a steep, humid catchment. *Water Resour. Res.* 26: 2821-2832.

Merricks TC, Cherry DS, Zipper CE, Currie R, Valenti T (2007) Coal-mine hollow fill and settling pond influences on headwater streams in southern West Virginia, USA. *Environ. Monit. Assess.* 129: 359-378.

Miller J, Barton C, Agouridis C, Fogel A, Dowdy T (2012) Evaluating soil genesis and reforestation success on a surface coal mine in Appalachia. *Soil Sci. Soc. Am. J.* 76:950-960.

Miller AJ, Zegre NP (2014) Mountaintop Removal Mining and Catchment Hydrology. *Water* 6:472-479.

Murphy JC, Hornberger JM, Liddle RG (2014) Concentration-discharge relationships in the coal mined region of the New River basin and Indian Fork sub-basin, Tennessee, USA. *Hydrol. Process.* 28:718-728.

Negley T, Eshleman K (2006) Comparison of stormflow responses of surface-mined and forested watersheds in the Appalachian mountains, USA. *Hydrol. Process.* 20: 3467-3483.

Orndorff ZW, Daniels WL, Zipper CE, Eick M, Beck M (2015) A column evaluation of Appalachian coal mine spoils' temporal leaching behavior. *Environ. Pollut.* 204: 39-47.

Pond GJ, Passmore ME, Borsuk FA, Reynolds L, Rose CJ (2008) Downstream effects of mountaintop coal mining: comparing biological conditions using family- and genus-level macroinvertebrate bioassessment tools. *J. N. Am. Benthol. Soc.* 27: 717–737.

Pond GJ, Passmore ME, Pointon ND, Felbinger JK, Walker CA, Krock KJ, Fulton JB, Nash WL (2014) Long-term impacts on macroinvertebrates downstream of reclaimed mountaintop mining valley fills in central Appalachia. *Environ. Manag.* 54: 919-933.

Ritter JB, Gardner TW (1993) Hydrologic evolution of drainage basins disturbed by surface mining, Central Pennsylvania. *Geol. Soc. Am. Bull.* 105: 101-115.

Roberts JA, Daniels WL, Bell JC, Burger JA (1988) Early stages of mine soil genesis in Southwest Virginia spoil lithosequence. *Soil Sci. Soc. Am. J.* 52: 716–723.

Rose AW, Cravotta CA (1998) Geochemistry of coal mine drainage. In: Smith MW, Schueck J (Eds.), Brady KBC. Coal Mine Drainage Prediction and Pollution Prevention in Pennsylvania. Pennsylvania Department of Environmental Protection, 22p.

Scherrer S, Naef F (2003) A decision scheme to identify dominant flow processes at the plot-scale for the evaluation of contributing areas at the catchments-scale. *Hydrol. Process*. 17: 391–401.

Sena K, Barton C, Angel P, Agouridis C, Warner R (2014) Influence of spoil type on chemistry and hydrology of interflow on a surface coal mine in the Eastern US coalfield. *Water Air Soil Poll.* 225: 2171.

Sencindiver JC, Ammons JT (2000) Minesoil genesis and classification. Ch. 23., in: Reclamation of Drastically Disturbed Lands. R. I. Barnhisel, W.L. Daniels, and R.G. Darmody (Eds.) Agronomy Series No. 41. American Society of Agronomy. Madison, WI.

Sidle RC, Noguchi S, Tsuboyama Y, Laursen K (2001) A conceptual model of preferential flow systems in forested hillslopes: evidence of self-organization. *Hydrol. Process.* 15: 1675– 1692.

Simmons J, Currie W, Eshleman K, Kuers K, Monteleone S, Negley T, Pohlad B, Thomas C (2008) Forest to reclaimed land use change leads to altered ecosystem structure and function. *Ecol. Appl.* 18: 104–118.

Singer PC, Stumm W (1970) Acidic mine drainage: the rate-determining step. *Science* 167(3921):1121-3.

Timpano AJ, Schoenholtz SH, Zipper CE, Soucek DJ (2010) Isolating Effects of Total Dissolved Solids on Aquatic Life in Central Appalachian Coalfield Streams. In: Proceedings, National Meeting of the American Society of Mining and Reclamation, Pittsburgh, PA, pp 1284-1302.

US EPA (2011) The Effects of Mountaintop Mines and Valley Fills on Aquatic Ecosystems of the Central Appalachian Coalfields. EPA/600/R-09/138F.

Wiley JB, Evaldi RD, Eychaner JH, Chambers DB (2001) Reconnaissance of Stream Geomorphology, Low Streamflow, and Stream Temperature in the Mountaintop Coal-Mining Region, Southern West Virginia, 1999-2000. USGS Water-Resources Investigations Report 01-4092.

CHAPTER III: Vegetation Influences Near-Surface Hydrological Characteristics on a Surface Coal Mine in Eastern USA

Elyse V. Clark and Carl E. Zipper

Citation: Clark EV, Zipper CE (2016) Vegetation influences near-surface hydrological characteristics on a surface coal mine in eastern USA. *Catena* 139: 241-249. DOI 10.1016/j.catena.2016.01.004

ABSTRACT

Mining processes alter natural landscapes worldwide, and methods for restoration of mined areas are widely studied. Establishment of vegetation is essential to mined land restoration. Prior research has addressed vegetative influence on erosion and runoff, but effects of vegetation type on surface hydrologic processes are less studied. We measured infiltration rates and observed subsurface flow paths in mine soils on a reforested area and a grassed area on a former surface coal mine in the eastern United States. The two areas were constructed and reclaimed fourteen years prior to our study using processes similar in all aspects except vegetation. MiniDisk tension infiltrometers and Brilliant Blue FCF dye staining analyses were utilized to evaluate near-surface flow processes in the vegetated mine soils. Mean infiltration rates were 16.5 ± 10.7 cm hr^{-1} and 10.4 ± 7.7 cm hr^{-1} for the reforested and grassed areas, respectively. Infiltration rates, hydraulic conductivities, dye coverage, and dye stained areas were higher statistically in the reforested area. The grassed area had constant dye coverage with depth but more flow paths than the reforested area. A transition from vegetation-controlled subsurface flow to abiotic-control at greater depths was evident in the stained soil profiles. Results highlight the heterogeneous nature of mine soils and the influence of vegetation type in development of mine soil hydrologic processes.

3.1 INTRODUCTION

Surface mining for ores and minerals disturbs landscapes and influences water resources in many world regions (Atanackovíc et al. 2013; Younger and Wolkersdorfer 2004); thus methods for restoring environmental quality on mine sites are widely studied. Vegetation establishment is commonly viewed as essential to restoration of environmental quality on mine sites (Barnhisel et al. 2000; Bradshaw and Chadwick 1990). Furthermore, the presence of suitable and productive vegetation is often necessary for economic post-mining land use, for the development of viable post-mining ecosystems, and is generally required for legal compliance (Cao et al. 2008; MacDonald et al. 2015; Skousen and Zipper 2014).

The establishment and development of vegetative cover on mine sites also contributes to restoration of hydrologic processes, including infiltration capacity (Jorgensen and Gardner 1987; Loch 2000; Moreno-de las Heras et al. 2009; Parr and Bertrand 1960) and erosion control (Carroll et al. 2000; Duran-Zuazo and Pleguezuelo 2008; Moreno-de les Heras et al. 2009; Ritter and Gardner 1993). Mechanisms associated with these effects include those which have been observed on natural soils, including soil organic matter accumulation and soil aggregation (Bronick and Lal 2005), the inhibition of soil crusting (Awadhwal and Thierstein 1985), and development of subsurface channels in association with plant rooting (Beven and Germann 1982; Sidle et al. 2001). Despite these well-known beneficial effects of vegetation on surface hydrologic properties, few studies have described how hydrologic influences differ among vegetation types on the highly disturbed landscapes that constitute reclaimed mines.

Coal surface mining typically disturbs large amounts of earth materials. Following coal extraction, the disturbed materials are placed back on the mined surface as “mine spoil”, which is often shaped to a post-mining landform and then vegetated. With plant community development and weathering, the surface-applied spoils develop into mine soils over time (Haering et al. 1993; Roberts et al. 1988; Sencindiver and Ammons 2000), and associated soil hydrologic properties and processes change over time with mine soil development (Guebert and Gardner 2001; Jorgensen and Gardner 1987; Ritter and Gardner 1993).

Studies on mine soils have shown that soil and hydrologic properties are not static, but develop over time, and in association with the plant community. Plant communities change after initial revegetation of unmanaged mine areas, as unplanted species invade, become established, and grow (Fields-Johnson et al. 2012; Holl 2002). As mine soils age, plant communities develop and plant rooting extends deeper, influencing mine soil properties (Akala and Lal 2001; Haering et al. 1993; Roberts et al. 1988; Rodrigue and Burger 2004). Although typically constructed from raw rock fragments with little to no prior vegetative influence, mine soils develop identifiable horizons and structure within several years after placement (Roberts et al. 1988; Sencindiver and Ammons 2000), and that development continues as time progresses (Ciolkosz et al. 1985; Thomas et al. 2000).

Soil hydrologic properties can also change in the years following reclamation; hence, in association with the plant community and soil morphology. On surface coal mines in eastern USA, infiltration capacities increased with time in the years following reclamation (Jorgensen and Gardner 1987; Ritter and Gardner 1993), while increasing

soil porosity and macropore and structural development were also observed to occur (Guebert and Gardner 2001; Jorgensen and Gardner 1987). Although reduced infiltration and greater storm runoff commonly occurs on mined landscapes relative to natural systems (Biemelt et al. 2005; Moreno-de las Heras et al. 2009; Negley and Eshleman 2006; Simmons et al. 2008), with time, mined landscapes may evolve to have decreased runoff and higher sustained baseflow (Griffith et al. 2012; Guebert and Gardner 2001; Ritter and Gardner 1993), or have less stream discharge overall due to increased evapotranspiration associated with plant community development (Sena et al. 2014).

Mine soil hydrologic changes include the development of subsurface flow paths over time. In native soils, typical subsurface flow processes include matrix flows and/or preferential flows, which can be observed in soils using dyes and tracers (e.g. Anderson et al. 2009; Weiler and Flühler 2004). Previous studies have observed that both matrix and preferential flows are also common in mine soils. In 16 year-old forested German lignitic mine soils, iodine staining showed preferential "finger flow" paths were common in the subsurface within the upper 60 cm of soil (Hangen et al. 2004; Hangen et al. 2005). Dye stainings also showed preferential flow paths common along coarse-fragment surfaces and through macropores in Appalachian mine soils with herbaceous vegetation (Guebert and Gardner 2001). These prior studies, however, did not determine if or how infiltration and subsurface flow differed or was influenced by vegetation type.

The benefits of mine-site revegetation for purposes of surface stabilization, erosion control, and post-mining land use are well-known. We expect that the plant communities established during and following reclamation influence mine soil hydrologic development as well, but those relationships have not been well-studied. Few

studies have documented subsurface flow patterns occurring in mined landscapes and even fewer have documented influences on mine soil hydrologic properties and processes by vegetation type. As mining disturbances expand globally, improved scientific understanding of how surface vegetation influences the hydrology of reclaimed mine landscapes can aid restoration of such areas.

In this study, two areas on a surface mine in Central Appalachia, USA, reclaimed with similar reconstruction techniques but differing vegetation were studied to compare hydrologic properties and processes on reclaimed landscapes. Specifically, mine soil infiltration rates, hydraulic conductivities, and subsurface flow paths in the contrasting vegetated areas were analyzed. Results from this study can inform reclamation scientists about the hydrologic development of reclaimed landscapes and the influence of vegetative cover on these processes over time.

3.2 MATERIALS AND METHODS

3.2.1 Study Area

The study area is located in Wise County, in the Appalachian Plateau geologic province of Virginia, USA (Figure 3.1). The dominant geology is the Pennsylvanian-age Wise Formation, consisting of horizontally oriented sandstones, siltstones, shales and coal seams (Nolde et al. 1986; Haering et al. 2005) that are typically low in pyritic sulfur (Howard 1988). Two areas of contrasting vegetation were identified on the mine site: a fully grassed hillslope and a reforested hillslope (Figure 3.2). Both areas were constructed in 2000 and reclaimed by applying a topsoil substitute of mixed sandstone and shale over a reconstructed slope comprised of undifferentiated ("run of mine") spoil. Grading techniques were applied as advised by university researchers, and consisted of

end-dumping spoils into closely-spaced piles, then using a dozer to lightly-grade the material to a thickness of 1.2 to 1.8 m (Sweigard et al. 2007). The experimental areas occur on the same reconstructed landform, have a south-facing aspect, are separated by ~500 m, and were reclaimed contemporaneously. The two areas also have similar ages, climates (mean annual rainfall of 120 mm), spoil types, and aspect; thus the main difference between the two areas is vegetative cover.

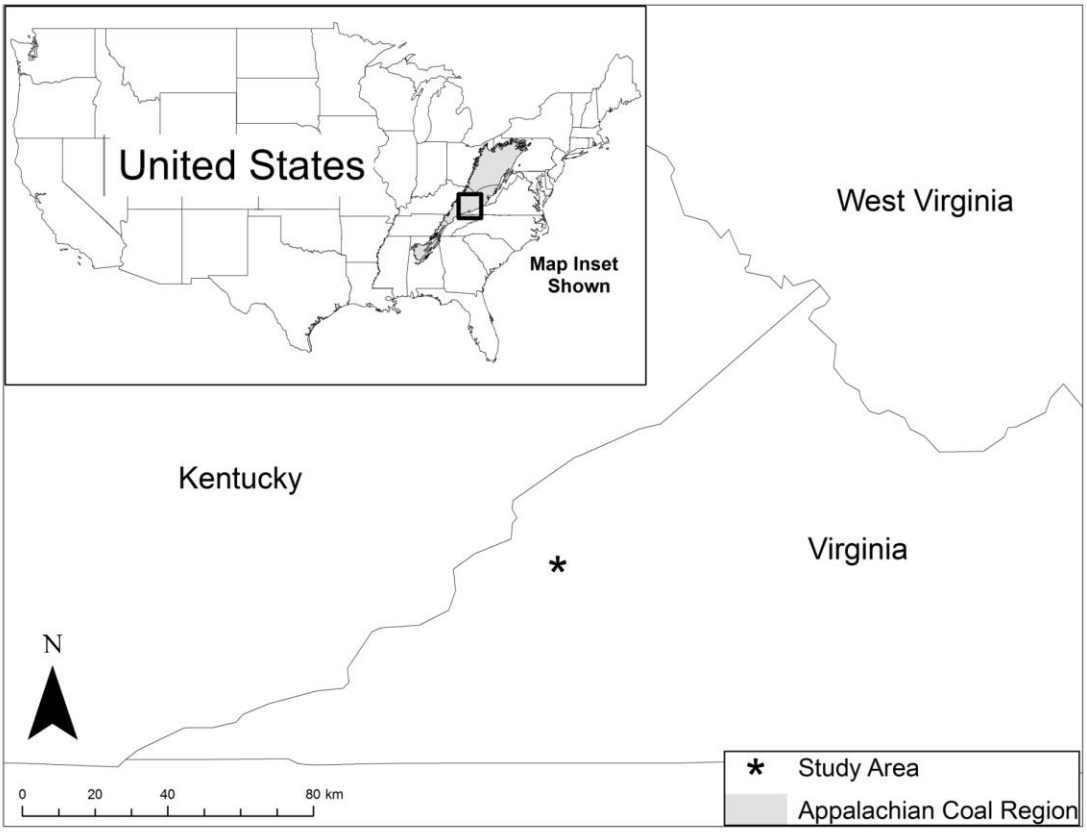

Figure 3.1 Location of the study area in southwestern Virginia, USA. The Appalachian coalfields of the United States are shown in gray.

Figure 3.2 The left photo is of the reforested area and the right photo is of the grassed area. Both photos show the dye staining apparatus in place during a dye staining experiment.

The grassed area (Figure 3.2) was vegetated using traditional reclamation grasses and legumes in ~2001. The conventional seeding mix used on this mine site includes the following grasses: orchardgrass (*Dactylis glomerata*), perennial ryegrass (*Lolium perenne*), redtop (*Agrostis gigantean*), and weeping lovegrass (*Eragrostis curvula*) and the following legumes: birdsfoot trefoil (*Lotus corniculatus*) and ladino clover (*Trifolium repens*). Because the seeded grasses tend to dominate in the years following reclamation, this site is described as "grassed". However, the slopes are now fully covered with a herbaceous cover that is dominated by sericea lespedeza (*Lespedeza cuneata).* Autumn olive (*Eleagnus umbellata)* and black locust *(Robinia pseudoacacia)*, which established as volunteer species, are also present, but sparse, in the grassed area. To limit the influence of trees on results in the grassed area, field experiments were conducted in locations away from the influence of these volunteers. The grassed area had 100 % vegetative cover, and the average slope was 45 % (Table 3.1). Soil texture of nine samples were estimated in the field using "texture-by-feel" analyses (Thien 1979), and consisted of coarse sand to silt loam with most soils consisting of a loamy texture.

Table 3.1 Descriptions of site conditions.

Veg. Type	% Cover Range*	% Cover Mean	Slope (%) Range	Slope (%) Mean	Soil and Surface Description
Reforested	40-100	75	40-65	50	Silt loam to fine sand, thick leaf litter, coarse fragments
Grassed	100	100	30-50	45	Silt loam to coarse sand, very rocky, no leaf litter

*Herbaceous cover

The reforested area (Figure 3.2) was initially grassed in ~2001 and then planted in early 2002 with a mix of native hardwood trees including the following: tulip poplar (*Liriodendron tulipifera),* white oak (*Quercus alba),* Northern red oak (*Quercus rubra),* chestnut oak (*Quercus prinus),* sugar maple *(Acer saccharum),* and white ash (*Fraxinus Americana)* that have grown well and are creating a woody plant community with a closed canopy in some places. Visible estimations of non-woody vegetative cover in the reforested areas ranged from 40 to 100 % cover, with an average slope of 50 % (Table 3.1). Field-estimated soil texture (Thien 1979) of nine samples ranged from fine sand to silt loam, with most soils having a sandy loam texture.

3.2.2 Field experiments

Tension Infiltration

Each area (~100 m x 100 m) was measured and divided into thirds vertically and across the slope to establish a grid for sampling transects. Cross-slope transects were established near the center of each area's upslope, midslope, and downslope segments, and vertical-slope transects were established on the right, middle, and left side of each area. Nine sampling locations were established for each slope position, three on each transect. Individual sampling locations will henceforth be referred to by transect and location (i.e. Reforested Upslope-Left, Grassed Midslope-Right, etc).

To control for antecedent moisture conditions, the infiltration tests took place over a two day rainless period (7/16/2014-7/17/2014), two days after a 10 mm rain event. Before conducting the infiltration tests, herbaceous vegetation was cut to the top of the organic soil horizon (O horizon) carefully as not to disturb soil structure. Soil O horizons were thicker in the reforested (3-7 cm) than in the grassed areas (0-5 cm) on average, but were removed from all sampling areas prior to the infiltration tests because they did not provide solid contact layers. Mini Disk tension infiltrometers (Decagon Devices, Inc.) with 4.5 cm disc diameters were used for the infiltration tests. A total of 54 infiltration tests were completed on the two areas (27 individual tests per vegetation type). A suction of -2 cm was consistently used for all infiltration tests and the drop in water level in the water chamber was manually recorded every 30 seconds until steady-state conditions were achieved. The tension infiltration test was repeated three times at each sampling point by moving the infiltrometer approximately 50 cm laterally along the slope. Cumulative infiltration (*I*) was calculated using the method of Zhang (1997) and Eq. 3.1:

$$I = C_1 t + C_2 \sqrt{t} \tag{3.1}$$

where *I* is cumulative infiltration, C_1 (m s^{-1}) is a parameter related to hydraulic conductivity (*k)*, C_2 (m s^{-1}) is a parameter related to soil sorptivity, and *t* is the time interval. The parameter C_1 was then used to calculate *k* in the following equation:

$$k = \frac{C_1}{A} \tag{3.2}$$

where C_1 is the slope of the curve of *I* vs $\sqrt{t}$. The *A* parameter relates parameters of a given soil type to the dimensions of the Decagon infiltrometer disk and was calculated as follows:

$$A = \frac{11.65\left(n^{0.1}-1\right)\exp[2.92(n-1.9)\propto h_0}{(\propto r_0)^{0.91}} \qquad \text{n} \geq 1.9$$

$$A = \frac{11.65\left(n^{0.1}-1\right)\exp[7.5(n-1.9)\propto h_0}{(\propto r_0)^{0.91}} \qquad \text{n} < 1.9 \tag{3.3}$$

where n and $\propto$ are the van Genuchten parameters for a given soil type as determined by Carsel and Parrish (1988). Soil texture was determined in the field and the appropriate texture class for van Genuchten parameters was selected. The r_0 is the disk radius (2.25 cm), and the h_0 is the suction at the disk surface (-2.0 cm for all tests).

Dye Staining Experiment

Three dye staining experiments were conducted on each vegetated area: one each at the upslope, midslope, and downslope positions. Brilliant Blue FCF (BB) dye was chosen for this study due to its good visibility in soils, low toxicity, low sorption, and transport properties similar to water (Flury and Flühler 1995). An apparatus was used to apply a dye solution to the reclaimed soil surface (Figure 3.2). The apparatus is a wooden structure ~ 1 m long by ~0.5 m wide that has extendable/ retractable legs on one end. The top of the apparatus is placed on the ground and the bottom of the apparatus with the extendable legs is placed downslope, then the legs are adjusted to level the dye application vessel, and clamped. A 62.5 L plastic bin (500 by 350 cm, in the horizontal dimension) with 2mm diameter holes drilled into the flat bottom in an equidistant grid was placed atop the apparatus and leveled to ensure even dye distribution on the surface. For each application, a total of 32 L of dye solution at a concentration of 4 g L^{-1} was poured into the plastic bin. The dye solution emerged from the drilled holes, falling directly onto the soil surface over a period of 10-15 minutes, and was allowed to infiltrate for one hour.

The application site surface was then excavated, beginning two meters downslope from the lower edge of the application area and gradually moving upslope until the BB dye was found. Once BB dye was found, a soil profile was excavated. After completing the first soil profile, the application area was excavated upslope in equal distances in order to create four soil profiles total. For example, if dye was found 100 cm downslope of the application area, soil profiles were produced at 25, 50, 75, and 100 cm downslope from the dye application area. To prepare a profile, the subsurface was carefully excavated by hand to prevent the disturbance of soil structure, then a flat tool was used to carefully scrape away excess material that may have filled in voids or macropores during excavation. The soil profile was extended laterally and vertically until a 30 x 30 cm wooden frame with an internal grid could be placed flat against the profile with the top of the frame aligned with the soil surface. An opaque plastic sheet was placed above the application area to reduce the interference of sunlight and associated shading with the profile. The profile was then photographed from a distance of one meter using a Nikon Coolpix digital camera. Extensive field notes and observations were taken to ensure accurate and precise digitization of the dye movement. If dye was found deeper than the 30 cm frame, the site was excavated deeper, if possible using hand tools with moderate effort, and a second profile was prepared beneath the top profile.

3.2.3 Data Analysis

The digital images were uploaded and cropped to the edge of the wooden frame, then imported into the photo editing software Image J, a Java-based open-source image processing program (Abràmoff et al. 2004). First, the number of pixels within the frame was determined and used to set the scale (i.e. *n* pixels= 30 cm) for converting the photo to

field-scale measurements. The color threshold of the image was adjusted to exclude all non-blue colors, then double-checked with the detailed field notes to ensure consistency. The image was then converted to an 8-bit color palette, changing all colors except blue into grayscale. The area of dye was measured using the "Measure Particles" tool, producing an output of dye coverage area in the profile recorded in x-y coordinates. The x-y output data was then broken into four equal-depth bins of 75 mm (depth quartiles), as per the wooden frame's internal grid. The area of dye within each depth quartile was calculated and used to produce profiles of dye coverage with depth. Each distinct dye-stained area was identified by the software; these were tallied by mid-point depth, depth-quartile, and area. If a stained area was bisected by the wooden frame's internal grid, the individual pieces were tallied as separate areas. Each separately dye-stained area was interpreted to represent a flow path. Mean numbers of flow paths per depth quartile were calculated by determining the number of separately stained areas in 5 mm horizontal segments, then averaged over the depth quartiles. Lastly, the stained areas were ordered by size; and those stained areas within the top 5 % (95^{th} quantile) by area were analyzed separately to investigate patterns of stained area size with depth.

Statistical Analysis

All statistical analyses were completed using the softwares JMP (v. 11.0, SAS Institute: Cary, N.C.) and R (R Core Team 2013). For the infiltration tests, outliers were identified using the Generalized Extreme Studentized Deviate (ESD) test for multiple outliers (Rosner 1983) and those values considered outliers statistically were omitted from further analyses. All identified outliers were high values. A Shapiro-Wilk test was used to confirm non-normal data. Mann Whitney tests were used to test for statistical

differences between the reforested and grassed areas for mean infiltration rates, numbers of flow paths, and dye-stained areas. A Steel-Dwass test was also utilized to identify any statistical differences among infiltration rates and dye stainings based on the within-area locations (upslope, midslope, and downslope). Regression analysis was used to test variables such as the numbers of flow paths and mean patch-size areas for significant trends with depth in the dye profiles. All statistical tests were conducted at the $\alpha = 0.05$ significance level.

3.3 RESULTS AND DISCUSSION

3.3.1 Infiltration Rates and Hydraulic Conductivity

Infiltration rates were highly variable in both the grassed and the reforested areas (Figure 3.3), but most infiltration rates were < 40 cm hr^{-1}. There were no apparent infiltration-rate trends with slope location, but differences among slope locations were found. Of the nine locations tested on each vegetation area (each with three replicate infiltration rates measured and averaged) two major outliers occurred, one in each vegetated area (Figure 3.3); all three data points at both outlier locations had infiltrations of > 40 cm hr^{-1} and were identified as outliers. These six data points skewed the data distribution; mean infiltration rates were 22.2 ± 19.6 and 21.4 ± 31.8 cm hr^{-1} for the reforested and grassed areas, respectively. The measured infiltration rates of these outliers are greater than typical infiltration values observed in soils. The heterogeneous nature of mine soil materials with variable in-spoil hydraulic conductivities may have enabled water to be displaced from the infiltrometer quickly and account for outlying infiltration values. A matrix of large coarse fragments just below the soil surface may also account for the large infiltration values. Greer (2015) conducted a geophysical

analysis of our sites and found high rock contents close to the surface in some areas, a finding that is consistent with our results. Wells et al. (1983) and Taylor et al. (2009) found that runoff from loosely placed Appalachian mine soils could not be produced by rainfall-runoff experiments due to high infiltration rates enabled by high rock contents of the materials.

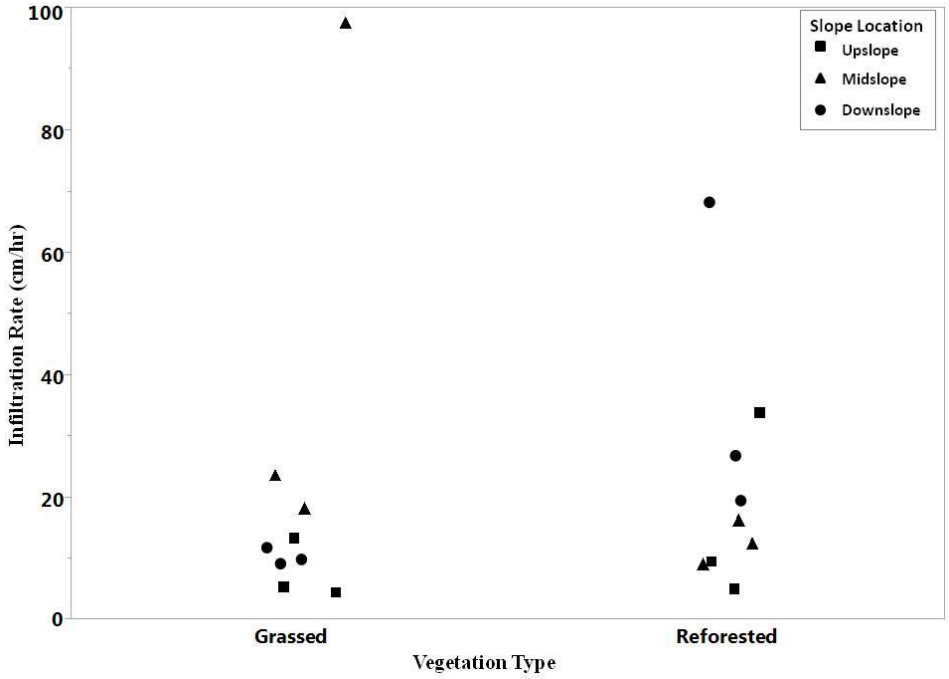

Figure 3.3 Comparison of infiltration rates in the reforested and grassed areas. Each symbol is a mean of three infiltration tests.

High outliers were excluded from statistical comparisons as the likely cause for the outlying values is not influenced by vegetation. Excluding outliers, the reforested infiltration rates ranged from 1.4 - 38.2 cm hr^{-1} and the grassed area infiltration rates ranged from 2.5 - 28.1 cm hr^{-1} (Table 3.2). Mean infiltration rates were 16.5 ± 10.7 cm hr^{-1} and 10.4 ± 7.7 cm hr^{-1} for the reforested and grassed areas, respectively. Mean infiltration was more rapid on the reforested areas than on the grassed areas ($p \leq 0.05$), implying that vegetation influences infiltration rates on these loosely-graded mine soils.

Table 3.2 Infiltration rates and hydraulic conductivities in the reforested and grassed areas.

Test Area	Infiltration Rate (cm hr^{-1})			Hydraulic Conductivity (cm s^{-1})
	Range	*Median*	*Mean*[†]	*Mean*[†]
FOR-UP	1.4-38.2	9.0	16.0±14.5[ab]	0.00129
FOR-MID	5.7-22.7	12.6	12.6±4.7[a]	0.00115
FOR-DOWN	10.8-32.8	23.7	23.0±8.7[b]	0.00222
Reforested (all)			16.5±10.7[*]	0.00147[*]
GR-UP	3.6-24.4	4.7	7.6±6.8[a]	0.00055
GR-MID	8.6-28.1	14.4	16.0±7.6[ab]	0.00079
GR-DOWN	2.5-27.4	9.0	10.2±7.7[a]	0.00045
Grassed (all)			10.4±7.7	0.00057

[†] Test area mean values followed by the same letter are not significantly different from one another.
[*] Designates experimental area means that are significantly greater than the other vegetated cover ($p<0.05$).

Mean infiltration rates in both the reforested and grassed areas were greater than measured rates at other mine sites. Prior studies have shown infiltration rates ranging from 0.3 cm hr^{-1} to 13.5 cm hr^{-1} on Appalachian surface-mined sites, whereas forested references had measured infiltration rates ranging from 5.3 to 45.0 cm hr^{-1} (Guebert and Gardner 2001; Jorgensen and Gardner 1987; Shukla et al. 2004; Simmons et al. 2008). In prior studies, the lowest infiltration rates occurred on the youngest mine soils (1-4 yr old) comprised of a mix of soil and spoils that may have been compacted by mining equipment (Jorgensen and Gardner 1987), and the highest infiltration rates occurred on the oldest mine soils (> 25 yr) that had a topsoil amendment added to the mine soil surface and was reclaimed to hayland/pasture land use (Shukla et al. 2004). Reynolds and Reddy (2012) measured infiltration rates on different aged arid and semi-arid mine sites in Wyoming, USA and found that 5-15-year-old plots had the smallest infiltration rates, whereas 20-25-year-old plots had comparable infiltration rates to reference plots.

The mine soils in our study were 14 years old and covered with a topsoil substitute that was loosely-graded for the purpose of avoiding soil compaction, promoting infiltration of water into mine spoils, and providing a suitable medium for vegetation re-establishment (Sweigard et al. 2002). Therefore, the difference in infiltration rates between this study area and other mine sites is likely a function of mine soil construction technique and time; however, it is also important to note that the difference in infiltration rates could be due to measurement technique, as studies have shown infiltration rates and hydraulic conductivity values are influenced by and are dependent on the methods used to measure infiltration (e.g. Mohanty et al. 1994; Reynolds et al. 2000).

Calculated hydraulic conductivities (*k*) ranged from 3.1×10^{-3} to 3.0×10^{-4} cm s^{-1}. Reforested area *k* values ranged from 3.1×10^{-3} to 5.0×10^{-4} cm s^{-1} (mean = 1.5×10^{-3} cm s^{-1}) and are greater, on average, than those of the grassed area (range: 1.2×10^{-3} to 3.0×10^{-4} cm s^{-1}, mean = 5.7×10^{-4} cm s^{-1}). Hawkins (2004) measured saturated hydraulic conductivities of Appalachian mine spoils at depths below the influence of vegetation using monitoring wells, piezometers, and slug tests. Resulting values ranged from 4.45×10^{-9} to 7.58×10^{-3} cm s^{-1}. Our measured values are within that range, and our overall mean (1.47×10^{-3} cm s^{-1}) is similar to the mean values found by Hawkins (2004) (1.93×10^{-3} cm s^{-1}), and greater than the Hawkins (2004) minimum values. Higher *k* values suggest in-spoil water movement is in response to larger substrates, whereas a smaller *k* suggests flow through finer material and/or compacted zones with little void space due to spoil settling or in-filling of voids with smaller particles. Therefore, based on the limited range in magnitude and larger *k* values measured in our study, it appears that a majority

of near-surface flows in these mine soils are controlled by soil matrices with large particle sizes capable of transporting soil water through the mine soil rapidly.

K values and infiltration rates in the two areas were highly variable, implying abiotic factors such as spoil type, degree of weathering and surface microtopographies are likely influential factors in the transport of rainwater into and through the subsurface. The variability of the results also highlights the highly disturbed and heterogeneous composition of mine soils at the hillslope scale, but also at the microscale. It is understood that the soil infiltration and hydraulic conductivity measurements in this study were measured at a microscale and covered a very small area on two reclaimed hillslopes, but similar observations within and between the vegetated areas indicate similar conditions throughout the reclaimed hillslopes. Both vegetative covers had mean infiltration rates greater than other mine sites, and no gullying or erosional areas were visible on either hillslope, indicating that the loose-grading technique was adequate for limiting runoff and erosion, and promoting rainwater infiltration into the mine soil on this mine site. Since the two vegetated areas were similarly reclaimed and controlled for abiotic factors such as age, reclamation technique and aspect, results indicate that the influence of growing trees significantly increases rainwater infiltration and transport of rainwater through the shallow subsurface relative to herbaceous vegetation effects.

3.3.2 Dye Staining

Six dye stainings were applied at an upslope, midslope, and downslope location on each of the two vegetated areas. Four soil profiles were prepared for each of the six stainings, but only two profiles were able to be excavated below 300 mm. All other profiles were too compacted, too rocky, or both to be excavated below the 300 mm depth

with moderate physical effort using hand-operated shovels and picks. In the data analysis that follows, only the ≤ 300 mm depth data are considered.

Both visual interpretations (Figure 3.4) and data analyses reveal that most staining occurred within the profiles as distinct and separate areas, and those areas occurred in a wide range of sizes. Each stained area is interpreted as a cross-section of a separate flow path, but with no assumption of flow path orientation relative to the profile plane. The large contiguous areas were interpreted as matrix flows, and smaller stained areas with no contact by other dye stainings or those with a clear direction of travel were interpreted as macropore or preferential flows. Dye was present in a wide range of patch sizes, suggesting a gradient of flow mechanisms, and both matrix and preferential flows. Dye movement appeared to be controlled by factors such as heterogeneity of substrate materials and densities, voids, presence of variably-sized rocks (with preferential flows along their outer surfaces), and plant roots. Large stained areas suggestive of matrix flows occurred close to the soil surfaces in the profiles, with lower boundaries that appeared to be controlled by "contact zones" of dissimilar material, likely the bulk spoil that was used to construct the landform prior to application of the topsoil substitute.

Visible differences between the soil profiles influenced by the two vegetation types included the stained area distributions and the numbers of individual stains (Figure 3.4). The reforested profiles typically had greater matrix staining near the top of the profile (Figures 3.5 and 3.6) that transitioned to a preferential pattern with depth along coarse root channels and around obstructions (large rocks and voids) in the material. Evident in many of the grassed profiles were staining patterns consisting of small patches of dye that were randomly dispersed throughout the profile. In this type of dye

movement, it appears the dye preferentially traveled through tiny cracks and pores in the spoil material with little interaction or exchange with the soil matrix. The dye-staining patterns appear to reflect the predominant rooting patterns of the two vegetation types. The grassed mine soils had a dense matrix of fine roots that appeared evenly distributed throughout the upper portions of the soil profile (top 5-10 cm on average, maximum 20 cm), whereas the reforested mine soils had fewer fine roots near the surface and had larger roots at depth in the subsurface.

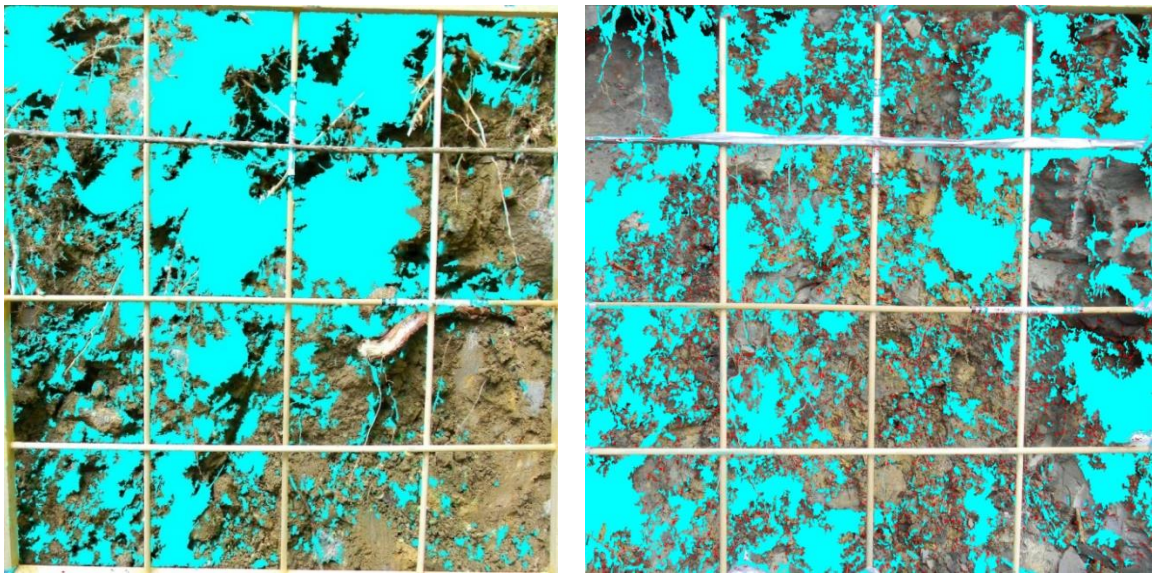

Figure 3.4 Dye profile examples for the reforested (left) and grassed (right) areas.

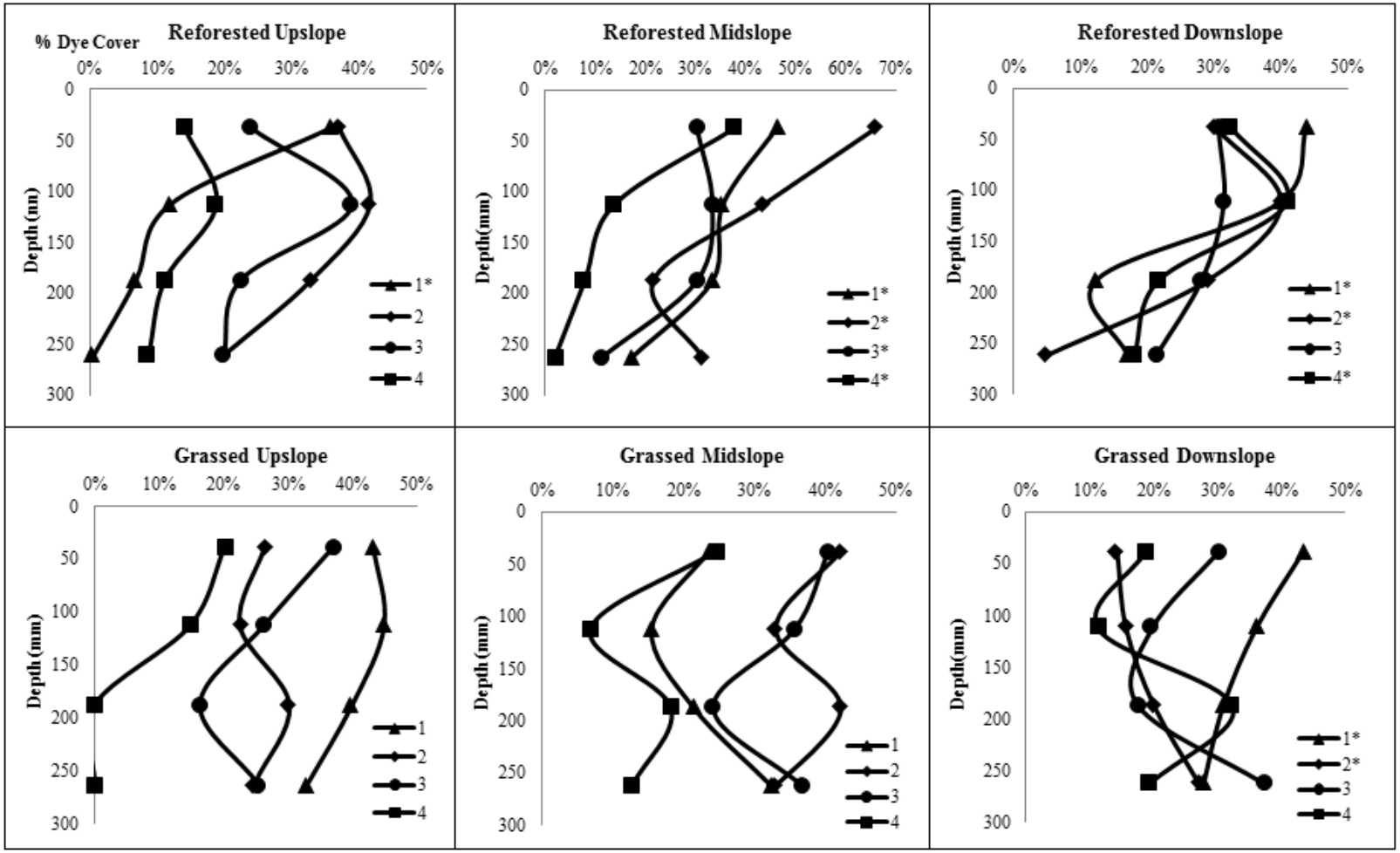

Figure 3.5 Profiles of % dye cover with depth for the reforested and grassed areas. The legend represents the four soil profiles created at each staining from the most upslope (1) to the furthest downslope (4). Labels denoted with * in the legend indicate a significant trend in dye coverage with depth ($p<0.05$).

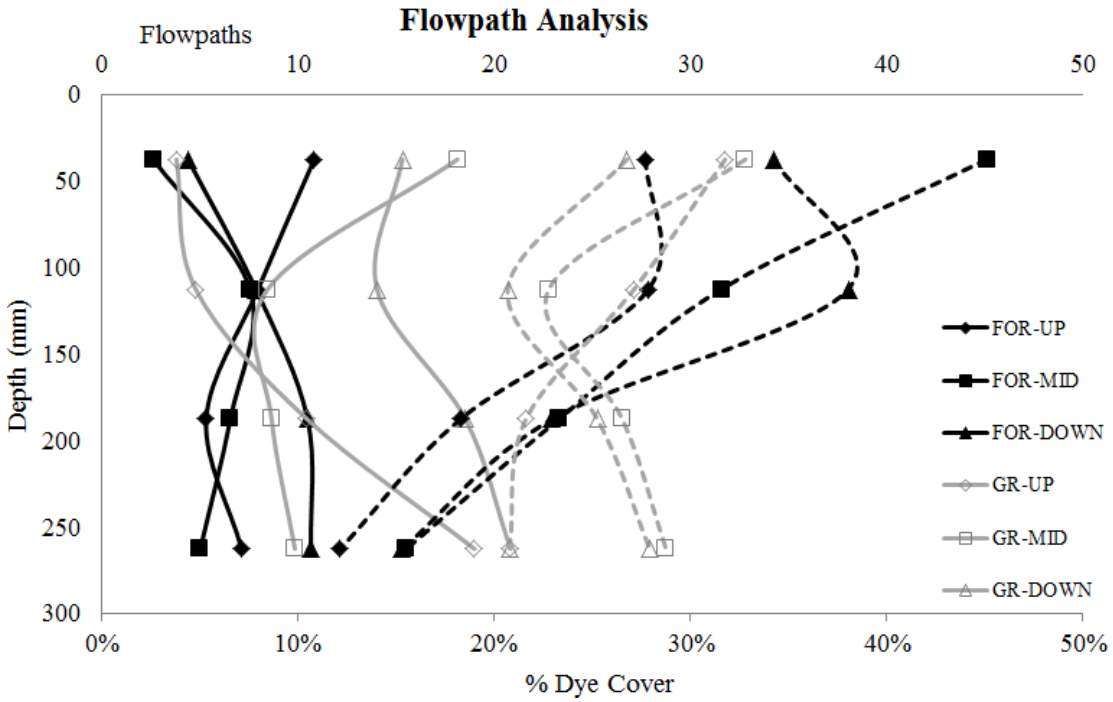

Figure 3.6 Profiles of the number of flowpaths (solid lines) per depth quartile and % dye cover (dashed lines) for the reforested and grassed areas with depth.

The reforested dye staining profiles had < 45-50 % of soil stained at all depths, excluding one profile (Reforested-Midslope 2). The greatest dye coverage was in the upper 150 mm and generally decreased in coverage with depth. No reforested profiles had > 30 % of the soil stained below the 250 mm depth. Furthermore, a majority of the reforested profiles (8 of 12) exhibited declining dye coverage with depth ($p \leq 0.05$) (Figure 3.5).

Like the reforested profiles, the grassed profiles had < 50 % stained area for all profiles. However, a majority of the profiles (10 out of 12) had no significant trend in coverage with depth, and only two profiles had a significant increase or decrease in stained area with depth ($p \leq 0.05$) (Figure 3.5). Stained area coverage within the grassed profiles was variable with depth, and dye coverage changed by no more than 20 % with depth in all the grassed profiles.

Flow Path Distributions with Depth

There were significantly more flow paths in the grassed area than in the reforested area ($p \leq 0.001$) (Figure 3.6), and the average numbers of flow paths in the reforested and grassed dye profiles, averaged over all depth quartiles (i.e. mean number of flow paths per soil profile), were 7.2 ± 4.8 and 12.7 ± 7.8, respectively (Table 3.3). In the grassed area, the average number of flow paths increased based on slope location; the upslope location had an average of nine flow paths, the midslope staining averaged 11 flow paths, and the downslope location averaged 17 flow paths overall. Similar trends were not present in the reforested area.

Table 3.3 Results of the dye staining analyses for the reforested and grassed areas.

Test Area	Stained Area Range (% profile area)	Stained Area Mean (% profile area) †	Mean Visible Flow Paths†	Individual Stained Areas† *Mean (mm²)*	*95th Quantile (mm²)*
For-Up	0.07 - 50.32	21.53[a]	7.82[a]	56.97[a]	858.95[ab]
For-Mid	1.89 - 74.92	28.91[a]	5.45[a]	60.59[a]	858.87[ab]
For-Down	3.75 - 48.89	27.64[a]	8.36[a]	51.34[a]	802.75[ab]
For-ALL		26.03	7.21	55.85[**]	837.64[*]
Gr-Up	5.42 - 53.36	28.94[a]	9.52[a]	50.26[ab]	1100.69[a]
Gr-Mid	6.10- 48.7	27.71[a]	11.28[ab]	34.04[bc]	702.15[bc]
Gr-Down	8.31- 50.89	25.15[a]	17.18[b]	22.75[c]	419.36[c]
Gr-ALL		27.26	12.66[*]	32.97	680.41

† Test area mean values followed by the same letter are not significantly different from one another.
[*] Designates experimental area means that are significantly greater than the other vegetated cover ($p < 0.05$).
[**] Designates experimental area means that are significantly greater than the other vegetated cover ($p < 0.001$).

In the reforested stainings, dye coverage generally decreases with depth (Figure 3.5), whereas the number of flow paths remains constant (Figure 3.6). This pattern suggests that as dye moves deeper into the subsurface of the reforested area, flow paths narrow and become increasingly preferential with depth. The dye coverage and flow path patterns in the grassed stainings are variable with depth (Figure 3.6), though regression analysis did not indicate a significant difference in the number of flow paths with depth.

There were, however, significantly more flow paths overall in the grassed area in the 225-300 mm depth quartile (Figure 3.6) than the reforested area ($p \leq 0.05$). Greater stained areas and more flow paths at depth in the grassed profiles suggest a different flow mechanism. In the reforested area, it is possible that coarse roots are extending deeper into the reforested mine soil and creating conduits for dye movement through the subsurface, enabling the dye to move preferentially through flow paths along the root system. In contrast, the lack of a dense root system at depth in the grassed area may lead to the dye spreading out into many flow paths through tiny voids and macropores in the subsurface, hence more flow paths occur overall in the grassed soil.

Stained-Area Size Distributions

A total of 14,670 unique stained areas were identified in the 24 soil profiles: ~5,800 and 8,800 individual stained areas for the reforested and grassed areas, respectively. The average sizes of the individual stained areas were greater in the reforested (55.8 ± 374.5 mm^2) than in the grassed (32.9 ± 248.9 mm^2) profiles (Table 3.3). Most of the individual stained areas were < 25 mm^2 for both the reforested (88%) and the grassed (90%) staining; the < 25 mm^2 stainings occur at all depths in the profiles. In contrast, 338 of the total reforested and 336 of the total grassed stainings were ≥ 75 mm^2, representing the 95th quantile or largest 5% of total stained areas in the profiles.

We interpreted the largest individual stained areas as indicators of dye transfer through zones of matrix flow (if no apparent direction of movement was apparent), thus the distribution of the largest stained areas (95th quantile) was analyzed separately to evaluate the likelihood of large stained areas occurring at depth in the subsurface. The largest individual stain detected by our technique was 8,953 mm^2 in the reforested area

and 9,847 mm² in the grassed area. Larger stained areas may have occurred; but if so, their measurements were limited by the frame. Large stained areas occurred at all depths of the profiles in both vegetated areas; however, the largest stained areas occurred predominantly in the top quartile (0-75 mm). Regression analysis indicated a significant decrease in stained area with depth in the profiles ($p \leq 0.001$) of both the reforested and grassed profiles. The average stained-area patch size was significantly larger in the reforested profiles than in the grassed profiles ($p \leq 0.05$) (Table 3.3).

3.3.3 Summary

Both the infiltration and dye-staining analyses indicate clear differences between the grassed and reforested areas. In the grassed area, dense rooting systems in the top ~10cm of soil correspond with apparent matrix flows, as revealed by the dye staining in the near-surface soil. Below the root-influenced soil in the grassed area, subsurface flow patterns transition to apparent control by abiotic factors. The transition to abiotic-influenced transport of dye through the subsurface combined with the increased number of flow paths relative to the near-surface soil indicates that flow through the grassed mine soil becomes increasingly random through visibly disconnected flow paths with depth.

Dye staining patterns in the reforested areas differed from those in grassed areas, which we interpret as evidence for differing flow patterns. The presence of larger stained areas in the reforested mine soils indicates a prevalence of matrix flow; however, increasingly-preferential flow at depth indicates flow-path connectivity in the subsurface, likely in response to root penetration. Dye staining results are complemented by the reforested area's larger infiltration rates and hydraulic conductivity values, which imply

that the reforested area is effective at promoting rainwater infiltration into and through the soil matrix.

The dye staining analyses highlighted the disturbed nature of mine soils, as flow was concentrated around voids and large rock fragments in the subsurface, and dye penetration below 30 cm was rare. Prior studies on mine soils have found differing subsurface flow patterns and shallower depths of dye penetration relative to native soils (Cey and Rudolph 2009; Wang and Zhang 2011). Hangen et al. (2004, 2005) reached similar conclusions in their study of German lignitic mine soils which found that subsurface flow paths are heterogeneous, both spatially and temporally, and are influenced by factors atypical of native soils (e.g. large coarse fragment content, high bulk density, compaction, soil repellency). Dye staining of eastern United States mine soils also found shallow dye penetration and subsurface flow predominantly along coarse-fragment surfaces and through macropores (Guebert and Gardner 2001). Although differing morphologically from native soils, it is evident that the mine soils in this study enable hydrologic functions such as rainwater infiltration and associated reduction of overland flow, and downward water movement along developed pathways in the subsurface. Furthermore, these developed flow pathways likely evolved over time in response to vegetation establishment and growth. Hence, it appears that near-surface hydrological processes in these mine soils have been influenced increasingly by biotic factors with time and plant community development.

Hydrologic processes have evolved over time in both the reforested and grassed areas, as seen in the infiltration rates and subsurface flow patterns reported in this study. However, observed hydrologic differences between the two vegetation types indicate that

vegetating mined land with trees may promote greater rainwater infiltration, enable faster soil matrix transport, and enhance subsurface transport via preferential flow paths, though these observed patterns may differ depending on factors such as rainfall intensity and duration, scale of measurement, and experimental methodologies. The findings of this study are consistent with well-known and documented influences by forest vegetation on natural landscapes (e.g. Beven and Germann 1982; Lange et al. 2008; Liang et al. 2011). Trees planted in non-mined environments have been found to aid the development of soil structure and to enable increased infiltration and more effective transport of water vertically downward relative to herbaceous plants (Alaoui et al. 2011; Dexter 1991; Oades 1993); our study reveals that emerging forest vegetation has similar influences in a mined-land environment.

3.4 CONCLUSIONS

Infiltration capacities and subsurface flow patterns varied by vegetation type on an eastern United States mine site. Fourteen years after vegetation establishment on loosely-graded mine soils, infiltration rates and hydraulic conductivities were significantly greater statistically on areas revegetated with forest trees than on areas revegetated with grasses but now dominated by herbaceous vegetation. Flow path types and patterns also differed visually and quantitatively between vegetation types, indicating a likelihood that the mine soils developed differing hydrologic properties and patterns of subsurface flow in response to post-mining vegetation type. Future research should determine if the apparent vegetation-type influences on mine soil hydrologic properties observed here occur more widely, apply other soil imaging techniques and/or tracers to further describe and understand hydrologic influence differences among vegetation types,

and determine if hydrologic properties and processes of mine soils that have been reforested successfully become similar to those of unmined forest soils with continued forest ecosystem development over time. Such research would assist in understanding deeper subsurface flow mechanisms beyond the scope of this study, as well as the influence of other vegetative covers on soil hydrologic processes, and thus improve the understanding of surface mine hydrology on a larger scale.

3.5 ACKNOWLEDGEMENTS

The authors would like to thank Dr. Robert Krenz for his gracious assistance with the infiltration and dye staining analyses, Kevin McGuire for providing infiltrometers, and Red River Coal Co. and Powell River Project for coordination and site access. The authors would also like to thank the three anonymous reviewers who assisted in manuscript improvement. This research was sponsored in part by the Appalachian Research Initiative for Environmental Science (ARIES) and the Virginia Tech Institute for Critical Technology and Applied Sciences (ICTAS). The views, opinions, and recommendations expressed herein are solely those of the authors and do not imply any endorsement by ARIES employees, other ARIES-affiliated researchers or industrial members. Funding for Carl Zipper's participation was provided in part, by the Virginia Agricultural Experiment Station and the Hatch Program of the National Institute of Food and Agriculture, U.S. Department of Agriculture.

3.6 REFERENCES

Abràmoff MD, Magalhães PJ, Ram SJ (2004) Image processing with ImageJ. *Biophotonics International* 11: 36-42.

Alaoui A, Caduff U, Gerke HH, Weingartner R (2011) Preferential flow effects on infiltration and runoff in grassland and forest soils. *Vadose Zone J*. 10: 367-377.

Anderson AE, Weiler M, Alila Y, Hudson RD (2009) Dye staining and excavation of a lateral preferential flow network. *Hydrol. Earth Syst. Sc.* 13: 935-944.

Atanackovíc N, Dragišić V, Stojković J, Papić P, Zivanović V (2013) Hydrochemical characteristics of mine waters from abandoned mining sites in Serbia and their impact on surface water quality. *Environ. Sci. Pollut. Res. Int.* 20: 7615-7626.

Awadhwal NK, Thierstein GE (1985) Soil crust and its impact on crop establishment: A review. *Soil Till. Res.* 5: 289-302.

Barnhisel RI, Darmody RG, Daniels WL (2000) Reclamation of Drastically Disturbed Lands (Agronomy No. 41). American Society of Agronomy, Madison, WI.

Beven K, Germann P (1982) Macropores and water-flow in soils. *Water Resour. Res.* 18: 1311-1325.

Biemelt D, Schapp A, Kleeberg A, Grünewald U (2005) Overland flow, erosion, and related phosphorus and iron fluxes at plot scale: a case study from a non-vegetated lignite mining dump in Lusatia. *Geoderma* 129: 4-18.

Bradshaw AD, Chadwick MJ (1980) The Restoration of Land: the Ecology and Reclamation of Derelict and Degraded Land. Univ of California Press.

Bronick CJ, Lal R (2005) Soil structure and management: A review. *Geoderma* 124: 3-22.

Cao X (2007) Regulating mine land reclamation in developing countries: The case of China. *Land Use Policy* 24: 472-483.

Carroll C, Merton L, Burger P (2000) Impact of vegetative cover and slope on runoff, erosion, and water quality for field plots on a range of soil and spoil materials on central Queensland coal mines. *Aust. J. Soil Res.* 38: 313-328.

Carsel RF, Parrish RS (1988) Developing joint probability distributions of soil water retention characteristics. *Water Resour. Res.* 24: 755-769.

Cey EE, Rudolph DL (2009) Field study of macropore flow processes using tension infiltration of a dye tracer in partially saturated soils. *Hydrol. Process*. 23: 1768-1779.

Decagon Devices, Inc. Undated. Mini Disk Infiltrometer User's Manual Version 10. Decagon Devices, Inc. Pullman, WA.

Dexter AR (1991) Amelioration of soil by natural processes. *Soil Till. Res.* 20: 87-100.

Duran-Zuazo VH,Pleguezuelo CRR (2008) Soil-erosion and runoff prevention by plant covers. A review. *Agron. Sustain. Dev*. 28: 65-86.

Flury M, Flühler H (1995) Tracer characteristics of Brilliant Blue FCF. *Soil Sci. Soc. Am. J.* 59: 22–27.

Greer BM (2015) Electrical Resistivity Imaging of Preferential Flow through Surface Mine Valley Fills with Comparison to Other Land Forms. M.S. Thesis, Virginia Tech.

Griffith MB, Norton SB, Alexander LC, Pollard AI, LeDuc SD (2012) The effects of mountaintop mines and valley fills on the physiochemical quality of stream ecosystems in the central Appalachians: A review. *Sci. Total Envi.* 417-418: 1-12.

Guebert MD, Gardner TW (2001) Macropore flow on reclaimed surface mines: infiltration and hillslope hydrology. *Geomorphology* 39: 151-169.

Haering KC, Daniels WL, Roberts JA (1993) Changes in mine soil properties resulting from overburden weathering. *J. Environ. Qual.* 22: 194-200.

Haering KC, Daniels WL, Galbraith JM (2005) Mapping and classification of southwest Virginia mine soils. *Soil Sci. Soc. Am. J*. 69: 463-472.

Haigh MJ, Sansom B (1999) Soil compaction, runoff and erosion on reclaimed coal-lands (UK). *International Journal of Surface Mining, Reclamation and Environment* 13: 135-146.

Hangen E, Gerke HH, Schaaf W, Hüttl RF (2004) Flow path visualization in a lignitic mine soil using iodine-starch staining. *Geoderma* 120: 121-135.

Hangen E, Gerke HH, Schaaf W, Hüttl RF (2005) Assessment of preferential flow processes in a forest-reclaimed lignitic mine soil by multicell sampling of drainage water and three tracers. *J. Hydrol.* 303: 16-37.

Hawkins JW (2004) Predictability of surface mine spoil hydryologic properties in the Appalachian Plateau. *Ground Water* 42: 119-125.

Howard JL, Amos DF, Daniels WL (1988) Phosphorus and potassium relationships in southwestern Virginia coal-mine spoils. *J. Environ. Qual.* 17: 695-700.

Jorgensen DW, Gardner TW (1987) Infiltration capacity of disturbed soils: temporal change and lithologic control. *Water Resour. Bull*. 23: 1161-1172.

Lange B, Luescher P, Germann PF (2008) Significance of tree roots for preferential infiltration in stagnic soils. *Hydrol. Earth Syst. Sci. Discuss.* 5: 2373-2407.

Liang WL, Kosugi K, Mizuyama T (2011) Soil water dynamics around a tree on a hillslope with or without rainwater supplied by stemflow. *Water Resour. Res.* 47.

Loch RI (2000) Effects of vegetation cover on runoff and erosion under simulated rain and overland flow on a rehabilitated site on the Meanda Mine, Tarong, Queensland. *Aust. J. Soil Res.* 38: 299-312.

Macdonald S E, Landhäusser SM, Skousen J, Franklin J, Frouz J, Hall S, Jacobs DF, Quideau S (2015) Forest restoration following surface mining disturbance: challenges and solutions. *New Forest*s 1-30.

Mohanty BP, Kanwar RS, Everts CJ (1994) Comparison of saturated hydraulic conductivity measurement methods for a glacial-till soil. *Soil Sci. Soc. Am. J.* 58: 672-677.

Moreno-de Las Heras M, Merino-Martín L, Nicolau JM (2009) Effect of vegetation cover on the hydrology of reclaimed mining soils under Mediterranean-Continental climate. *Catena* 77: 39-47.

Negley T, Eshleman K (2006) Comparison of stormflow responses of surface-mined and forested watersheds in the Appalachian mountains, USA. *Hydrol. Process.* 2: 3467-3483.

Nolde JE, Lovell JA, Whitlock WW, Miller RI (1986) Geology of the Norton Quadrangle, Virginia. Virginia Div. of Mineral Resources Publ. 65. Commonwealth of Virginia. Department of Mines, Minerals, and Energy. Division of Natural Resources. Charlottesville, VA.

Oades JM (1993) The role of biology in the formation, stabilisation and degradation of soil structure. *Geoderma* 56: 377–400.

Parr JF, Bertrand AR (1960) Water Infiltration into Soils. *Adv. Agron.* 12: 311-363.

R Core Team (2013) R: A language and environment for statistical computing. R Foundation for Statistical Computing, Vienna, Austria. URL http://www.R-project.org/.

Reynolds WD, Bowman BT, Brunke RR, Drury CF, Tan CS (2000) Comparison of tension infiltrometer, pressure infiltrometer, and soil core estimates of saturated hydraulic conductivity. *Soil Sci. Soc. Am. J.* 64: 478– 484.

Reynolds B, Reddy KJ (2012) Infiltration rates in reclaimed surface coal mines. *Water Air Soil Poll.* 223: 5941:5958.

Ritter JB, Gardner TW (1993) Hydrologic evolution of drainage basins disturbed by surface mining, Central Pennsylvania. *Geol. Soc. Am. Bull.* 105: 101-115.

Roberts JA, Daniels WL, Bell JC, Burger JA (1988) Early stages of mine soil genesis in Southwest Virginia spoil lithosequence. *Soil Sci. Soc. Am. J.* 52: 716–723.

Rosner B (1983) Percentage points for a generalized ESD many-outlier procedure. *Technometrics* 25: 165-172.

Sena K, Barton C, Angel P, Agouridis C, Warner R (2014) Influence of spoil type on chemistry and hydrology of interflow on a surface coal mine in the Eastern US coalfield. *Water Air Soil Poll.* 225: 2171.

Sencindiver JC, Ammons JT (2000) Minesoil genesis and classification. Ch. 23., in: Reclamation of Drastically Disturbed Lands. R. I. Barnhisel, W.L. Daniels, and R.G. Darmody (Eds.) Agronomy Series No. 41. American Society of Agronomy. Madison, WI.

Shukla MK, Lal R, Underwood J, Ebinger M (2004) Physical and hydrological characteristics of reclaimed minesoils in southeastern Ohio. *Soil Sci. Soc. Am. J.* 68: 1352-1359.

Sidle RC, Noguchi S, Tsuboyama Y, Laursen K (2001) A conceptual model of preferential flow systems in forested hillslopes: evidence of self-organization. *Hydrol. Process.* 15: 1675– 1692.

Simmons J, Currie W, Eshleman K, Kuers K, Monteleone S, Negley T, Pohlad B, Thomas C (2008) Forest to reclaimed land use change leads to altered ecosystem structure and function. *Ecol. Appl.* 18: 104–118.

Skousen J, Zipper CE (2014) Post-mining policies and practices in the Eastern USA coal region. *International Journal of Coal Science & Technology* 1: 135-151.

Sweigard R, Burger JA, Zipper CE, Skousen JG, Barton CD, Angel PN (2007) Low compaction grading to enhance reforestation success on coal surface mines. U.S. Office of Surface Mining Reclamation and Enforcement, Appalachian Regional Reforestation Initiative, Forest Reclamation Advisory No. 3.

Taylor TJ, Agouridis CT, Warner RC, Barton CD, Angel PN (2009) Hydrologic characteristics of Appalachian loose-dumped spoil in the Cumberland Plateau of eastern Kentucky. *Hydrol. Process.* 23: 3372-3381.

Thien SJ (1979) A flow diagram for teaching texture-by-feel analysis. *J. Agron. Educ.* 8: 54-55.

Wang K, Zhang R (2011) Heterogeneous soil water flow and macropores described with combined tracers of dye and iodine. *J. Hydrol.* 397: 105–117.

Weiler M, Flühler H (2004) Inferring flow types from dye patterns in macroporous soils. *Geoderma* 120: 137-153.

Wells LG, Ward AD, Phillips RE (1983) Predicting Infiltration and Surface Runoff from Reconstructed Spoils and Soils. Water Resources Research Institute, University of Kentucky: Lexington, Kentucky.

Younger PL, Wolkersdorfer C (2004) Mining impacts on the fresh water environment: technical and managerial guidelines for catchment scale management. *Mine Water Environ*. 23: 2-80.

Zhang R (1997) Determination of soil sorptivity and hydraulic conductivity from the disk infiltrometer. *Soil Sci. Soc. Am. J.* 61: 1024-1030.

Zipper CE, Burger JA, Skousen JG, Angel PN, Barton CD, Davis V, Franklin JA (2011) Restoring forests and associated ecosystem services on Appalachian coal surface mines. *Environ. Manage.* 47: 751-765.

CHAPTER IV: Modeling Patterns of Total Dissolved Solids Release from Central Appalachia, USA Mine Spoils

Elyse V. Clark, Carl E. Zipper, W. Lee Daniels, Zenah W. Orndorff and Matthew J. Keefe

Citation: Clark EV, Zipper CE, Daniels WL, Orndorff ZW, Keefe MJ (2017) Modeling patterns of total dissolved solids release from Central Appalachia, USA mine spoils. *Journal of Environmental Quality* 46:55-63. DOI 10.2134/jeq2016.04.0149

ABSTRACT

Surface mining in the Central Appalachian coalfields (USA) influences water quality as the interaction of infiltrated waters and oxygen with freshly-exposed mine spoils releases elevated levels of total dissolved solids (TDS) to streams. Modeling and predicting the short- and long-term TDS release potentials of mine spoils can aid in the management of current and future mining-influenced watersheds and landscapes. In this study, the specific conductance (SC, a proxy variable for TDS) patterns of 39 mine spoils over a sequence of 40 leaching events were modeled using a five parameter nonlinear regression. Estimated parameter values were compared to six rapid spoil assessment techniques (RSATs) to assess predictive relationships between model parameters and RSATs. Spoil leachates reached maximum values, 1,108 ± 161 µS cm^{-1} on average, within the first three leaching events, then declined exponentially to a breakpoint at the 16^{th} leach on average. After the breakpoint, SC release remained linear with most spoil samples exhibiting declines in SC release with successive leaching events. The SC asymptote averaged 276 ± 25 µS cm^{-1}. Only three samples had SCs > 500 µS cm^{-1}at the end of the 40 leaching events. Model parameters varied with mine spoil rock and weathering type, and RSATs were predictive of four model parameters. Unweathered samples released higher SCs throughout the leaching period relative to weathered

samples, and rock type influenced the rate of SC release. The RSATs for SC, total sulfur, and neutralization potential may best predict certain phases of mine spoil TDS release.

4.1 INTRODUCTION

Increasing soluble salt concentrations in freshwaters are a global concern (Cañedo-Argüelles et al. 2016; Williams 2001), as such increases have the potential to impact aquatic life at species, community, and ecosystem levels (Cañedo-Argüelles et al. 2013; Pond et al. 2008). Soluble salt increases in freshwaters are exacerbated by numerous anthropogenic activities including agriculture, water use and treatment, urbanization, de-icing road salt applications, and mining (Cañedo-Argüelles et al. 2013; Steele and Aitkenhead-Peterson 2011). Surface mining methods cause excess soluble salts in streamwater via disturbance of geologic materials, which, upon exposure to ambient O_2 and H_2O, undergo geochemical reactions resulting in the release of soluble ions that discharge to surface waters (Li et al. 2014; Orndorff et al. 2015).

In the Appalachian coalfields of the eastern United States, the dominant ion-producing processes occurring in disturbed mining materials, termed mine spoils, include pyrite oxidation, feldspar hydrolysis, and carbonate dissolution (Daniels et al. 2013; Orndorff et al. 2015). Appalachian mine spoil exposure to ambient environmental conditions typically releases dissolved SO_4^{2-}, HCO_3^-, Ca^{2+}, and Mg^{2+} to water, as well as lesser amounts of other major cations and trace elements (Pond et al. 2008; Skousen et al. 2000; Timpano et al. 2015). Collectively, the dissolved ions are called total dissolved solids (TDS). Electrical conductivity (EC) and specific conductance (SC, which is EC corrected to 25° C), are easily measured proxy variables for TDS (Hem 1989; Timpano et

al. 2010); SC is often measured as a TDS proxy when assessing aquatic ecosystems influenced by Appalachian surface mining (Cormier et al. 2013; Pond et al. 2008).

Typical SC values of Appalachian streams lacking significant anthropogenic influence are < 200 µS cm^{-1} (Merricks et al. 2007; Pond et al. 2008; Fritz et al. 2010), whereas mining-influenced waters range from < 500 to > 3,000 µS cm^{-1} (Hartman et al. 2005; Merricks et al. 2007; Lindberg et al. 2011; Evans et al. 2014). Elevated TDS in mining-influenced streams has been linked to altered aquatic macroinvertebrate communities, likely due to organism exposure to excess soluble salts (Hartman et al. 2005; Pond et al. 2008; Timpano et al. 2015), and these community alterations have been detected at SCs > 300 µS cm^{-1} (Cormier et al. 2013) and > 500 µS cm^{-1} (Pond et al. 2008). Previous studies have shown that mining-influenced streams with elevated SC often have fewer sensitive aquatic taxa present than non-mining-influenced streams (Pond et al. 2008, 2014), and these aquatic community effects have been observed ≥ 15 years after mining has ceased (Merricks et al. 2007; Pond et al. 2014).

The ability to predict mine spoil TDS release potentials prior to mining disturbance can aid in the environmental management of mining-influenced landscapes and watersheds. Prior studies have shown the chemistry of waters produced by Appalachian mine spoils depends on both rock type and degree of weathering (Evans et al. 2014; Orndorff et al. 2015; Daniels et al. 2016). Central Appalachian mine spoils are typically of clastic sedimentary origin (i.e. sandstones, siltstones, mudstones and shales) that have been subjected to varying degrees of *in situ* weathering prior to mining disturbance. Studies to date indicate that, upon weathering and leaching, sandstones typically produce lower SCs than more finely textured clastics, and that mine spoils

originating from close to the original land surface that are visibly weathered (oxidized and leached) prior to mining have lower SCs than mine spoils originating from deeper in the geologic column and not visibly weathered (Agouridis et al. 2012; Daniels et al. 2013, 2016; Sena et al. 2014; Orndorff et al. 2015). Furthermore, the SCs of mine spoil leachates are often at maximum values early in the leaching process and decline in subsequent leaching events. Levels of SC in mine spoil leachates may "stabilize" over time, but generally remain well above the natural background levels typical of the region's unmined reference streams (Agouridis et al. 2012; Evans et al. 2014; Sena et al. 2014). Although these observations of leaching patterns have emerged from a combination of laboratory and field studies, there is still a lack of knowledge about modeling and predicting the potential SC leaching levels and temporal SC release patterns of Appalachian mine spoils, which have considerable variation depending on rock type and pre-mining weathering status.

Mine spoil TDS release patterns generated by laboratory columns demonstrate a general correspondence with field behavior (Evans et al. 2014; Sena et al. 2014; Ross 2015; Daniels et al. 2016); however, such studies are time consuming and labor intensive. Methods for characterizing and predicting mine spoil TDS release that are less time and labor intensive are needed. In this study, 39 mine spoil samples collected from Central Appalachian surface coal mines were characterized using column leaching and rapid spoil assessment techniques (RSATs). Specific objectives were to (1) develop a model of mine spoil SC release patterns, and (2) examine relationships between estimated SC model parameters and RSAT results. This research was intended to improve scientific

understanding and prediction of mine spoil TDS leaching patterns, and to aid development of mine reclamation techniques to minimize TDS elution from mine spoils.

4.2 MATERIALS AND METHODS

4.2.1 Spoil Collection and Classification

Thirty-nine freshly-fractured mine spoil samples of known stratigraphic origin were collected from active surface coal mines in Kentucky, Virginia, and West Virginia (Figure 4.1). Bulk spoils were characterized by the following weathering types: unweathered, weathered, or mixed weathering (Table 4.1). Unweathered spoils (UW) are gray in color, and originate from beneath weathered strata. Weathered spoils (WX) are visibly altered relative to UW due to the brown coloration of Fe-oxides. Mixed-weathering spoils (MXW) have both weathered and unweathered zones within the spoil sample. Spoils were also characterized by the following rock types: sandstones (SAND), mudstones (MUD), mixed rock (MXR), or shales. A classification of MXR implies that a rock has no more than 80% of one rock type (Orndorff et al. 2015). For further details on the mine spoil properties, see Daniels et al. (2016).

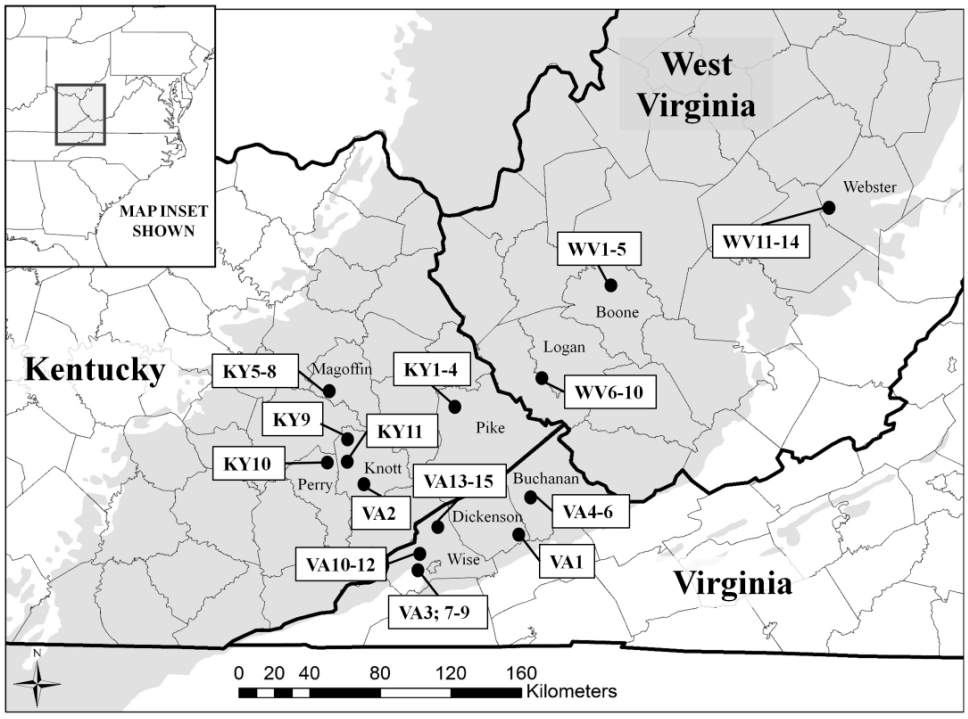

Figure 4.1 Location map of the 39 Central Appalachian spoils collected in Kentucky, Virginia, and West Virginia. The Appalachian coalfields of the eastern United States are shown in gray.

Table 4.1 Mine spoil sample numbers by rock and weathering type (n=39). Numbers of samples excluded from the analyses are in parentheses.

	Weathering Type			
Rock Type	**UW**	**MXW**	**WX**	**Total**
MUD	7 (1)	--	4	11(1)
MXR	4 (1)	3	--	7 (1)
SAND	10	4	3	17
SHALE	(2)	--	--	(2)
Total	21(4)	7	7	35 (4)

4.2.2 Column Leaching

Spoil samples were ground to < 2 mm and back-blended with finer-textured spoil materials, then placed into 40 cm long PVC pipes with a 7.4 cm inside diameter. Subsamples of each spoil material were placed into three PVC leaching columns. Reported results are averages of the three replicate samples. Columns were leached with a pH 4.6 solution, which is a solution commonly used in leaching studies as it resembles

regional rainfall pH values more closely than deionized water (Halvorson and Gentry 1990). To initialize the column leaching experiment, simulated rainfall was slowly added to the leaching columns until the maximum unsaturated water holding capacity was reached. The first 2.5 cm of leached water was collected and analyzed as Leach 0. After the initial leachate was collected, the columns were dosed with 2.5 cm of simulated rainwater (pH 4.6) twice a week and the eluted leachate was collected and analyzed for SC. The experiment lasted for a total of 20 weeks (40 leaching events, Leaches 0-39). For a more detailed description of the column dimensions and leaching process see Orndorff et al. (2015).

4.2.3 Model Development

Previous studies (Orndorff et al. 2015; Daniels et al. 2016) and visual analyses of leachate data found that leachate SC from the column design utilized here typically peaked at Leach 0, 1 or 2; then decreased with subsequent leaching events in a decay pattern that appeared exponential. After the decay process, the leachate reached a change point, after which the pattern appeared linear through subsequent leaching events. In response to these observations, the leaching patterns of the 39 mine spoils were used to develop a model for the purpose of quantitatively describing the SC of waters produced during the leaching period.

Exponential nonlinear regression models are often used to model the concentration of a substance over a period of time. A nonlinear regression model has the following form:

$$Y_i = f(\boldsymbol{X_i}, \boldsymbol{\theta}) + \epsilon_i \quad (4.1)$$

where Y_i is the response of the i^{th} observation, $\boldsymbol{X_i}$ is a vector of observed values of the predictor variables for the i^{th} observation, and $f(\cdot)$ is a response function that is nonlinear in the parameter vector $\boldsymbol{\theta}$ (Bates and Watts, 1988). It is assumed that ϵ_i are independent and normally distributed with mean 0 and variance σ^2.

Based on the observation of non-linear leaching patterns, a five-parameter nonlinear segmented regression model was developed (Figure 4.2). The segmented regression includes a three-parameter exponential decay function and a linear regression function connected by a breakpoint (BP). The response function f, as a function of leach number $x_i (i = 0, 1, \dots, 39)$ and $\theta = (\theta_1, \theta_2, \theta_3, \beta_0, \beta_1, BP)$ is given by the following:

$$f(\boldsymbol{X_i}, \boldsymbol{\theta}) = \begin{cases} \theta_2 e^{-\theta_3 x_i} + \theta_1, & x_i < BP \\ \beta_0 + \beta_1 x_i, & x_i \geq BP. \end{cases} \tag{4.2}$$

In order for the exponential component and the linear component to be connected at $x_i = BP$, the relationship is as follows:

$$\theta_2 e^{-\theta_3 BP} + \theta_1 = \beta_0 + \beta_1 BP \tag{4.3}$$

and can be rearranged as shown in Eq. 5.4:

$$\beta_0 = \theta_2 e^{-\theta_3 BP} + \theta_1 - \beta_1 BP \tag{4.4}$$

Therefore, the nonlinear response function f used to model SC as a function of time is given by

$$f(\boldsymbol{X_i}, \boldsymbol{\theta}) = \begin{cases} \theta_2 e^{-\theta_3 x_i} + \theta_1, & x_i < BP \\ (\theta_2 e^{-\theta_3 BP} - \beta_1 BP + \theta_1) + \beta_1 x_i, & x_i \geq BP \end{cases} \tag{4.5}$$

where θ_2 describes the exponential peak, θ_3 is the exponential decay factor, BP is the leach at which the decay function changes to a linear function, β_1 is the slope of the linear segment, and θ_1 is the horizontal asymptote associated with the exponential decay segment. The θ_1 values are also similar to the SC associated with the BP leach.

Parameters of the regression were estimated using nonlinear least squares (Bates and Watts 1988). All samples were modeled from their peak concentration (i.e. largest SC value of all leaching events). If the peak SC was not at Leach 0 but at Leach 1 or 2, the leach(es) before the peak were omitted from the data set and the sample was modeled from the leach with the largest SC value.

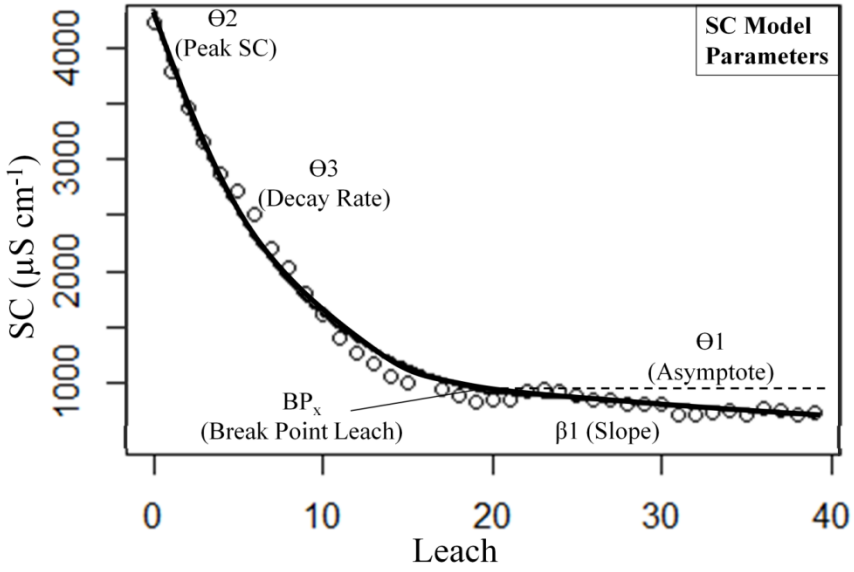

Figure 4.2 Diagram of specific conductance (SC) model parameters and the nonlinear regression for the spoil samples.

4.2.4 Rapid Spoil Assessment Techniques (RSATs)

Rapid spoil assessment techniques are laboratory analyses that characterize mine spoils within a shorter time period and require fewer resources than the column leaching procedure. In total, 14 RSATs were applied to the spoil samples in order to identify which RSATs may predict SC model parameters; however, two were omitted due to a lack of correspondence with model parameters (hydrogen peroxide potential acidity and calcium carbonate equivalent) and six were omitted because results were highly correlated with other RSATs. Therefore, six of the original 14 RSATs are presented in

subsequent text. Saturated paste SC (Rhoades 1982) and pH were measured by mixing ground spoils (<2 mm) with deionized water until a glistening paste formed, then suction-filtered after 2 hours to extract a liquid which was analyzed for pH and SC. Hydrogen peroxide SC and pH were determined by reacting a weak concentration (3 %) of H_2O_2 with a 1:1 sample to peroxide solution ratio, then analyzed. Total sulfur was measured using the dry combustion technique on a LECO S632 Sulfur Analyzer. Neutralization potential (NP), a test for the amount of neutralizing bases, was measured by adding HCl to the samples, boiling, then back-titrating with NaOH (Sobek et al. 1978).

4.2.5 Statistical Analyses

Model performance was evaluated using root mean square error (RMSE). The RMSE indicates the difference between measured data and model predicted values and is calculated as follows:

$$RMSE = \sqrt{\frac{1}{n-p}\sum_{i=1}^{n}(y_i - \hat{y}_i)^2} \tag{4.6}$$

where y_i and $\hat{y}_i$ are the observed and predicted values of n observations, considering p parameters, respectively.

Mann Whitney *U* and Kruskal-Wallis tests were performed using the software R (R Core Team 2013) to determine statistical differences ($\alpha = 0.05$) between SC model parameters based on rock or weathering type. If differences were found, a Steel-Dwass test for multiple nonparametric comparisons was used to identify rock-type or weathering-type effects. Spearman correlations between SC model parameters and RSATs were calculated. All values in the text after "±" indicate one standard error above/below the mean.

4.3 RESULTS AND DISCUSSION

4.3.1 Model Parameters

All samples were successfully modeled; however, model fit varied for different samples, and it is recognized that certain mine spoils may not conform to the proposed model due to differences in spoil chemistry, composition, mineralogy, etc. Models with the poorest fits were those producing (1) very high leachate SC and no apparent breakpoint or linear model component (Type I, Figure 4.3a), or (2) a "pseudo-peak" in the initial leaching events followed by a secondary peak later in the leaching period (Type II, Figure 4.3b). Two samples (VA2 and KY7) had Type I patterns, and two samples (WV7 and WV13) had Type II patterns; these samples were omitted from further analysis (Table 4.1). Type I samples, which were both shales, were omitted because 40 leaching events were not adequate to define model parameters, likely due to high S content in the samples continuing to oxidize throughout the leaching period. Type II samples were omitted because the geochemical drivers for these samples' TDS releases appear different than for other samples, likely due to differences in spoil mineralogy or fine particle size coatings affecting mineral reactivity during the leaching and weathering process. Discussion of results henceforth excludes these four omitted samples, and model parameters are subsequently discussed in order of appearance throughout the leaching period (Figure 4.2).

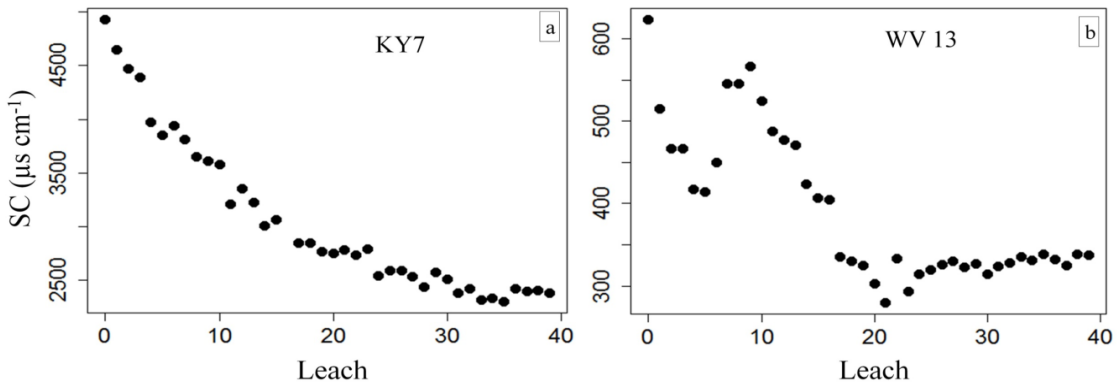

Figure 4.3 Examples of spoil samples omitted from analysis due to lack of correspondence with the nonlinear regression due to (a) Type I patterns and (b) Type II patterns.

Peak SC (θ_2)

The peak SC parameter (θ_2) ranged from 34 to 4,480 µS cm^{-1}, averaged 1,108 ± 161 µS cm^{-1}, and did not differ statistically among rock types (Figure 4.4). Among weathering types, the mean peak SC was lower for WX (618 ± 179 µS cm^{-1}) than for MXW and UW spoils (1,737 ± 534 and 1,181 ± 181 µS cm^{-1}, respectively). Samples with higher peak SCs tended to have significantly higher asymptote SCs (θ_1, Figure 4.2) at the end of the leaching study period ($\rho = 0.60; p \leq 0.001$) and also tended to have more steeply declining linear segment slopes ($\beta_1, \rho = -0.43; p \leq 0.01$) (Figure 4.5).

For all samples, peak SC was positively correlated with paste SC ($\rho = 0.72; p \leq 0.001$), H_2O_2 SC ($\rho = 0.70; p \leq 0.001$), and total sulfur ($\rho = 0.53; p \leq 0.01$), and negatively correlated with H_2O_2 pH ($\rho = -0.39; p \leq 0.05$) (Figure 4.6). Paste SC, H_2O_2 SC and total sulfur were correlated with the peak SC for most rock and weathering types (Table 4.2). The peak SC was also correlated with H_2O_2 pH in SAND, UW, and WX spoils.

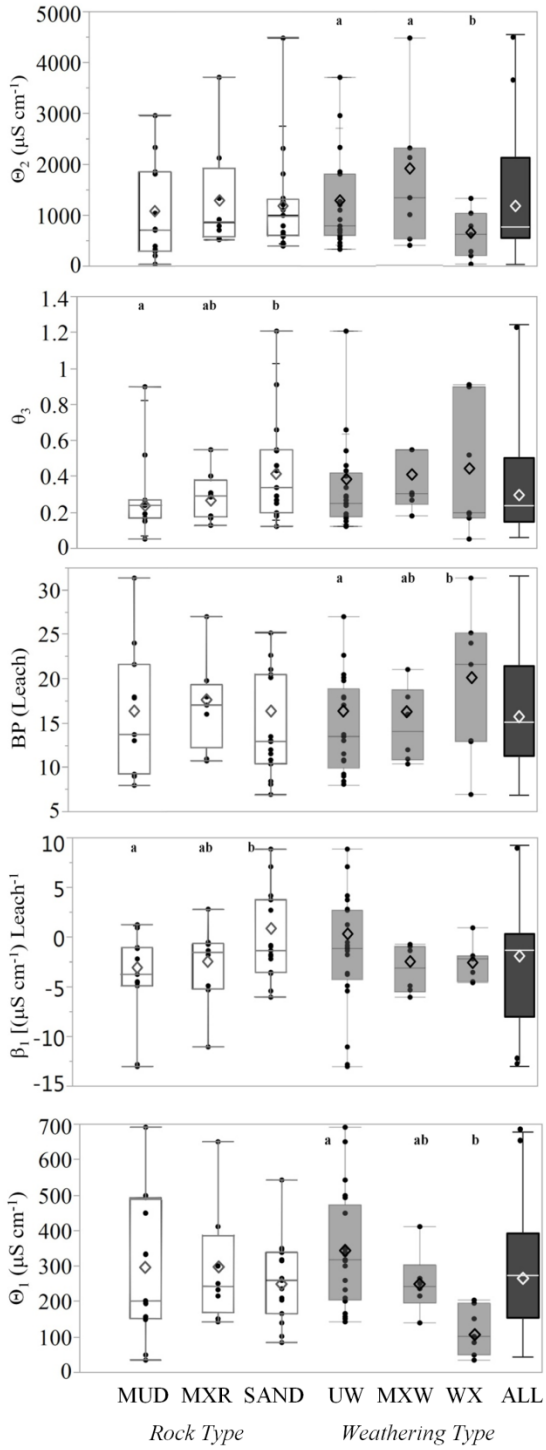

Figure 4.4 Box plots of estimated specific conductance model parameters illustrating the range of parameter values. Wide bars represent the minimum, 25th percentile, median, 75th percentile, and maximum values, respectively. Diamonds represent means. Mine spoils are classified by rock (MUD=mudstone, MXR=mixed rock, SAND=sandstone) and weathering (UW=unweathered, MXW=mixed weathering, WX=weathered) type. ALL designates all samples. Within each rock or weathering type, box plots with different letters are significantly different ($p \leq 0.05$). For model parameter symbol definitions see Figure 4.2.

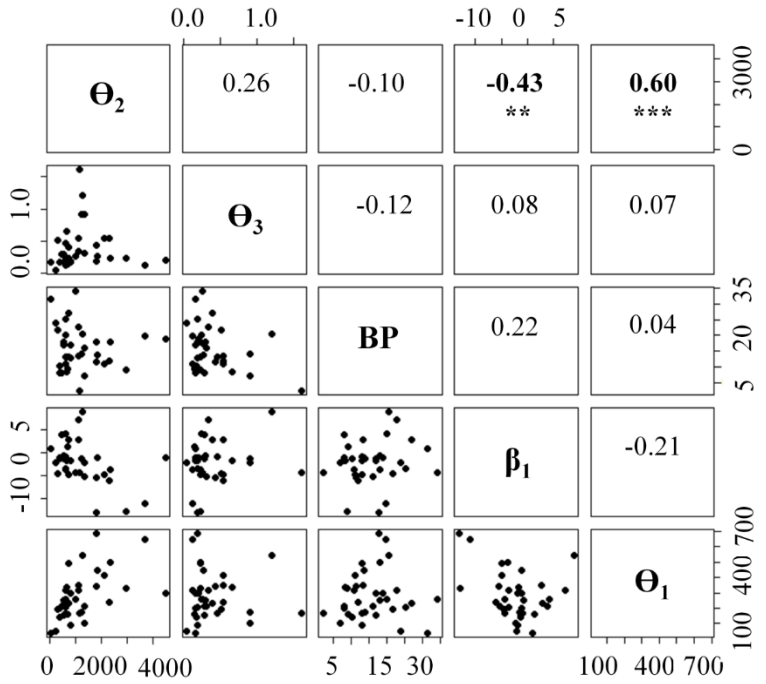

Figure 4.5 Correlations among estimated model parameters. Values followed by ** and *** denote $p \leq 0.01$, and $p \leq 0.001$, respectively. For model parameter symbol definitions see Figure 5.2.

Table 4.2 Correlation coefficients for significant relationships between estimated specific conductance model parameters and rapid spoil assessment tests.

Parameter	Class.	Paste SC	H_2O_2 SC	Paste pH	H_2O_2 pH	Total S	NP†
θ_2‡	MUD†	0.91***	0.91***			0.89**	
	MXR	0.86*	0.93*			0.77*	
	SAND	0.52*			-0.52*		
	UW	0.67***	0.64**		-0.59*	0.59**	
	MXW	0.93***			-0.82*		
	WX	0.86*	0.89**				
θ_3	MUD				-0.64*		
	UW	-0.48*	-0.43*			-0.47*	
BP	MUD			-0.75**	-0.61*		-0.69*
	UW			-0.56**	-0.52*		
	WX	-0.82*	-0.86*				
β_1	MXR	-0.79*	-0.93**			-0.79*	
	UW	-0.61*	-0.58**				
θ_1	MUD	0.92**	0.87**			0.89**	
	MXR	0.89**				0.86*	0.79*
	SAND	0.49*				0.52*	0.70**
	UW	0.71***	0.68***			0.58**	

† NP= Neutralization Potential, MUD=mudstone, MXR=mixed rock, SAND= sandstone, UW=unweathered, MXW=mixed weathering, WX=weathered

‡ For model parameter symbol definitions see Figure 4.2.

* Indicates $p \leq 0.05$, ** Indicates $p \leq 0.01$, *** Indicates $p \leq 0.001$.

Pre-mining weathering status had clear effects on the peak SC for individual mine spoils, likely because weathered spoils were pre-weathered and leached *in situ* and had smaller pools of potentially leachable soluble ions. Results suggest that paste SC has a strong predictive relationship with peak SC, likely because paste SC measures easily solubilized ions that contribute directly to the initial SC peak. A related study (Daniels et al. 2016) on mine spoil leachates also found a strong predictive relationship between peak SC and paste SC ($R^2 = 0.85$). Results suggest that total S also has a predictive relationship with peak SC. Higher total S typically indicates a sample may be more affected by S-oxidation and offsetting neutralization reactions (Orndorff et al. 2015), hence a higher peak SC.

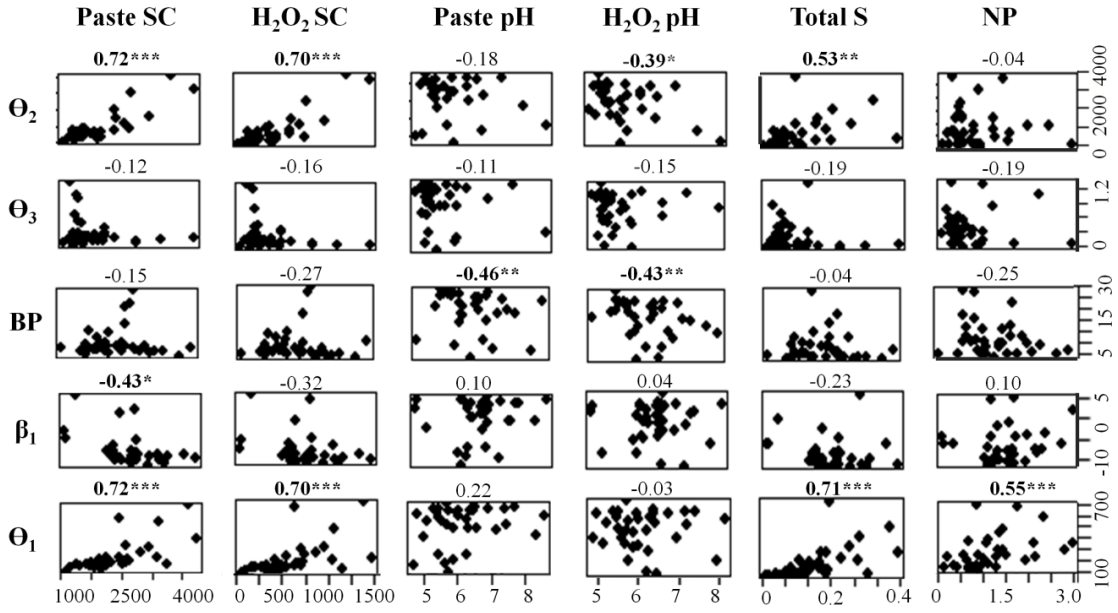

Figure 4.6 Correlations between estimated model parameters and rapid spoil assessment tests are shown. Significant correlations are in bold. Values followed by *, **, and *** indicate $p \leq 0.05$, $p \leq 0.01$, and $p \leq 0.001$, respectively. For model parameter symbol definitions see Figure 5.2

Exponential Decay Rate (θ_3)

The exponential decay rates (θ_3) ranged from 0.05 to 1.21 with a mean of 0.36 ± 0.04 (Figure 4.4), with relatively high decay rates indicating rapid exponential declines in SC release. Based on rock type, SAND had larger decay rates (0.45 ± 0.08) than MUD spoils (0.27 ± 0.05). The exponential decay rates did not differ statistically among weathering types.

Considering all spoils, exponential decay rates were not correlated with any RSATs (Figure 4.6). However, based on rock and weathering type, exponential decay rates were negatively correlated with paste SC, H_2O_2 SC and total S in UW spoils.

Rock type differences among exponential decay rates were most likely influenced by differences in spoil mineralogy and grain size. Larger surface areas associated with smaller grain sizes may result in a more uniform weathering of the MUD and MXR samples which slows over time as the easily-weatherable ions leach out. Comparatively, SAND spoils have different surface areas and greater abundances of primary mineral grains that likely contribute to faster SC decay rates relative to MUD and MXR spoils. Exponential decay rate prediction by RSATs was limited; therefore, other analyses such as mineralogical analyses or specific ion analyses may be necessary to predict spoil exponential decay rates.

Breakpoint (BP)

The breakpoint (BP) parameter ranged from Leach 7 to 31 and averaged 16 ± 1. Mean breakpoints for specific rock and weathering types ranged from Leach 15 to 19. Mean breakpoints did not differ by rock type, whereas WX spoils had higher breakpoints (Leach 19 ± 3) than MXW (Leach 15 ± 2) and UW (Leach 15 ± 1) spoils (Figure 4.4).

Modeled breakpoints were negatively correlated with both paste pH ($\rho = -0.46; p \leq 0.01$) and H_2O_2 pH ($\rho = -0.43; p \leq 0.01$) for all samples (Figure 4.6). Considering rock and weathering type, paste pH and H_2O_2 pH were negatively correlated with the breakpoint for MUD and UW spoils, and paste SC and H_2O_2 SC were negatively correlated with WX samples.

Pre-weathered samples required four more leaching events on average than UW samples to reach a BP, which may be attributed to WX spoils having less neutralizers and total sulfur overall ($p \leq 0.01$, Wilcoxon, data not shown). It is likely that the reactions responsible for SC release have already occurred to a larger extent in weathered spoils, thus the breakpoint occurs at a different time in the leaching process relative to unweathered samples. Results suggest that the breakpoints may be predicted by initial pH, as samples with lower pHs (i.e. less neutralizers) may require more leaching events to reach a BP relative to samples with higher pHs which contain larger masses of reactive neutralizers such as carbonates that continue to counteract Fe, Mn and S-oxidation reactions throughout the observed leaching period.

Linear Slope (β_1)

For the post-breakpoint parameters, the linear slope (β_1) parameter values ranged from -13.0 to 8.8 µS cm^{-1} $Leach^{-1}$ with nine increasing, 21 decreasing, and five slopes not significantly different from zero. Mean linear slope values were negative for all rock and weathering classification types; however, MUD spoils had smaller (i.e. more negative) average slopes (-3.7 ± 1.4 µS cm^{-1} $Leach^{-1}$) than SAND (-0.2 ± 1.0 µS cm^{-1} $Leach^{-1}$). Samples with more negative linear slopes were correlated with higher peak SCs ($\rho = -0.43; p \leq 0.01$) (Figure 4.5).

For all samples, the linear slope was negatively correlated with paste SC ($\rho = -0.43; p \leq 0.05$). Negative correlations between the linear slope and RSATs for SC also occurred in MXR and UW samples.

Rock type effects on the linear SC release slope are likely influenced by the same factors as the exponential decay rate (e.g. spoil mineralogy, grain sizes). Continuous weathering of finer-grained mudstones likely influences the more negative linear slope compared to the relatively constant or increasing linear slope of heterogeneous (i.e. larger primary mineral grains surrounded by cementing agents) sandstones. Paste SC is potentially predictive of the linear phase; samples with higher paste SCs tended to continue declining in TDS release during the linear phase, likely due to a larger availability of weatherable ions over more extended leaching periods. Comparatively, samples with lower paste SCs tended to have constant or slightly increasing linear slopes, indicating that SC release may have reached a near-equilibrium status driven by background mineral weathering rates (Sena et al. 2014).

Asymptote SC (θ_1)

The asymptote SC (θ_1) values for all samples ranged from 34 to 690 µS cm^{-1} and averaged 276 ± 25 µS cm^{-1} (Figure 4.4). Mean asymptote SC values did not differ by rock type but differed among weathering types. Mean asymptote SC values were the highest for UW (329 ± 33 µS cm^{-1}) and lowest for WX (118 ± 26 µS cm^{-1}). Only three samples, all unweathered, had asymptote SC values > 500 µS cm^{-1}, whereas the asymptote SC values of 22 samples (63%) were < 300 µS cm^{-1}. Samples with higher asymptote SCs tended to also have significantly higher peak SCs ($\rho = 0.60; p \leq 0.001$) (Figure 4.5).

The asymptote SC had positive correlations with paste SC, H_2O_2 SC, total sulfur, and the neutralization potential ($\rho = 0.55 - 0.72; p \leq 0.001$) for all samples (Figure 4.6). Paste SC, H_2O_2 SC and total sulfur also had strong correlations with the asymptote SC for certain rock and weathering types.

The asymptote SC mimicked the pre-mining weathering status, as samples that had been pre-weathered generally had lower asymptote SCs and samples that had not been pre-weathered typically had higher asymptote SCs. The asymptote SC had predictive relationships with the RSATs for SC, total S, and neutralization potential, suggesting that SC release is still influenced, to an extent, by sulfur oxidation and neutralization reactions at the end of the exponential decay period. Typically, samples with lower asymptote SCs also had lower paste SCs (1,000-1,500 µS cm^{-1}), total S (0 - 0.1 %), and neutralization potentials (0 - 1.0 %) relative to samples with higher asymptote SCs.

4.3.2 Model Error

Model error estimates (RMSE) indicated that model predicted SCs were under- or over-estimated by a minimum of 2 µS cm^{-1}, a maximum of 91 µS cm^{-1}, and a mean of 35 µS cm^{-1} relative to the collected data for all samples (Table 4.3). The highest overall RMSE occurred in modeling MUD (RMSE 44 µS cm^{-1}) and UW (RMSE 39 µS cm^{-1}) spoils, and the smallest error occurred in WX spoils (RMSE 24 µS cm^{-1}) on average.

Table 4.3 The Root Mean Square Error (μS cm^{-1}) for model-predicted specific conductance based on rock and weathering type.

Spoil Classification	RMSE (μS cm^{-1}) *(Mix, Max)*	*Mean*
All	(2.1, 91.5)	34.8
MUD	(2.1, 89.8)	44.3
MXR	(11.2, 91.5)	37.4
SAND	(10.2, 80.5)	27.1
UW	(10.9, 91.5)	38.9
MXW	(10.2, 80.5)	34.1
WX	(2.1, 53.2)	24.1

4.3.3 Summary of Modeling Results

Overall, the successful modeling of 35 of the 39 Central Appalachian spoils revealed clear patterns in leaching behavior. Each model parameter was significantly influenced by rock or weathering type, indicating that such mine spoil classifications are essential to characterizing TDS leaching behaviors. Weathering type only had significant effects on model parameters describing the SC at specific points in the leaching process (i.e. peak SC, breakpoint leach, and asymptote). Comparatively, rock type only had significant effects on the rates of SC release in the model (i.e. exponential decay rate and linear slope). Significant relationships between model parameters and RSATs implied that certain phases of the leaching process may be predicted by relatively rapid laboratory based RSATs. Considering all spoils, four of five model parameters were significantly correlated with at least one of the six RSATs analyzed; however, different RSATs were correlated with each model parameter.

4.3.4 Model Applications to Laboratory and Field Leaching Behavior

For model validation purposes, relating model results to laboratory- and field-leaching studies of Appalachian mine spoils may help confirm and improve the

understanding of spoil leaching patterns. Considering peak SC (θ_2), exponential decay (θ_3), and the transition from exponential decay to linear SC release (BP), few studies have characterized these phases of the leaching process. In their column leaching study of 15 Appalachian mine spoils which were a subset of the mine spoils analyzed in this study, Orndorff et al. (2015) found a mean peak SC of 1,468 ± 150 µS cm^{-1}, which was slightly higher than the 1,108 ± 161 µS cm^{-1} peak SC identified in this study, and also found significantly larger peak SCs in unweathered spoils relative to weathered spoils. A two-year field lysimeter study by Agouridis et al. (2012) in Kentucky, USA, similarly noted that weathered spoils had significantly lower SC discharges initially (829 ± 68 µS cm^{-1}) relative to unweathered spoils (1,032 ± 54 µS cm^{-1}). Prior studies found three to four leaching events were required for a pore volume, and that leaching patterns may cease exponential decay after five to seven pore volumes or approximately 15 to 20 leaching events (Orndorff et al. 2015). In the field, however, many months or years may be required to reach a full pore volume. A study of > 130 VFs by Evans et al. (2014) estimated that 15 to 25 years on average may be required to complete the exponential decay phase of the leaching process. In field leaching conditions, the variability of the exponential decay phase is likely influenced by factors such as spoil porosity and volume, preferential flow paths, and weathering front depth.

Laboratory and field studies characterizing the post-BP linear SC release (β_1) and the level at which SC release stabilizes (θ_1) are also limited. A field study on spoil leaching behavior reported that brown (WX) sandstones, gray (UW) sandstones, and MXW spoils had constant TDS release patterns nine years after placement, as SC was not decreasing temporally (Sena et al. 2014). Our results suggest, however, that certain spoils

may continue to increase or decrease in TDS release, although it is currently unknown if these patterns will continue over a longer period. For SC stabilization levels (θ_1), Orndorff et al. (2015) reported mean SC values of 374 and 129 μS cm^{-1} for unweathered and weathered spoils at the end of the leaching study period, respectively. Although not statistically significant, Sena et al. (2014) reported higher SCs in unweathered spoils (564 μS cm^{-1}) relative to weathered spoils (421 μS cm^{-1}) that were leached in the field for nine years. The SCs from prior studies and those reported in this study indicate that following the exponential decay phase, mine spoil leachate SCs still remain at levels elevated above natural background for a number of years (Sena et al. 2014; Ross 2015), and typically stabilize at SC levels above the 300 μS cm^{-1} benchmark intended to prevent > 5% extirpation of aquatic macrobenthic genera (Cormier et al. 2013).

4.3.5 Geochemical Drivers of Specific Conductance Release

Prior studies of Appalachian mine spoils indicate that rapid oxidation of trace pyrites occurs initially in freshly-exposed mine spoils, but slows over time (Orndorff et al. 2015), which is likely responsible for the modeled peak SC and exponential decay patterns. Once pyrite oxidation slows, the anion leaching pattern shifts from sulfate dominance to bicarbonate due to neutralization reactions, which may explain the post-BP and linear leaching model segments. Therefore, the interaction of rapid S-oxidation combined with kinetically slower carbonate- and feldspar-driven neutralization reactions appears to control temporal patterns of mine spoil TDS release.

Although certain model parameters had predictive relationships with RSATs, the inability to predict the exponential decay rate (θ_3) parameter indicates that certain phases of leaching were not explained by the RSATs used in this study. Other spoil assessments

such as mineralogical analyses and ion chemistry may assist in understanding the SC model parameters that were not predicted in this study.

4.3.6 Conclusions

The leaching patterns of central Appalachian mine spoils were modeled as a continuous nonlinear regression with an exponential phase and linear phase separated by a breakpoint. Each model parameter was significantly influenced by either rock- or weathering- type and all but one parameter had predictive relationships with rapid laboratory assessment techniques. Classification of spoil materials by weathering and rock type is essential to understanding leaching patterns of mine spoils. Future research should focus on improving the understanding of geochemical mechanisms governing TDS release rates and patterns throughout the leaching process, as well as focus on relating model predictions and data from laboratory studies to measured field data in order to evaluate temporal model conformance.

4.4 ACKNOWLEDGEMENTS

This project was sponsored by the Appalachian Research Initiative for Environmental Science (ARIES), Powell River Project, Virginia Tech Institute for Critical Technology and Applied Science, USDI Office of Surface Mining, Virginia Agricultural Experiment Station, and the Hatch Program of the National Institute of Food and Agriculture, U.S. Department of Agriculture. The views and recommendations expressed herein are solely those of the authors and do not imply endorsement by ARIES employees, other ARIES-affiliated researchers or industrial members.

4.5 REFERENCES

Agouridis CT, Angel PN, Taylor TJ, Barton CD, Warner RC, Yu X, Wood C (2012) Water quality characteristics of discharge from reforested loose-dumped mine spoil in eastern Kentucky. *J. Environ. Qual.* 41: 454-468.

Bates DM, Watts DG (1988) *Nonlinear Regression Analysis and Its Applications.* John Wiley & Sons, New York.

Cañedo-Argüelles M, Kefford BJ, Piscart C, Prat N, Schäfer RB, Schulz C (2013) Salinisation of rivers: an urgent ecological issue. *Environ. Pollut.* 173: 157-167.

Cormier SM, Suter GW, Zheng L (2013) Derivation of a benchmark for freshwater ionic strength. *Environ. Toxicol. Chem*. 32: 263-271.

Daniels WL, Orndorff ZW, Eick MJ, Zipper CE (2013) Predicting TDS release from Appalachian mine spoils. In: Craynon, J.R. (Ed.), Proc., Environmental Considerations in Energy Production, April 14-18, 2013, Charleston, WV. Society for Mining Metallurgy and Exploration, Englewood, CO, p. 275-285.

Daniels WL, Zipper CE, Orndorff ZW, Skousen JG, Barton CD, McDonald L, Beck M (2016) Predicting total dissolved solids release from central Appalachian coal mine spoils. *Environ. Pollut.* 216:371-379.

Evans DM, Zipper CE, Donovan PF, Daniels WL (2014) Long-term trends of specific conductance in waters discharged by coal-mine valley fills in central Appalachia, USA. *J. Am. Water Resour. Assoc.* 50: 1449-1460.

Fritz KM, Fulton S, Johnson BR, Barton CD, Jack JD, Word DA, Burke RA (2010) Structural and functional characteristics of natural and constructed channels draining a reclaimed mountaintop removal and valley fill coal mine. *J. North Am. Benthol. Soc*. 29: 673-689.

Halvorson HG, Gentry CE (1990) Long-term leaching of mine spoil with simulated precipitation. In: Proceedings of the 1990 Mining and Reclamation Conference and Exhibition, Charleston, WV. American Society for Surface Mining and Reclamation, Lexington, KY, pp. 27-32.

Hartman KJ, Kaller MD, Howell JW, Sweka JA (2005) How much do valley fills influence headwater streams? *Hydrobiologia* 532: 91-102.

Hem JD (1989) Study and Interpretation of the Chemical Characteristics of Natural Waters. Water Supply Paper 2254, 3rd edition, U.S. Geological Survey, Washington D.C., 263 p.

Li X, Park JH, Edraki M, Baumgartl T (2014) Understanding the salinity issue of coal mine spoils in the context of salt cycle. *Environ. Geochem. Hlth* 36: 453-465.

Lindberg TT, Bernhardt ES, Bier R, Helton AM, Merola RB, Vengosh A, DiGiulio RT (2011) Cumulative impacts of mountaintop mining on an Appalachian watershed. *Proceedings Natl. Acad. Sci.* USA 108:20929-20934.

Merricks TC, Cherry DS, Zipper CE, Currie R, Valenti T (2007) Coal-mine hollow fill and settling pond influences on headwater streams in southern West Virginia, USA. *Environ. Monit. Assess.* 129: 359-378.

Orndorff ZW, Daniels WL, Fanning DS (2008) Reclamation of acid sulfate soils using lime-stabilized biosolids. *J. Env. Qual*. 37:1447-1455.

Orndorff ZW, Daniels WL, Zipper CE, Eick M, Beck M (2015) A column evaluation of Appalachian coal mine spoils' temporal leaching behavior. *Environ. Pollut.* 204: 39-47.

Pond GJ (2010) Patterns of Ephemeroptera taxa loss in Appalachian headwater streams (Kentucky, USA). *Hydrobiologia* 641: 185–201.

Pond GJ, Passmore ME, Borsuk FA, Reynolds L, Rose CJ (2008) Downstream effects of mountaintop coal mining: comparing biological conditions using family- and genus level macroinvertebrate bioassessment tools. *J. N. Am. Benthol. Soc.* 27: 717-737.

Pond GJ, Passmore ME, Pointon ND, Felbinger JK, Walker CA, Krock KJ, Fulton JB, Nash WL (2014) Long-term impacts on macroinvertebrates downstream of reclaimed mountaintop mining valley fills in Central Appalachia. *Environ. Manage.* 54: 919-933.

R Core Team (2013) R: A language and environment for statistical computing. R Foundation for Statistical Computing, Vienna, Austria. URL http://www.R-project.org/

Rhoades JD (1982) Soluble salts. In: Methods of Soil Analysis, Part 2: Chemical and Microbiological Properties - Agronomy Mono. No. 9. ASA-SSSA, Madison, WI, USA.

Ross LC (2015) Effect of Leaching Scale on Prediction of Total Dissolved Solids Release from Coal Mine Spoils and Refuse. M.S. Thesis, Virginia Tech.

Sena K, Barton C, Angel P, Agouridis C, Warner R (2014) Influence of spoil type on chemistry and hydrology of interflow on a surface coal mine in the eastern US coalfield. *Water Air Soil Pollut.* 225: 2171.

Skousen JG, Sexstone A, Ziemkiewicz PF (2000) Acid mine drainage control and treatment. In : Barnhisel, R.I. et al. (Eds.), Reclamation of Drastically Disturbed Lands. Agronomy Monographs. #41. ASA, CSSA, and SSSA, Madison, WI, p. 131-168.

Sobek AA, Schuller WA, Freeman JR, Smith RM (1978) Field and laboratory methods applicable to overburden and minesoils, EPA 600/2-78-054, 203p.

Steele MK, Aitkenhead-Peterson JA (2011) Long-term sodium and chloride surface water exports from the Dallas/Fort Worth region. *Sci. Total Environ.* 409: 3021-3032.

Timpano AJ, Schoenholtz SH, Zipper CE, Soucek DJ (2010) Isolating effects of total dissolved solids on aquatic life in central Appalachian coalfield streams. In: Proceedings, National Meeting of the American Society of Mining and Reclamation, p. 1284-1302.

Timpano AJ, Shoenholtz SH, Soucek DJ, Zipper CE (2015) Salinity as a limiting factor for biological condition in mining-influenced Central Appalachian headwater streams. *J. Am. Water Resour. As.* 51: 240-250.

Williams WD (2001) Anthropogenic salinisation of inland waters. *Hydrobiologia* 466: 329-337.

CHAPTER V: Appalachian Coal Mine Spoil Elemental Release Patterns and Depletion

Elyse V. Clark, Carl E. Zipper, W. Lee Daniels, Zenah W. Orndorff, and Matthew J. Keefe

ABSTRACT

Elevated total dissolved solids (TDS) in Appalachian coal mining-influenced streams result from the interactions of oxygen and rainwaters with fractured mine rocks. Common minerals occurring in the sedimentary coal-bearing strata include silicates (quartz, feldspars, muscovite, chlorite and others), sulfides (pyrite), and carbonates (calcite, siderite); the weathering of these minerals releases soluble ions to streams. In this study, we determined mine spoil bulk composition and elemental depletion via column leaching, applied models to determine leaching patterns, compared model results among individual elements, and interpreted results to infer geochemical drivers of soluble element release from mine spoils. Temporal release patterns of 15 elements from 26 mine spoils were determined via column leaching. Two five-parameter segmented models, one an exponential decay function combined with linear function and the second a growth function combined with a linear function, were applied to the elemental leaching patterns. Of the elements analyzed, Al (60,711 mg kg^{-1}) and K (19,157 mg kg^{-1}) had the largest concentrations on average in the bulk spoil samples. Leaching patterns for major elements (Ca, Mg, S, Ca, Na, K) differed from elements commonly found in mine water discharges (Al, Mn) and from trace elements (As, Cu, Ni, Se). Major elements tended to require more leaches to decay and transition to a stabilized state relative to mine water and trace elements. Leaching patterns for three of the tested elements (Fe, Cd and Pb) were not modeled successfully. Sulfur, Ca and Se were most depleted during the leaching period. Overall, results indicated that certain ions (Ca, Mg and HCO_3) were

released to counter-balance the acid-production of S oxidation, whereas other elements, such as those released by feldspar hydrolysis (K, Na) were less associated with S oxidation but still contributed to overall TDS release from the mine spoils.

5.1 INTRODUCTION

The release of total dissolved solids (TDS) to streams by areas mined for coal in Appalachia has been the focus of many studies in recent times (e.g. Evans et al. 2014; Sena et al. 2014; Cook et al. 2015; Timpano et al. 2015). Predominant components of TDS in Appalachian streams influenced by coal mining are generally SO_4^{2-}, Ca^{2+}, Mg^{2+}, and HCO_3^-, but other trace elements also occur in mining-influenced streams (Pond et al. 2008; Lindberg et al. 2011). Appalachian surface coal mining entails fracturing and removing rock strata overlying coal seams; those rocks (termed mine spoils) are used after coal extraction to reconstruct landforms and the land surface, which exposes mine spoils to rapid geochemical weathering. Movement of infiltrated waters through the materials causes release of soluble elements to streams (Agouridis et al. 2012; Griffith et al. 2012).

The release of soluble elements from mine spoils affects freshwater streams, as altered aquatic macroinvertebrate community structure and aquatic taxa losses are commonly found in waters with elevated specific conductances (SC, measured as a proxy for TDS) (Pond et al. 2008; Cormier et al. 2013; Timpano et al. 2015). Waters with SCs > 300 µS cm^{-1} have been associated with the extirpation of 5% of aquatic genera in Appalachian streams (Cormier et al. 2013) and waters with SCs ≥ 500 µS cm^{-1} have been associated with altered assemblages of aquatic organisms and losses of taxonomic groups (Pond et al. 2008, 2014). In Appalachia's unmined reference streams, SC is

typically < 200 µS cm^{-1} and often < 100 µS cm^{-1} (Pond et al. 2008, 2014; Timpano et al. 2015).

Prior research has demonstrated patterns of SC and major ion release from Appalachian mine spoils in both laboratory and field experimental settings (Sena et al. 2014; Orndorff et al. 2015; Daniels et al. 2016; Clark et al. 2017). In a study of 15 mine spoils placed in leaching columns intended to simulate field leaching conditions, Orndorff et al. (2015) showed that S, Ca, Mg, K and Na concentrations in leachates tended to decline over the leaching period, whereas the HCO_3^- ion concentrations tended to increase during early phases of leaching and then stabilized as leaching continued. Sena et al. (2014) demonstrated declines of electrical conductivity and S in waters leached from field lysimeters on a Kentucky coal mine over a period of nine years.

Although general patterns of major element release from Appalachian mine spoils have been documented, quantitative analyses of leaching patterns have not been performed. Furthermore, general release patterns of trace elements have not been documented nor quantitatively analyzed. Trace elements of ecotoxicological concern released from mine spoils and potentially found in mining-influenced waters at elevated concentrations include As, Cd, Cu, Ni, Pb, Se and Zn (Bryant et al. 2002; Hartman et al. 2005; Pond et al. 2008). Quantitative models of elemental release patterns can improve understanding of the leaching behaviors of individual elements. By enabling comparisons of individual element release patterns, quantitative elemental release models can also improve the understanding of mine spoil weathering processes and geochemical drivers of elemental release.

The geochemistry of mining-influenced waters is ultimately influenced by the mine rock mineralogy, the weathering reactions that result in elemental leaching, and the pre-mining weathering extent of the mine rocks. Typical central Appalachian mine rocks are sedimentary in origin and include Pennsylvanian-aged sandstones, siltstones, mudstones, and shales (Daniels et al. 2016). Prior studies have indicated that silicate minerals such as quartz (SiO_2), feldspars ($(Na,Ca)AlSi_3O_8$; $KAlSi_3O_8$), micas ($KAl_2(AlSi_3O_8)(OH)_2$-muscovite) and other clays, sulfide minerals such as pyrite (FeS_2), carbonate minerals such as calcite ($CaCO_3$) and siderite ($FeCO_3$), and other oxyhydroxides such as goethite (FeO(OH)) commonly occur in central Appalachian mine rocks (Cravotta 2008; Blowes et al. 2014; Johnson 2016). The weathering of these minerals directly influences mine spoil elemental leaching patterns and, by extension, the chemistry of waters discharged from mine spoils.

The objectives of this study were to: (1) determine the bulk chemical composition of central Appalachian mine spoils of varying rock types and weathering extents; (2) examine individual mine spoil elemental release patterns via leaching in laboratory columns, and model and compare those patterns; (3) determine the degree of elemental depletion after leaching, and (4) infer the geochemical factors influencing elemental release from mine spoils. Overall, results were intended to improve the understanding of essential processes influencing the release of chemical constituents from Appalachian mine spoils.

5.2 MATERIALS AND METHODS

Twenty-six spoil samples were collected from active surface coal mines in Virginia, West Virginia, and Kentucky (Figure 5.1). Spoil samples were collected from

identifiable rock strata that had been freshly fractured and included samples collected from multiple strata and of different weathering extents. West Virginia samples (n = 11) sourced from the Kanawha and Allegheny Formations, Kentucky samples (n = 10) sourced from the Princess and Four Corners Formations, and Virginia samples (n = 5) sourced from the Norton, Four Corners, and Middle and Lower Wise Formations (Daniels et al. 2016). These 26 samples were selected from the larger dataset described by Daniels et al. (2016) because of the availability of complete datasets for all 15 elements of focus in this study.

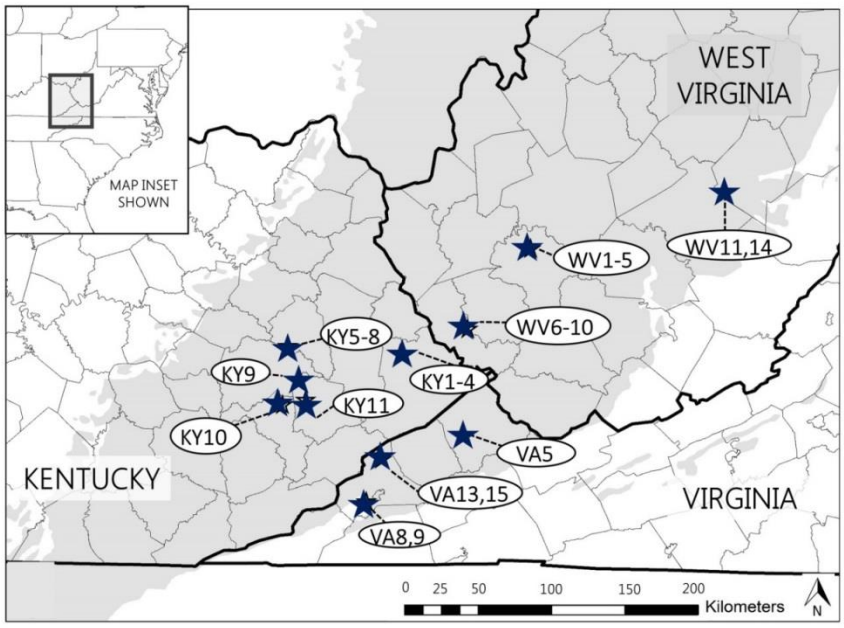

Figure 5.1 Location map of the 26 collected mine spoils. The Appalachian coalfields are indicated by gray coloration.

Initial characterization of the mine spoil samples included spoil classification by rock type. Rock types included mudstones (n = 7), mixed rocks (n = 6), and sandstones (n = 13). The term "mixed rocks" describes a spoil that had ≤ 80 % of a single rock type (mudstone or sandstone). Samples were also classified by the following weathering extents: unweathered (n = 17), mixed weathering (n = 6) and weathered (n = 3);

weathering status was inferred from initial physical and chemical properties such as Fe-oxide coatings, pH and EC.

5.2.1 Mine Spoil Bulk Chemical Composition

Prior to bulk chemical analysis, all spoil samples were ground to a fine powder with a mortar and pestle and homogenized. The elements Al, Ca, Fe, K, Mg, and Na were analyzed using a PANalytical Axios Advanced X-Ray Fluorescence (XRF) spectrometer. Total S was determined via dry combustion and a LECO S-analyzer. The elements As, Cd, Cu, Mn, Ni, Pb, and Se were analyzed using microwave-assisted acid digestion with concentrated HNO_3 and HCl as detailed in EPA Method 3051a and an Agilent 720 ICP-OES. Spoil bulk chemical compositions are reported as mg kg^{-1} spoil.

Assuming that finer materials in the leaching columns (described in Section 5.2.2) were responsible for the reactions driving ion release, sieve analysis was used to determine the weight of fine particles (< 0.25 mm) packed into the leaching columns. The typical weight of fine materials in the columns ranged from 46-510 g and averaged 213 g, indicating the proportion of finer materials in the packed columns ranged from 2.5 - 24.2 % and averaged 11.4 % of the total mass. The mass of the finer materials in the columns (kg) was multiplied by the bulk chemical composition of the mine spoils (mg kg^{-1}) to determine the mass (mg) of each element in the finer materials within each column.

5.2.2 Leaching Experiment

After sieving as described above, the rock fragments for the 26 mine spoils were ground to < 1.25 cm, then re-blended with finer materials. Each spoil sample was measured to 1,200 cm^3 and packed into a 40 cm tall PVC leaching column with a 7.4 cm inner diameter. An endcap with a 60 mm drill hole was placed on the bottom of the

leaching column, to allow for leachate drainage into Nalgene sample bottles via a Tygon tube. Further details about the column packing process are described in Orndorff et al. (2015).

The application of a pH 4.6 solution to each leaching column initiated the column leaching experiment. The solution is commonly used in leaching studies as it resembles regional rainfall pH values more closely than deionized water (Halvorson and Gentry 1990). The solution was slowly applied until the maximum unsaturated water holding capacity was reached. As leachate started draining from the columns, more water was applied until 125 mL of eluted leachate had drained; this water sample was considered Leach 0. Subsequent leaching consisted of a bi-weekly dosing of the columns with 125 mL of solution using a perforated cup and collecting the leachate. The column experiment lasted for a total of 20 weeks or 40 leaches. The collected leachates for each leach were analyzed immediately or appropriately preserved. Spoil samples were run in triplicates, i.e. three leaching columns per sample, and results presented are averages of the triplicates.

Leaches 0-4 were analyzed for all mine spoil samples, and every 4^{th} leach on average after Leach 4 was analyzed for a minimum of 11 leaches and mean of 14 leaches per sample. pH was determined for each leachate sample. Leachate concentrations of S were determined using EPA Method SW 846 6010B and a Spectro ARCOS ICP-ES Model FHS16. Most S was likely in the oxidized form SO_4^{2-}, but concentrations reported here are S. A Shimadzu TOC analyzer was used to determine inorganic carbon, which was converted to HCO_3^- assuming all inorganic carbon was in the bicarbonate form. The As, Al, Ca, Cd, Cu, Fe, K, Mg, Mn, Na, Ni, Pb, and Se concentrations were determined

using a Thermo Electron Corporation ICP-MS X-Series and EPA Method SW 846 6020A. For the purposes of data interpretation, results henceforth are categorized into three classifications: (1) major elements, including Ca, Mg, S, K, Na, and the HCO_3^- ion, (2) elements that are often problematic in coal mine water releases (Al, Fe, and Mn; Rose and Cravotta 1998), which we collectively term mine water elements, and (3) trace elements, including As, Cd, Cu, Ni, Pb, and Se.

5.2.3 Leachate Modeling

A previous study on the 39 samples that include the 26 samples analyzed here developed a model of SC leaching from the column leaching data (Clark et al. 2017), and a similar modeling approach was used in this study.

Nonlinear Segmented Exponential Decay and Linear Function Model

As Clark et al. (2017) showed, mine spoil leaching patterns conform to a nonlinear segmented regression model comprised of an exponential decay function combined with a linear function as follows:

$$f(X_i,\theta) = \begin{cases} \theta_2 e^{-\theta_3 x_i} + \theta_1 & , \quad x_i < BP \\ (\theta_2 e^{-\theta_3 BP} - \beta_1 BP + \theta_1) + \beta_1 x_i & , \quad x_i \geq BP, \end{cases} \qquad [5.1]$$

where the leaching model has five parameters (Figure 5.2a). The θ_2 parameter, also termed the peak, describes the maximum release at Leach 0, θ_3 is the exponential decay constant, the breakpoint (BP) indicates the leach at which the decay function changes to linear, β_1 is the linear function slope, and θ_1 describes the release conditions associated with the asymptote of the exponential decay segment. When the β_1 values are not significantly different from zero ($p > 0.05$), θ_1 can be interpreted to reflect the leaching

conditions at the end of the leaching period. Clark et al. (2017) validated the model using SC values; here we extend the model to examine the leaching patterns of other elements.

Before modeling, leachate concentrations (mg L^{-1}) were converted to a mass basis (mg), then these values were modeled using Eq. 5.1 and the software R (R Core Team, 2013). Using the model output equation, the mass released for leaches in which data was not measured initially were interpolated. Due to the magnitude of variation between mass releases of the various elements, the data were then transformed to a percent of total value to compare leaching patterns of different elements as follows:

$$Percent\ of\ Total = \left[\frac{mass\ \ of\ element\ leached\ in\ Leach(n)}{total\ mass\ of\ element\ leached}\right] * 100, \qquad [5.2]$$

where the total mass leached of each element was calculated as the sum of mass (mg) leached in all leaches. The mass released in each leach (n = 0,1,2,…,40) was divided by the total mass leached, then multiplied by 100 to transform the data to a percent of total mass leached value.

For model parameter conversion from mass release to a percent of total basis, no transformation was needed for the θ_3 (exponential decay constant) parameter because it is unitless. The break point (BP) also did not need a transformation as the units (Leach) are independent of the mass released. The model parameters θ_2 (peak), β_1 (linear slope), and θ_1 (asymptote) results in mass (mg) were converted to the percent of total and model results presented hereafter are on a percent of total basis (Figure 5.2a).

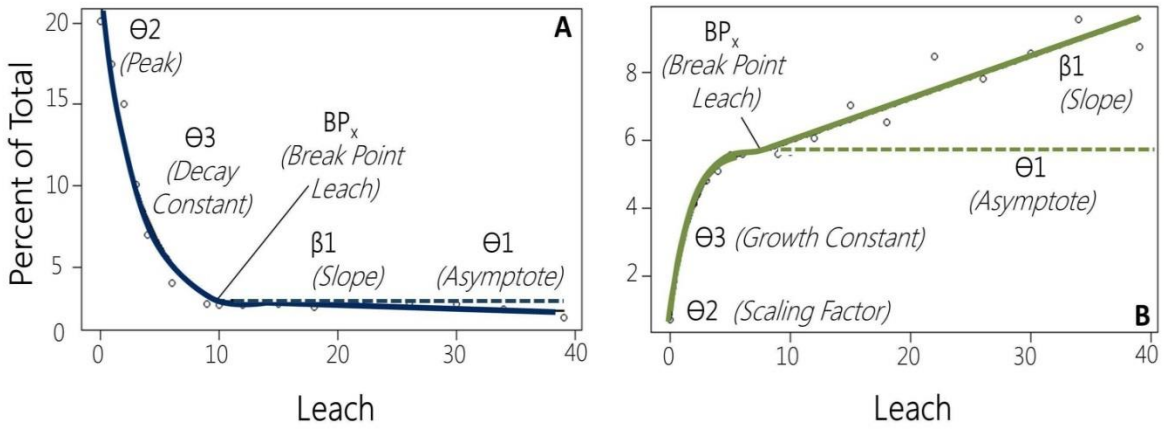

Figure 5.2 Leaching pattern model parameters for all (a) Ca, Mg, S, K, Na, Al, Mn, Cu, Ni, and Se models using Eq. 5.1 and for (b) HCO_3^- using Eq. 5.3. Both (a) and (b) are examples of the S and HCO^{3-} models of sample WV4, respectively.

The elements Ca, Mg, S, K, Na, Al, Fe, Mn, As, Cd, Cu, Ni, Pb, and Se were analyzed for model conformance. If a sample had < 20% of the leaches with data below detection limits (BDL), those BDLs were set to half of the concentration of the detection limit before modeling.

Nonlinear Segmented Growth and Linear Function Model

A second model was developed to describe the leaching patterns of other measured variables that did not conform to Eq. 5.1. Specifically, prior studies observed that the leaching patterns of pH and HCO_3^- appeared to increase rapidly in a nonlinear convex pattern from the first leach, reach a breakpoint, then continued to increase in a linear pattern or stabilized (Orndorff et al. 2015; Daniels et al. 2016). Thus, a five parameter segmented model with a growth function connected to a linear function by a breakpoint was developed as follows:

$$f(X_i,\theta) = \begin{cases} \theta_1(1-\theta_2 e^{\theta_3 x_i}) & , \quad x_i < BP \\ \theta_1(1-\theta_2 e^{\theta_3 BP}) - \beta_1 BP + \beta_1 x_i\,, & x_i \geq BP, \end{cases} \qquad [5.3]$$

where θ_2 is a scaling factor, θ_3 is the growth constant, BP is the leach at which the grown function changes to a linear function, β_1 is the slope of the linear segment, and θ_1 is the horizontal asymptote associated with the nonlinear growth segment (Figure 5.2b); this model is essentially the inverse of Eq. 5.1. Both pH and HCO_3^- were modeled with Eq. 5.3, and the HCO_3^- results are presented as percent of total release for conformance with the results from those elements modeled using Eq. 5.1. Where data were adequate for analysis, the regression parameters of both Eq. 5.1 and 5.3 were estimated using nonlinear least squares (Bates and Watts 1998) for individual elements and spoil samples.

5.2.4 Depletion Analysis

Calculating elemental depletion from the spoil samples via leaching can assist with understanding the relative amount of reactive materials that have been leached from the spoil materials or conversely, the relative amount of reactive materials that remain in the spoil materials after leaching. Both the bulk chemical composition and column leaching analyses were used to determine the depletion of individual elements as a result of the leaching process. The depletion or mass loss of the spoil sample during the leaching process was calculated using the following equation:

$$Depletion\ (\%) = \left(\frac{Total\ mass\ \ of\ element\ released\ via\ leaching\ (mg)}{Mass\ of\ element\ in\ the\ fine\ materials\ (mg)}\right) * 100, \qquad [5.4]$$

and the depletion percent was calculated for each element analyzed. The total mass released via leaching was calculated as the sum of the mass leached (mg) in all 40 leaching events for each element. The calculation of the mass in the finer materials (mg) is described in Section 5.2.1.

5.2.5 Statistical Analyses

For leachate modeling (Eq. 5.1 and 5.3), a β_1 (linear slope) value was considered significant when the slope was significantly different from zero ($p \leq 0.05$). Permutation tests determined significant differences between model parameter values of all elements as well as differences in percent depletion of all elements. Permutation tests are non-parametric tests with no distributional assumptions that permute (randomize) and resample observed data (Bonnini et al. 2014) to derive a test statistic and p-value under the null hypothesis that the elements analyzed have the same distribution.
Principal component analysis (PCA) is a multivariate statistical technique that reduces a data set down to a few components (i.e. principal components), allowing for the interpretation of the parameters that are influential on the whole data set with minimal loss of the original relationships between variables (Iscen et al. 2008). Using the software JMP (v. 11.0, SAS Institute), the elemental leaching patterns based on all five model parameters were analyzed using PCA in order to determine similarities of individual elements' leaching patterns.

5.3 RESULTS

5.3.1 Mine Spoil Bulk and Fine Fraction Composition

Of the measured elements, Al, Fe and K dominated the bulk mine spoil chemical composition (Table 5.1). The bulk K content (19,157 mg kg^{-1}) was one order of magnitude greater than all other major elements, Ca and Na had similar bulk compositions, and S had the lowest composition of all major elements.

Table 5.1 Bulk mine spoil composition (mg kg^{-1}; mean ± se), fine fraction mass (<0.25mm; mean ± se), peak leachate concentration (mg L^{-1}; mean ± se), asymptote leachate concentration (mg L^{-1}, mean ± se), and linear slope (mg L^{-1} $Leach^{-1}$, mean ± se) for each element.

Element Classification	Mine Spoil *(mg kg^{-1})*[*]	Mass Fines (*mg*)	θ_2-Peak *(mg L^{-1})*	θ_1- Asymptote (*mg L^{-1})*	β_1- Linear Slope *(mg L^{-1} $Leach^{-1}$)*
Major					
Ca	2,314±440	490±92	113±22	21.1±3.0	-0.34±0.13
Mg	5,233±617	1,087±80	80±16	14.6±2.1	-0.04±0.06
S	785±170	174±41	237±58	22.9±4.5	-0.50±0.16
HCO_3^-	--	--	8±2[†]	82.0±12.7	1.10±0.48
K	19,157±1,104	4,378±256	20±2	6.9±0.9	-0.13±0.02
Na	2,310±340	528±77	13±2	1.1±0.2	-0.04±0.01
Mine Water					
Al	60,711±4,274	13,719±927	4.2±0.8	0.04±0.01	-0.00031±0.00061
Fe	28,883±3,252	6,009±433	2.8±1.6[†]	0.13±0.05[†]	--[§]
Mn	526±81	115±23	7.9±4.1	0.46±0.19	-0.029±0.014
Trace					
As	5.24±0.64	1.16±0.14	0.0038±0.00036	0.00014±0.000018	-0.0000081±0.0000021
Cd	0.75±0.09	0.15±0.018	0.00215±0.00063[†]	BDL[‡]	--
Cu	14.88±1.99	3.08±0.32	0.095±0.022	0.00076±0.00017	-0.000051±0.000015
Ni	18.92±1.78	4.15±0.34	0.38±0.16	0.0076±0.0034	-0.00062±0.00028
Pb	10.97±0.93	2.41±0.19	0.017±0.004[†]	BDL[‡]	--
Se	2.57±0.10	0.64±0.08	0.17±0.06	0.0051±0.0019	-0.00023±0.000097

[*] Major elements and Al were measured with XRF; trace elements and Mn were measured with ICP-OES.

[†] Value calculated as the mean eluted concentration (mg L^{-1}) at Leach 0 for θ_2 of HCO_3^-, Fe, Cd, and Pb, and at Leach 39 for θ_1 of Fe.

[‡] BDL= Below Detection Limit; Detection Limits - Cd: 0.1 µg L^{-1}, Pb: 0.5 µg L^{-1}

[§] Linear slopes were not calculated for Fe, Cd and Pb.

On average, the mass of the fine materials placed into the leaching columns was 213 g, and fine materials comprised 11.4 % of the total spoil mass. The fine fraction mass (mg) of the elements in the mine spoils had similar relative compositions to the bulk mine spoil, with Al having the greatest and Cd having the least mass in the fine fraction.

5.3.2 Leachate Modeling Analysis

pH

All pH leaching patterns conformed to the segmented growth and linear function model in Eq. 5.3. The initial pH at Leach 0 for all samples ranged from 4.11 to 7.94 (median 4.6). After the initial leaches, the pH exhibited a growth pattern until a breakpoint (BP) at Leach 8 on average (Figure 5.3). Following the BP, the pH remained linear with an average slope of 0.0054 SU Leach^{-1}. For linear slopes (β_1), 54 % of the samples continued to have a significantly increasing pH through the end of the leaching period, 31 % had linear slopes not significantly different from zero, and 15 % had significantly decreasing linear slopes. Three of the four samples exhibiting decreasing slopes were collected from a single mine site in Kentucky. The pH associated with the growth segment's asymptote (θ_1; Figure 5.2b) ranged from 6.39 to 8.97 (median 8.0).

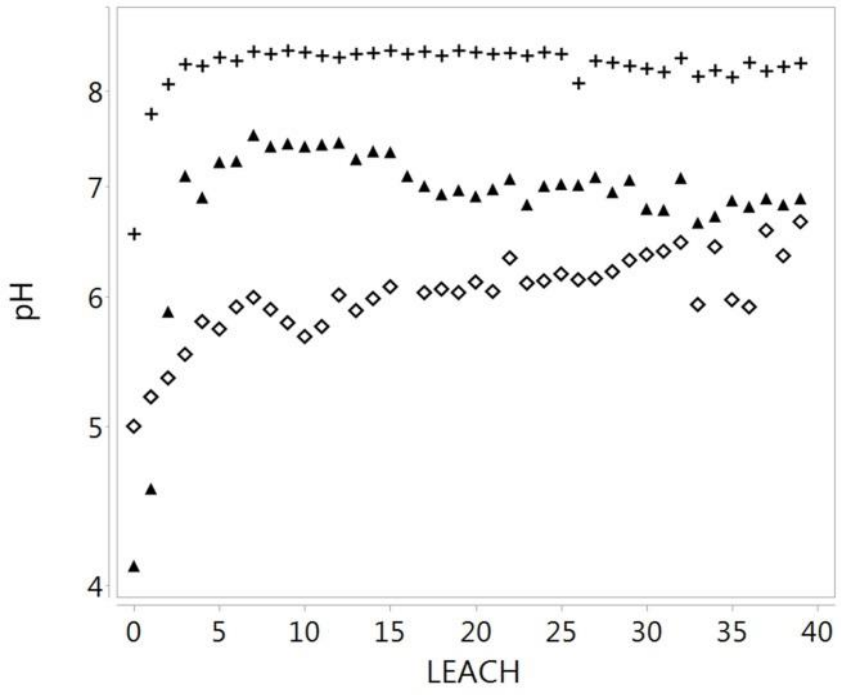

Figure 5.3 Representative pH leaching profiles showing one significantly increasing linear slope (◊, sample KY6), one significantly decreasing slope (▲; sample KY1), and one linear slope that is not significantly different from zero (+; KY2).

Major Elements: Ca, Mg, S, K, Na

All major elements conformed to the nonlinear regression model in Eq. 5.1 for all samples. Estimated peak (θ_2) parameter values were largest for Na (17.1 %) and smallest for K (6.1 %; Figure 5.4a, Figure 5.5). Potassium had the largest estimated exponential decay constant (θ_3) on average and S had the smallest; all elements transitioned from exponential decay to linear release at a BP between Leach 10 and 12 on average. All major elements had nominally negative slopes on average during the linear phase of leaching. However, a majority of the linear slopes (ranging from 54 % for K to 96 % for As and Se), although nominally negative, were not significantly different from zero. We termed linear slopes not statistically different from zero as "stabilized" in subsequent text. Sulfur had the most samples of all major elements that stabilized (85 %). Stabilized

linear slopes had similar leaching patterns as the exponential decay segment's asymptote (θ_1), thus θ_1 could be interpreted as an indicator of elemental release at the end of the leaching period. Estimated θ_1 parameter values were largest for K (2.2 %) and smallest for S (1.3 %) on average.

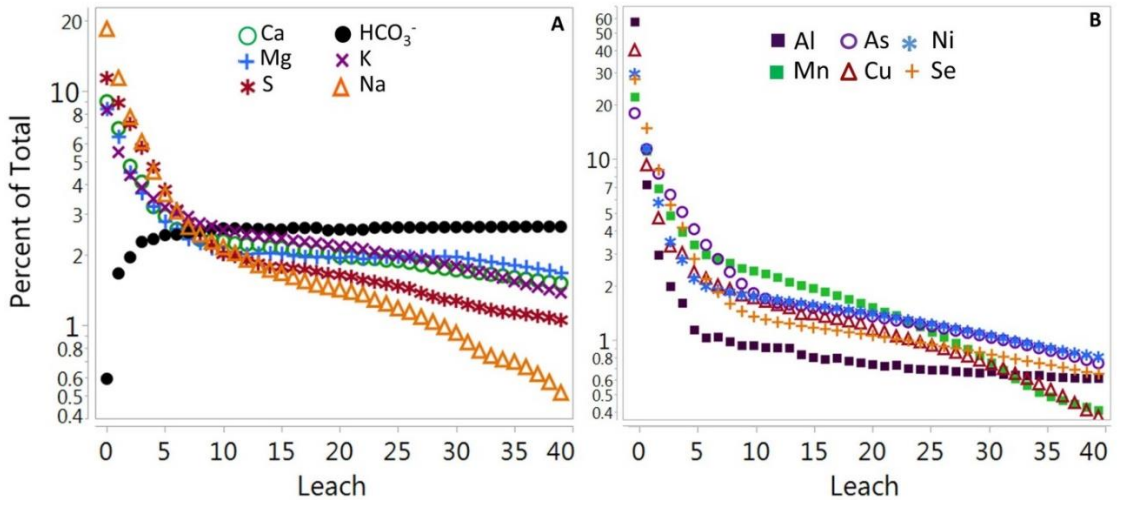

Figure 5.4 Median percentages of total mass release profiles for (a) the major elements Ca, Mg, S, K, Na, and the HCO_3^- ion, and (b) the mine water and trace elements Al, Mn, As, Cu, Ni and Se for each leach. Note the semi-log plot and difference in y-axis scales for percent of total release. Median leaching profiles were calculated as the median value for each leach across all 26 samples.

Considering actual leachate concentrations (mg L^{-1}) measured during the leaching experiment (Table 5.1), peak (θ_2) concentrations were largest for S (237 mg L^{-1}) and smallest for K (13 mg L^{-1}). The linear slopes stabilized for most samples with mean θ_1 values highest for S and smallest for K.

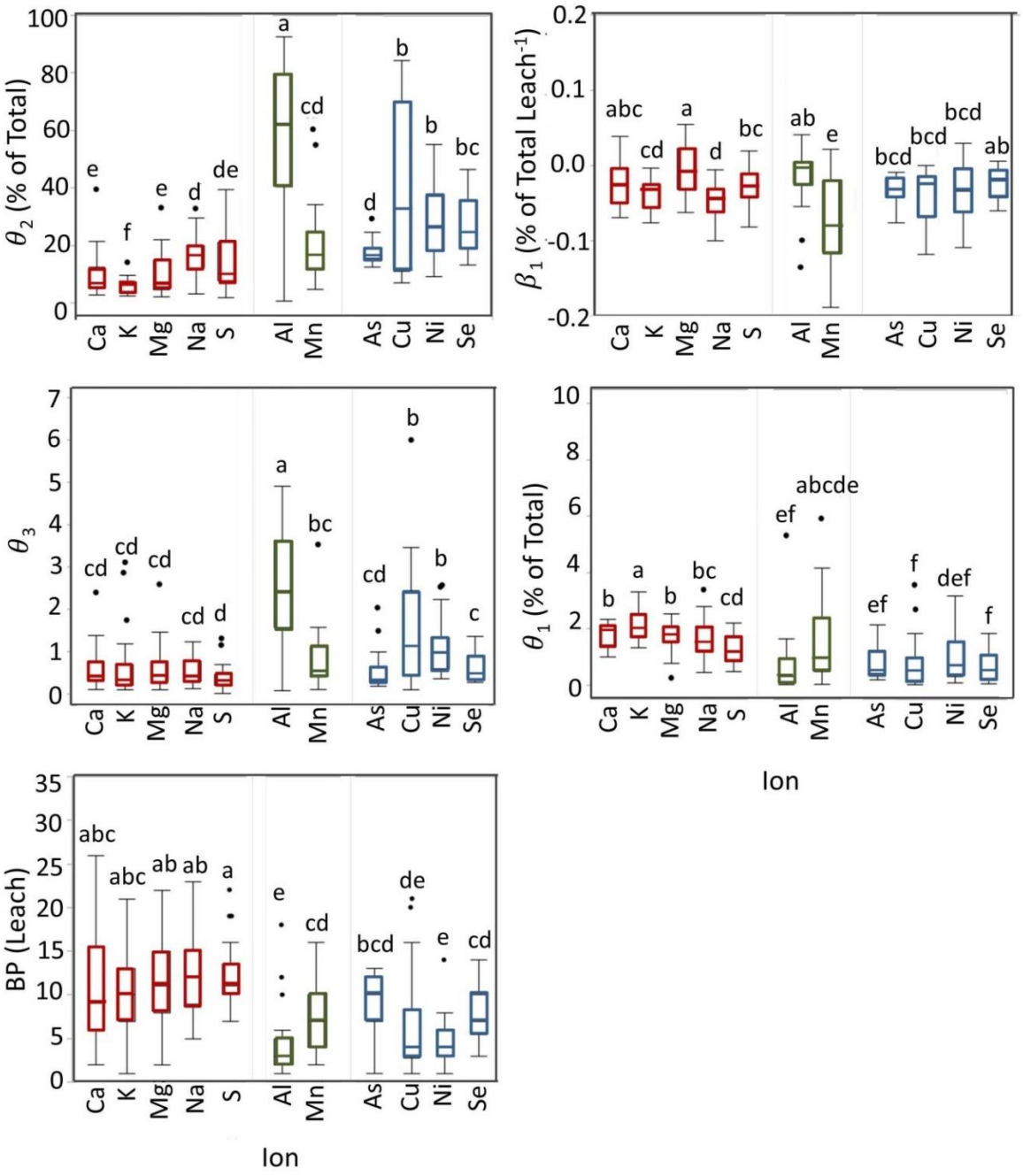

Figure 5.5 Boxplots of estimated model parameters ($\theta_2, \theta_3, BP, \beta_1, \theta_1$) for all elements illustrating the range of parameter values. The model parameters are defined as follows (Eq. 5.1):θ_2- peak, θ_3- exponential decay constant, BP-break point, β_1-linear slope, θ_1 – asymptote. The minimum, 25th percentile, median, 75th percentile, and maximum values are represented by wide bars. Data points indicate outlying parameter values. For each model parameter, elements connected by similar letters are not significantly different ($p>0.05$). Note that HCO_3^- is not included in statistical comparisons due to the use of a different model (Eq. 5.3).

Major Ion: HCO_3^-

The HCO_3^- conformed to the nonlinear regression model in Eq. 5.3 for 21of the 26 samples. For the samples which did not conform to the model, HCO_3^- leaching patterns tended to increase in concentration rapidly in the first three leaches, decrease rapidly for two to three leaches, then vary in concentration through the end of the leaching period as shown by the representative samples in Figure 5.6a.

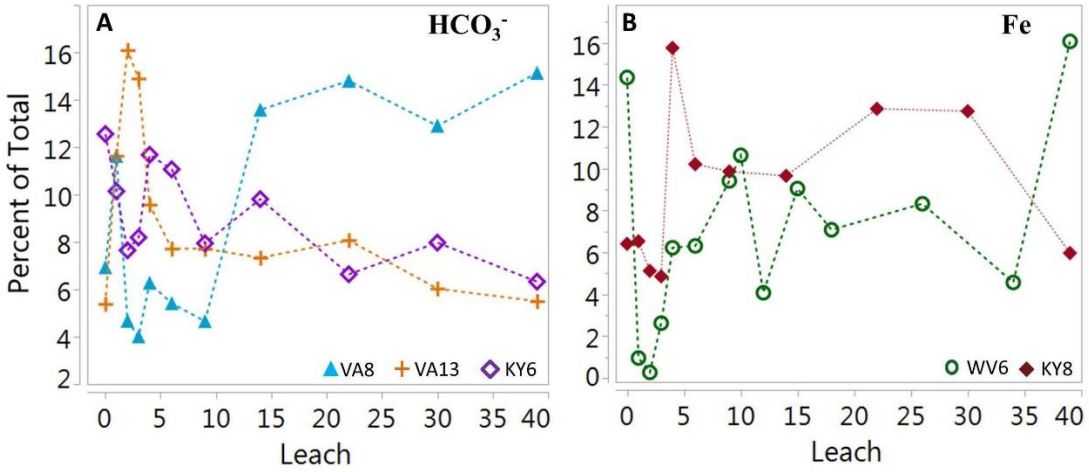

Figure 5.6 Percentage of total mass release profiles for (a) HCO_3^- leaching illustrating a lack of conformance to the nonlinear model of Eq. 5.3 for three samples which are representative of the five samples that could not be modeled; and (b) Fe leaching illustrating the lack of conformance to Eq 5.1 or Eq.5.3 for the WV6 and KY8 samples, which are representative of general Fe leaching patterns.

For the modeled samples, the mean percent of total mass leached at the beginning of the leaching period (θ_2) was 0.53 % (Figure 5.4a). Release of HCO_3^- experienced growth until Leach 10 on average, then transitioned to linear release. Approximately 40 % of samples had significantly increasing β_1 values, whereas 60 % significantly decreased or remained constant. The estimated asymptote (θ_1) parameter was 3.52 % on average.

Considering actual leachate concentrations (mg L^{-1}) measured during the leaching experiment, the mean initial HCO_3^- concentration was 8 mg L^{-1}, whereas the mean θ_1 concentration was 82 mg L^{-1} (Table 5.1). In the linear phase of leaching, HCO_3^- concentration increased at a rate of 1.10 mg L^{-1} per leach on average.

Mine Water and Trace Elements: Al, Fe, Mn, As, Cd, Cu, Ni, Pb Se

Iron leaching patterns did not conform to either model utilized in this study, as the patterns tended to either increase rapidly initially, decrease rapidly initially, release similar concentrations throughout the leaching period, etc. depending on the sample (Figure 5.6b). The average Fe leachate concentration was 2.8 mg L^{-1} at the beginning of leaching (i.e. mean concentration at Leach 0 for all samples) and 0.14 mg L^{-1} at the end of the leaching period (i.e. mean concentration at Leach 39 for all samples). Since Fe leaching patterns did not conform to either Eq. 5.1 or Eq. 5.3, subsequent text omits discussion of Fe leaching patterns due to lack of model conformance.

Cadmium and Pb appeared to conform to Eq. 5.1 (Figure 5.2a), but were not modeled due to a majority of leachate data BDL. For Cd, five samples were BDL (< 0.1 µg L^{-1}) in Leach 0, but by Leach 4, 58 % of the samples were BDL. Similarly for Pb, only three samples were BDL (< 0.5 µg L^{-1}) in Leach 0, but by Leach 4, 65 % of the samples were BDL for Pb. Thus, both Cd and Pb are excluded from the text henceforth due to lack of model conformance.

Aluminum had the highest percentage of total mass release of all elements at the peak (θ_2) with an average of 56.7 % (Figure 5.4b). Furthermore, Al also had the largest decay constant, earliest BP, and second smallest asymptote of all elements modeled (Figure 5.5). The estimated peak (θ_2) parameter values for the other mine water and trace

elements were largest for Cu (39.2 %) and smallest for As (17.2 %). Associated with the large θ_2 values (relative to major elements) were larger decay constants and earlier breakpoints (Leach 5-9 on average). Although mean linear slopes were nominally negative, As, Cu, Ni and Se had > 85 % samples with stabilized β_1 values, corresponding to mean $\theta_1$values ranging from 0.71 % (As) to1.53 % (Mn).

The actual leachate concentrations (mg L^{-1}) associated with the θ_2 were 3.7 and 5.3 mg L^{-1} for Al and Mn, respectively (Table 5.1). For the model-conforming trace elements, θ_2 was largest for Se (141 µg L^{-1}) and smallest for As (3.1 µg L^{-1}) on average. Due to stabilized β_1 values, the mean θ_1 values associated with the end of the leaching period were largest for Ni (5.15 µg L^{-1}) and smallest for Al (0.08 µg L^{-1}).

Statistical Analysis of Leaching Model Parameters

For individual element statistical comparisons, Al had a significantly higher peak values, as well as significantly larger exponential decay constants than all other elements (Figure 5.5). Potassium had a significantly smaller percentage of total mass release (6.1 %) at the peak relative to all other elements. Lastly, Mn had significantly more negative linear slopes (β_1) on average than all other elements, indicating that Mn mass release continued to decline for ~ 40 % of the samples through the end of the leaching period.

Although the leaching profiles of the major, mine water, and trace elements appear similar, there were key differences in their leaching patterns. Peak release differed among the mine water, trace, and major elements as all had significantly different θ_2 values on average, with the mine water elements having the greatest (37.9 %) and major elements having the least (11.4 %) mean percentage (Table 5.2). Similar statistical relationships occurred for the decay constants (θ_3), as mine water elements decayed

significantly faster than trace and major elements. No significant differences occurred between the break point leach of the mine water and trace elements; however, both had BPs significantly earlier in the leaching cycle relative to major elements. After the breakpoint, the linear slopes of both the major and mine water elements were significantly different from one another, but trace elements were not significantly different than either the major or mine water elements. The asymptote (θ_1) parameter values indicated that major elements were still releasing significantly more relative mass (1.73 % of the total mass released) than both the mine water and trace elements.

Table 5.2 Leaching model results showing estimated parameter values (mean ± se) for elemental classifications.

Element Class.[*]	θ_2 -Peak (%)	θ_3 –Decay Constant	Break Point (Leach)	β_1 – Linear Slope (% Leach^{-1})	θ_1 - Asymptote (%)
Major [†]	11.4±0.7^{c}	0.54±0.05^{c}	11±0^{a}	-0.029±0.003^{a}	1.73±0.05^{a}
Mine Water	37.9±4.0^{a}	1.64±0.21^{a}	6±1^{b}	-0.048±0.005^{b}	1.14±0.19^{b}
Trace	29.4±2.1^{b}	1.00±0.10^{b}	7±0^{b}	-0.032±0.004^{ab}	0.82±0.08^{b}

[*] Major, mine water, and trace element parameter values followed by different letters within a column are significantly different ($p \leq 0.05$). Statistics based off means of all major, mine water, and trace element parameter values, respectively.
[†] HCO_3^- not included in statistical analysis due to the use of a different model (Eq. 3).

A principal component analysis (PCA) of the five model parameters from Eq. 5.1 indicated similarities in modeled leaching patterns of various elements. Principal component 1 (PC1), which explained 64.3 % of the variation in the dataset, had positive loadings of the trace elements and Al, and negative loadings of Mg, Ca, S, Na and K (Figure 5.7), with the model parameters associated with the exponential decay function having the largest influence. Principal component 2 (PC2), which explained 21.0 % of the total variation in the data set and was highly influenced by β_1, had positive loadings of Ca, Mg, S, As, Se and Al, and negative loadings of Na, K, Ni, Cu and Mn.

Overall, the PCA indicated that certain elements were more similar to one another than to others in terms of leaching patterns. All major elements, which had negative

loadings for PC1, plotted near each other in Figure 5.7, but there was still separation into a grouping of Ca, Mg and S, and a second grouping of Na and K. The trace elements, which all had positive loadings for PC1, similarly separated into two groups as follows: the anions As and Se, and the cations Ni and Cu. Lastly, the mine water elements Al and Mn did not appear to have similar leaching patterns to any other elements, nor to each other.

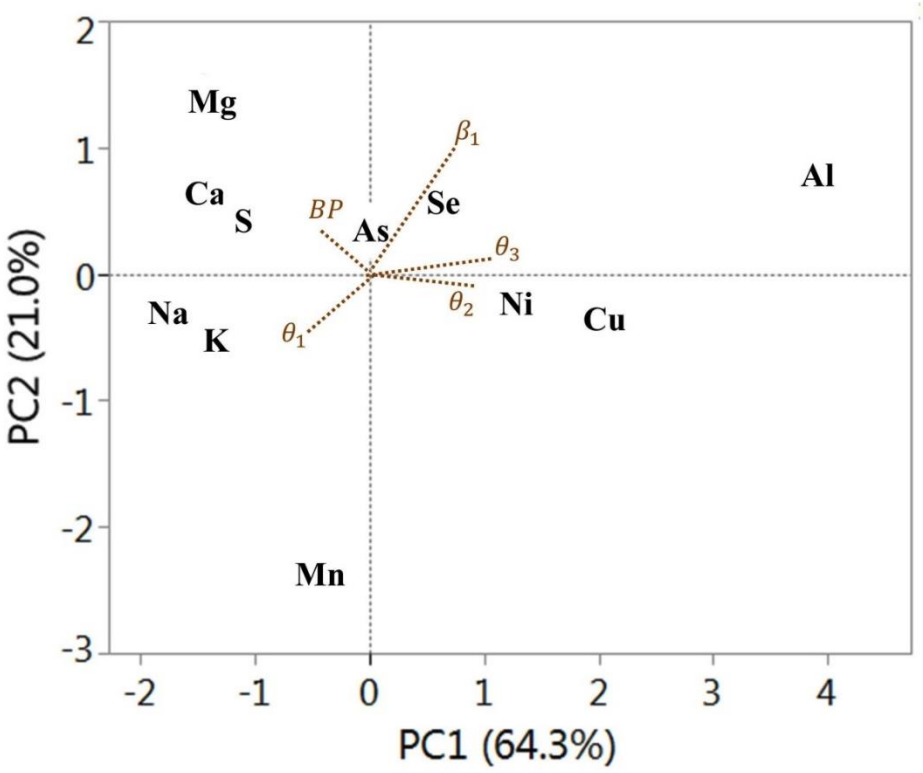

Figure 5.7 Principal Component Analysis biplot illustrating the relative loadings of all elements. Leaching model parameters are show in brown. Principal components 1 and 2 accounted for 64.3 and 21.0% of the dataset's variation, respectively.

5.3.3 Elemental Depletion Analysis

Using the results presented in Table 5.1 and Section 5.3.2, the percent depletion of each element that occurred during the leaching process was calculated using Eq. 5.4. The depletion percent is interpreted as an indicator of the amount of material that has

been leached from the system via weathering reactions, but its inverse can also indicate the amount of potentially-reactive materials remaining in the system.

Median depletion percentages ranged from 0.0063 % (Al) to 109 % (S) for all samples (Table 5.3). More than half of the samples had S depletion percentages > 100 % indicating that S reactions in larger particle sizes may also have significantly contributed to release. The large difference between median and mean percent depletion of S and Se were largely influenced by a single outlying spoil sample, KY4, which was an unweathered mudstone that leached relatively large amounts of S and Se.

Table 5.3 Mean, median, and range of major, mine drainage, and trace element depletion (%).

Element Classification*	Mean % Depletion†	Median % Depletion	Range
Major			
Ca	50.93[b]	29.91	5.19-146.96
Mg	11.89[c]	8.25	0.58-37.30
S	159.03[a]	109.59	28.09-628.61
K	1. 10[f]	1.01	0.13-3.55
Na	2.98[d]	2.08	0.23-11.83
Mine Water			
Al	0.0083[h]	0.0063	0.00088-0.033
Fe‡	0.021[--]	0.0079	0.0007-0.17
Mn	6.65[cde]	1.71	0.094-56.04
Trace			
As	0.42[fgh]	0.38	0.16-1.11
Cu	1.02[fgh]	0.47	0.082-3.71
Ni	4.87[defg]	0.72	0.18-39.97
Se	30.94[bcdef]	6.00	1.04-233.39

* Major elements and Al were measured with XRF; trace elements and Mn were measured with ICP.
† Depletion percentage values followed by different letters are significantly different ($p \leq 0.05$).
‡ Iron depletion percentages were determined by linear interpolation between measured leachate concentrations due to lack of model conformance and thus results were not included in statistical analysis.

After S, Ca and Se had the second and third highest mean depletion percentages. All major elements were characterized by at least 1 % of the original mass being depleted via leaching. For the trace elements, As, Cu and Ni all had median depletion percentages < 1 %. Selenium was the most depleted of the trace elements, with a median depletion of

6 %. Aluminum had the smallest percent depletion of all elements (0.0083 % on average) and was significantly different than all other elements except As and Cu. Although Fe did not conform to the leaching models in this study, depletion was still calculated via linear interpolation between measured data points to infer the relative amount of Fe leached (0.021 % on average).

5.4 DISCUSSION

Overall, the leaching model and depletion analyses indicated clear differences in the release patterns of major, mine water, and trace elements from mine spoils.

5.4.1 Initial Leaching Patterns

In the initial stage of leaching (i.e. Leach 0), it is apparent that all of the elements analyzed except Fe and the ion HCO_3^- had high levels of release as the column leaching experiment was initiated. This initial "flush" of elements from the mine spoils is likely due to decreasing the particle size of the mine spoils before placement into the columns and thus increasing reactive surface area of the particles. When oxygen and water, which drive mineral weathering, come into contact with the freshly-fractured mineral surfaces in the leaching columns, it is likely that rapid weathering ensues and elements leach out, resulting in the leaching patterns modeled above. Although not measured in this study, prior column leaching studies have showed that the initial leachates may also elute colloidal-sized particles that also contribute to the overall flux of elements released initially (Parker 2013).

Since Appalachian mine spoils typically contain trace amounts of reactive pyrite (Diehl et al. 2012), which is the most common form of S in rocks of similar geologic origin (Martino et al. 2014), pyrite oxidation is likely initiated once the oxygen and water

begin to interact with the materials. Pyrite oxidation is a highly acid-forming reaction that results in the release of the products SO_4^{2-}, Fe^{2+}, and H^+ (Singer and Stumm 1970). Evidence for pyrite oxidation occurring in the initial phase of the leaching experiment includes the large concentration of S eluted relative to all other elements and high initial SCs as reported by Clark et al. (2017). Accumulated secondary soluble sulfosalts may also have been present in the materials (Pérez-López et al. 2009) and their dissolution may have contributed to the high initial leaching of S. In addition to pyrite oxidation, it is evident that other geochemical factors influence initial release patterns due to the fact that most other elements also had relatively high releases in the initial leaches. These reactions may be acid-consuming reactions that occur in conjunction with the highly acid-forming pyrite oxidation. Examples of such reactions would include those on fractured silicate mineral edges, carbonate dissolution reactions, and feldspar hydrolysis.

Carbonate minerals ($CaCO_3$; $MgCO_3$, $FeCO_3$) may occur either as individual grains or as cements in the mine spoils (Daniels et al. 2016; Johnson 2016), and the dissolution of these minerals likely result in the release of Ca and Mg in addition to buffering the acid-generation of S oxidation. Prior studies have shown that siderite ($FeCO_3$), which is known to occur in these mine rocks, can naturally form a solid solution with Mg, Ca, and Mn (Morrison et al. 1990; Rose and Cravotta 1998), which may further contribute to the release of these elements during the initial phases of leaching. Siderite, however, would not be expected to contribute to net neutralization reactions (Skousen et al. 1997).

Carbonate mineral dissolution reactions in acid waters will also consume acidity as such in the following calcite dissolution reaction in which HCO_3^- is also formed.

$$CaCO_3 + H^+ = Ca^{2+} + HCO_3^- \quad [5.5]$$

Relatively low concentrations of HCO_3^- were released initially (8 mg L^{-1} on average) from the leaching columns, indicating that some carbonate dissolution was occurring early in the leaching period, but not to the same degree as the kinetically-rapid S oxidation. Sulfide oxidation with direct neutralization by carbonates may also occur (Bethke 2008) as follows:

$$FeS_2 + 2CaCO_3 + 3.75O_2 + 1.5\ H_2O = Fe(OH)_3 + 2SO_4^{2-} + 2Ca^{2+} + 2CO_2 \quad [5.6]$$

which could also explain the presence of higher Ca and S in the initial leachates relative to HCO_3^-.

Plagioclase and potassium feldspars, which are aluminosilicate minerals known to occur in Appalachian mine rocks (Blowes et al. 2014, Johnson 2016), also weather via acid-consuming hydrolysis reactions such as the following simplified reaction:

$$KAlSi_3O_8\ (\text{K-feldspar}) + H^+ + H_2O = K^+ + Al_2Si_2O_5(OH)_4\ (\text{kaolinite}) + H_4SiO_4 \quad [5.7]$$

in which K, Na or Ca is released depending on the type of feldspar weathering. The weathering of other aluminosilicates such as chlorite ($Mg_2Al_2SiO_5(OH)_4$) and muscovite ($KAl_3Si_3O_{10}(OH)_2$) may also contribute to the release of Mg and K during the initial stages of leaching. Prior studies have hypothesized that such reactions are responsible for most Na, K, and Mg release, as well as some of the Ca release during mine spoil weathering (Rose and Cravotta 1998).

Aluminum had the greatest percentage of mass release (57 %) during the initial stages of leaching relative to all other elements. This is likely due, at least in part, to the colloidal-size particles eluted initially from the columns. Such colloids may be comprised of Al-bearing clay minerals or aluminosilicates (e.g. kaolinite, illite, chlorite, muscovite),

hence the relatively high release of Al initially. In addition to colloid elution, some dissolved Al may have been released, as the median pH initially was 4.58 and Al is generally soluble at these pH values. As the pH increased rapidly in the first few leaches, Al likely became less mobile as evidenced by the very low Al release after the initial peak, indicating that most Al was retained within the leaching column materials.

For the trace elements, which released a higher total percentage of mass at the peak (i.e. Leach 0; 29.4 % on average) relative to the major elements (11.4 % on average), the initial releases of these ions are likely attributed to the reactions described above. Prior studies have indicated that pyrite can host other trace elements such as As, Cu, Ni, Pb, Se and Zn (Tuttle et al. 2009), and specifically in the coalfields of Appalachia, As and Se may be enriched in pyrites associated with coal-bearing formations (Yudovich and Ketris 2005, Yudovich and Ketris 2006, Diehl et al. 2012). Furthermore, the As and Se leaching patterns had positive loadings in PC2 (like S), indicating that leaching of these ions may be related to S oxidation. It is important to note, however, that relative to As and S, Se released a higher percentage of total mass at the beginning of the leaching period. Such results may indicate the presence of other forms of Se that may contribute to the overall leaching pattern of Se such as elemental Se^{o} crystals (Yudovich and Ketris 2006) in the materials, lead selenide (PbSe) micro-crystals, which have been reported to occur in Appalachian coal samples (Coleman et al. 1993), inorganic or organic Se forms associated with coal (Yudovich and Ketris 2006), or other sulfide minerals (Dreher and Finkleman 1992).

Both Cu and Ni can substitute into pyrite as mentioned above, indicating that the leaching of these minerals could be associated with S oxidation to an extent. The negative

loading on PC2; however, would indicate a different geochemical influence for Cu and Ni. Prior studies have shown that Cu can substitute for Fe, Ca and Mg into carbonate minerals such as siderite ($FeCO_3$), calcite ($CaCO_3$), and dolomite ($CaMg(CO_3)_2$) (Veizer 1983, Cravotta 2008). Nickel has a similar ionic radius to Fe and Mg and thus can substitute into the common Fe- and Mg- bearing minerals such as goethite and illite (Massoura et al. 2006). Lastly, both Cu and Ni have been found to substitute into the crystal lattice of the silicate mineral chlorite (Suarez et al. 2011). The minerals illite, goethite, chlorite and siderite have previously been identified in Appalachian coal mine rocks (Johnson 2016); thus the release of Cu and Ni may be more influenced by the weathering of these minerals rather than S oxidation.

5.4.2 Exponential Decay Phase

The exponential decay phase of the leaching process required 4-12 leaches on average for all elements. As previously mentioned, pyrite oxidation appears to be the main geochemical driver of the leaching patterns observed in this study, and the exponential decay phase appears to correspond to the declining of the S oxidation rate. Such a decline is likely influenced by both physical and geochemical factors.

Pyrite weathering is initiated on the surface of the mineral grains, specifically in microcracks, micropores, fissures, and around the corners (Ciminelli and Ossei-Asare 1995). As weathering continues, it becomes more difficult for the drivers of pyrite weathering (O_2, H_2O) to penetrate through to the internal mineral grain areas, thus slowing the rate of pyrite oxidation. Similar mechanisms would also be expected for the other minerals weathering in the mine spoils. Thus, after the initial flush of easily-leachable elements from mineral surfaces, reaction rates decline due to a slowing of

elemental release from those surfaces; hence the exponential decay release patterns exhibited by the spoils.

Another factor that slows reaction rates during the exponential decay phase is Fe-oxide deposition on mineral surfaces. Prior studies have shown that as pyrite weathers, the formation of Fe-oxides and Fe-oxyhydroxides can coat mineral surfaces as precipitates that may inhibit further interaction of H_2O and O_2 with the mineral surfaces, resulting in a decrease in the pyrite oxidation rate (Ahonen and Tuovinen 1995; Caldeira et al. 2010). The fact that Fe release patterns were seemingly random and did not conform to either model and that depletion percentages were so low relative to other elements (< 0.025 % on average), indicates high Fe retention in the leaching columns. Hence, it appears that Fe precipitation occurred in the columns, likely as Fe-coatings on minerals, and inhibited further mineral weathering. Such coatings have been observed on the mineral surfaces of sulfides as well as carbonate minerals (Al et al. 2000).

Another effect of Fe-oxide coatings on the mineral surfaces is that it prevents water-oxygen-mineral contact, which may suppress metal solubilization (Ahonen and Tuovinen 1995) and contribute to retention of other elements. Prior studies have shown that at near-neutral pHs such as those in mine tailings containing large amounts of carbonates, trace elements are retained in the solid phase due to adsorption, precipitation and co-precipitation processes of these trace elements with oxyhydroxides, sulfates and insoluble Fe^{3+} (Blowes et al. 1991; Xu et al. 1997; Cravotta and Trahan 1999; Robbins et al. 1999). Specifically, adsorption of the metals Cd, Cu, Ni and Pb was extensive (Blowes et al. 1998), as evidenced by these trace elements occurring in higher concentrations on mineral surfaces rather than the interior of mineral grains (Al et al.

2000). Such adsorption effects may explain the faster decay of the trace elements relative to the major elements.

During the exponential decay phase for the elements with release patterns conforming to the decay model, pH and HCO_3^- were experiencing growth and the pH rapidly increased from 5.16 initially to 7.86 after 8 leaches on average. Thus, as the S oxidation slows via the mechanisms described above, it appears that carbonate dissolution reactions are enhanced, hence the increase in HCO_3^- and pH.

5.4.3 Linear Phase

During the linear phase of leaching, release of all elements (and the HCO_3^- ion) stabilized (i.e. the β_1 slope was not significantly different from zero) for at least 54 % of samples, and release of S, Na, Al, As, Ni and Se stabilized for at least 85 % of the samples. The high stabilization percentage of S and the trace elements associated with pyrite (As, Se), indicates that S oxidation did slow considerably during the exponential decay phase. The S depletion percentage > 100 % on average appears to suggest that pyrite oxidation neared completion; however, it is more likely that larger particle sizes (> 0.25 mm) were also contributing to S release in addition to fines. Thus, the relatively high stabilization rates for all elements suggest that in the linear phase, equilibrium between the weathering rate and depletion/leaching rate was reached.

The elements with relatively lower stabilization percentages (i.e. Ca, Mg, HCO_3^-, Mn) are associated with carbonate minerals (calcite, siderite, ankerite), and therefore their continued dissolution may indicate a shift to carbonate dissolution dominance in the linear phase rather than S oxidation (Daniels et al. 2016). Approximately 25 % of spoil samples had decreasing linear slopes for Ca, Mg, and Mn; however, those same samples

had increasing linear slopes for HCO_3^- and pH. Such results suggest a continuation of acid-consumption and HCO_3^- release independent of the Ca, Mg and Mn release, likely via the carbonate buffering system.

Lastly, 46 % of samples exhibited significantly decreasing β_1 slopes for K. It is apparent that K release in the linear phase differs from the other elements analyzed, which may be due to the fact that K occurs in multiple minerals (K-feldspar, muscovite, clay minerals) in these spoil samples that may continue to weather in the linear phase of leaching.

Overall, since most elements had a majority of samples that stabilized in release through the linear leaching phase, the linear phase may reflect "pseudo-background" weathering rates of the mine spoils. The term "pseudo-background" is used because leachate concentrations, although stabilized, are still elevated above natural background concentrations observed in waters and soils unaffected by surface coal mining (Hartman et al. 2005; Pond et al. 2008).

5.4.4 Implications for Mine Spoil Management

Multiple elements of aquatic ecotoxicological concern were analyzed in this study (Al, As, Cd, Fe, Pb, Ni and Se) and leachate concentrations were transformed from total recoverable concentrations to dissolved concentrations using conversion factors (US EPA 1996) to determine potential ecotoxicological effects of the leachates. An element was considered of ecotoxicological concern if dissolved leachate concentrations were elevated above the acute and/or chronic water quality criteria recommended by the US EPA for protection of aquatic life in freshwater streams (US EPA 2017). The discussion below is based on leaching column results; however, we presume that if mine spoils similar to

those tested in this study were placed into mine spoil fills in the field, similar leaching results would be expected, although no studies have been concluded to date that demonstrate this presumption.

For the mine water elements, leachate concentrations of Fe and Al were 2.8 and 42x larger, respectively, than the chronic toxicity criteria at the peak, with Al concentrations 5x larger than the acute toxicity criterion, but were both below the chronic toxicity criteria at the end of the leaching period. For the trace elements, As leachate concentrations did not exceed ecotoxicological thresholds at any point in the leaching period. Cadmium concentrations exceeded both the acute and chronic criterion at the beginning of the leaching period, then quickly fell below detection and the criteria. Both Ni and Pb were not greater than the acute criteria, but were above the chronic toxicity criteria (52 µg L^{-1} and 2.5 µg L^{-1}, respectively) in the initial leaches. Lastly, the chronic aquatic life criterion for Se is 3.1 µg L^{-1}, thus the peak leachate concentration (140 µg L^{-1} on average) was ~ 45x larger, but neared criterion concentrations by the end of the leaching period. Overall, these results suggest that Cd, Pb, and Ni leachate concentrations are at levels that may impact aquatic life at the beginning of leaching, but not during the later stages of leaching. The Se leachate concentrations are of ecotoxicological concern during all phases of leaching, whereas As was not leached at concentrations greater than ecotoxicological criteria in these mine spoils.

It is well-established that current mining practices lead to the generation and release of TDS to streams (Hartman et al. 2005; Agouridis et al. 2012; Sena et al. 2014); however, it is less known how long TDS release will continue and how release patterns will change over time. Evans et al. (2014) found that 15-25 years were required for SCs

to decline to ≤ 500 μS cm^{-1} on average in VF discharges. Daniels et al. (2016) found that mine spoils leached in laboratory columns for 40 leaches had a general correspondence to field-leaching patterns that had stabilized within nine years on 0.5-1.5 m depth study plots on a Kentucky mine site. Using the same nonlinear regression model and spoil samples as this study, Clark et al. (2017) found that it took 16 leaches, on average, for SC release to stabilize at levels of 250-300 μS cm^{-1} in mine spoils.

In this study, the major elements Ca, Mg, Na, K and S tended to have similar leaching patterns and model forms as the TDS model in Clark et al. (2017), suggesting that as *in situ* mine spoils weather, major element release would be expected to mimic overall TDS release. The mine water element (Al, Fe, Mn) and trace element (As, Cd, Cu, Ni, Pb, Se) release patterns from *in situ* mine spoils would not be expected to mimic overall TDS release due to their more rapid decay and stabilization. These patterns have been observed in a study of 15 central Appalachian valley fill discharge streams, which found that all major elements were still being released at elevated levels 11-33 years after reclamation. In those same streams, dissolved As, Cd, Cu and Pb concentrations were all below detection limits and Fe concentrations were not of aquatic toxicity concern, whereas Al and Se concentrations were still slightly elevated above chronic toxicity criteria (Pond et al. 2014). Such results indicate that observations from these laboratory and modeling results are similar to field observations in mining-influenced streams in the region.

5.5 CONCLUSIONS

The elemental release patterns from central Appalachian mine spoils placed in leaching columns in the laboratory differed by relative abundances in the mine spoils (i.e.

major elements, trace elements), with major element leaching patterns tending to release proportionately less mass in the beginning of the period and stabilize later in the leaching period relative to trace elements. The pH and HCO_3^- ion had inverse release patterns of all other measured variables. Geochemically, the leaching patterns of Ca, Mg, S, HCO_3^-, As and Se were likely most influenced by pyrite oxidation and carbonate dissolution reactions occurring in the leaching columns, whereas Na, K, Ni and Cu were likely influenced by aluminosilicate hydrolysis and other weathering reactions. Iron oxide coatings appear to be the cause of exponential decay of elemental release due to the inhibition of mineral weathering. Most elements stabilized in release near the end of the leaching period, indicating an equilibrium was reached. Levels of stabilization were above background concentrations found in reference streams, and several elements had concentrations above ecotoxicological thresholds for aquatic life impacts. Future studies should relate laboratory leaching patterns to field leaching patterns of individual elements, determine how release of individual elements to stream discharges change over time, as well as utilize geochemical modeling to better understand specific mineralogical sources of elements in leachates.

5.6 ACKNOWLEDGEMENTS

The authors would like to thank Dr. Nicholas Basta and Shane Whitacre at the Ohio State University for laboratory analyses assistance. This project was sponsored by the Appalachian Research Initiative for Environmental Sciences (ARIES), Powell River Project, Virginia Tech Institute for Critical Technology and Applied Sciences, and the USDI Office of Surface Mining. The views and recommendations expressed herein are

solely those of the authors and do not imply endorsement by ARIES employees, other ARIES-affiliated researchers, or industrial members.

5.7 REFERENCES

Agouridis CT, Angel PN, Taylor TJ, Barton CD, Warner RC, Yu X, Wood C (2012) Water quality characteristics of discharge from reforested loose-dumped mine spoil in eastern Kentucky. *J. Environ. Qual*. 41: 454-468.

Ahonen L, Tuovinen OH (1995) Bacterial leaching of complex sulfide ore samples in bench-scale column reactors. *Hydrometallurgy* 37: 1-21.

Al TA, Martin CJ, Blowes DW (2000) Carbonate-mineral/water interactions in sulfide-rich mine tailings. *Geochim. Cosmochim. Acta* 64(23): 3933-3948.

Bates DM, Watts DG (1988) *Nonlinear Regression Analysis and Its Applications.* John Wiley & Sons, New York.

Bethke CM (2008) *Geochemical and Biogeochemical Reaction Modeling* (2nd ed.). New York: Cambridge University Press.

Blowes DW, Jambor JL, Hanton-Fong CJ, Gould WD (1998) Geochemical, mineralogical and microbiological characterization of a sulfide-bearing, carbonate-rich, gold mine tailing impoundment, Joutel, Quebec. *Appl. Geoch.* 13(6): 687-705.

Blowes DW, Ptacek CJ, Jambor JL, Weisener CG, Paktunc D, Gould WD, Johnson DB (2014). The geochemistry of acid mine drainage. Holland HD, Turekian KK (Eds.), Treatise on Geochemistry, 2nd Edition, Elsevier, p 131-190.

Blowes DW, Reardon EJ, Jambor JL, Cherry JA (1991) The formation and potential importance of cemented layers in inactive sulfide mine tailings. *Geochim. Cosmochim. Acta* 55: 965-978.

Bonnini S., Corain, L., Marozzi, M., & Salmaso, L. (2014). *Nonparametric Hypothesis Testing: Rank and Permutation Methods with Applications in R* (1st ed.). Chichester, West Sussex: John Wiley & Sons, Inc.

Bryant G, McPhilliamy S, Childers H (2002) A survey of the water quality of streams in the primary region of mountaintop/valley fill coal mining. Mountaintop Mining/Valley Fills in Appalachia Programmatic Environmental Impact Statement. US Environmental Protection Agency, Philadelphia. EPA 9-03-R-00013.

Caldeira CL, Ciminelli VST, Osseo-Asare K (2010) The role of carbonate ions in pyrite oxidation in aqueous systems. *Geochim. Cosmochim. Acta* 74:1777-1789.

Clark EV, Zipper CE, Daniels WL, Orndorff ZW, Keefe MJ (2017) Modeling patterns of total dissolved solids release from Central Appalachia, USA, mine spoils. *J. Environ. Qual.* 46:55-63.

Ciminelli VST, Osseo-Asare K (1995) Kinetics of pyrite oxidation in sodium carbonate solutions. *Metall. Mater. Trans.* B 26: 209-218.

Coleman L, Bragg LJ, Finkleman RB (1993) Distribution and mode of occurrence of selenium in US coals. *Environ. Geochem. Hlth* 15 (4): 215-227.

Cook NA, Krometis LH, Sarver EA, Huang J (2015) Inorganic constituents of conductivity in five central Appalachian watersheds with mixed source-driven pollutants. *Ecol. Eng.* 82: 175-183

Cormier SM, Suter GW, Zheng L (2013) Derivation of a benchmark for freshwater ionic strength. *Environ. Toxicol. Chem.* 32: 263-271.

Cravotta CA (2008) Dissolved metals and associated constituents in abandoned coal-mine discharges, Pennsylvania, USA. Part 2: Geochemical controls on constituent concentrations. *Appl. Geochem.* 23: 203-226.

Cravotta CA, Trahan MK (1999) Limestone drains to increase pH and remove dissolved metals from acidic mine drainage. *Appl. Geochem.* 14:581-606.

Daniels WL, Zipper CE, Orndorff CW, Skousen JG, Barton CD, McDonald L, Beck M (2016) Predicting total dissolved solids release from central Appalachian coal mine spoils. *Environ Pollut* 216: 371-379.

Diehl SF, Goldhaber MB, Koenig AE, Lowers HA, Ruppert LF (2012) Distribution of arsenic, selenium, and other trace elements in high pyrite coals: Evidence for multiple episodes of pyrite formation. *Int. J. Coal Geol.* 94:238-249.

Dreher GB and Finkleman RB (1992). Selenium mobilization in a Powder River basin surface coal mine. *Environ. Geol. Water Sci.* 19(3):155-167.

Evans DM, Zipper CE, Donovan PF, Daniels WL (2014) Long-term trends of specific conductance in waters discharged by coal mine VFs in Central Appalachia, USA. *J. Am. Wat. Res. Assoc.* 50(6): 1449-1460.

Griffith MB, Norton SB, Alexander LC, Pollard AI, LeDuc SD (2012) The effects of mountaintop mines and valley fills on the physiochemical quality of stream ecosystems in the central Appalachians: A review. *Sci. Total Envi.* 417-418: 1-12.

Halvorson HG, Gentry CE (1990) Long-term leaching of mine spoil with simulated precipitation. In: Proceedings of the 1990 Mining and Reclamation Conference

and Exhibition, Charleston, WV. American Society for Surface Mining and Reclamation, Lexington, KY, pp. 27-32.

Hartman KJ, Kaller MD, Howell JW, Sweka JA (2005) How much do valley fills influence headwater streams? *Hydrobiologia* 532: 91–102.

Iscen, C.F., Emiroglu, O., Ilhan, S., Arslan, N., Yilmaz, V., and Ahiska, S. (2008). Application of multivariate statistical techniques in the assessment of surface water quality in Uluabat Lake, Turkey. *Environ. Monit. Assess*. 114 (1-3), 269-276.

Johnson D (2016) Geochemical Properties of Soils and Associated Overburden of the Pottsville Group in Central Appalachia. Virginia Polytechnic Institute and State University. Ph.D. Dissertation.

Lindberg TT, Bernhardt ES, Bier R, Helton AM, Merola RB, Vengosh A, DiGiulio RT (2011) Cumulative impacts of mountaintop mining on an Appalachian watershed. *P Nat Acad Sci USA* 108:20929-20934.

Martino RL, Grady WC, Lukey HM, Scott GW, Harrison J, Karukus M (2014) Paleoenvironmental analysis of the Glenalum Tunnel coal and roof rock, southern West Virginia-Implications for sulfur origin and trends. *Int. J. Coal Geol.* 136 (15): 75-98.

Massoura TS, Echevarria G, Becquer T, Ghanbaja J, Leclerc-Cessac E, Morel JL (2006) Control of nickel availability by nickel bearing minerals in natural and anthropogenic soils. *Geoderma* 136 (1-2): 28-37.

Morrison JL, Atkinson SD, Sheetz BE (1990) Delineation of potential manganese sources in the coal overburdens of western Pennsylvania. In: Proceedings of the 1990 Mining and Reclamation Conference and Exhibition, Charleston, West Virginia, 23-26 April, 1990: Morgantown, WV, West Virginia University, v. 1, pp. 249-256.

Orndorff ZW, Daniels WL, Zipper CE, Eick M, Beck M (2015) A column evaluation of Appalachian coal mine spoils' temporal leaching behavior. *Environ. Pollut.* 204: 39-47.

Parker HM (2013) Effects of Various Saturation Levels, Leaching Solution pH, and Leaching Cycle on Electrical Conductivity from Coal Mine Spoil Leachate. Virginia Polytechnic Institute and State University. M.S. Thesis.

Pérez-López R, Cama J, Nieto JM, Ayora C, Saaltink MW (2009) Attenuation of pyrite oxidation with a fly ash pre-barrier: Reaction transport modelling of column experiments. *Appl. Geochem.* 24: 1712-1723.

Pond GJ, Passmore ME, Borsuk FA, Reynolds L, Rose CJ (2008) Downstream effects of mountaintop coal mining: comparing biological conditions using family- and genus-level macroinvertebrate bioassessment tools. *J N Am Benthol Soc* 27: 717–737.

Pond GJ, Passmore ME, Pointon ND, Felbinger JK, Walker CA, Krock KJ, Fulton JB, Nash WL (2014) Long-term impacts on macroinvertebrates downstream of reclaimed mountaintop mining valley fills in central Appalachia. *Environ. Manag.* 54: 919–933.

R Core Team (2013) R: A language and environment for statistical computing. R Foundation for Statistical Computing, Vienna, Austria. URL http://www.R-project.org/.

Robbins EI, Cravotta CA, Savela CE, Nord CL (1999) Hydrobiogeochemical interactions in anoxic limestone drains for neutralization of acidic mine drainage. *Fuel* 78: 259-270.

Rose AW, Cravotta CA (1998) Geochemistry of coal mine drainage. In: Smith MW, Schueck J (Eds.), Brady KBC. Coal Mine Drainage Prediction and Pollution Prevention in Pennsylvania. Pennsylvania Department of Environmental Protection, 22p.

Sena, K., C. Barton, P. Angel, C. Agouridis, and R. Warner. 2014. Influence of spoil type on chemistry and hydrology of interflow on a surface coal mine in the eastern US coalfield. *Water Air Soil Pollut.* 225:2171.

Singer PC, Stumm W (1970) Acidic mine drainage: the rate-determining step. *Science* 167(3921):1121-3.

Skousen J, Renton J, Brown H, Evans P, Leavitt B, Brady K, Cohen L, Ziemkiewicz P (1997) Neutralization potential of overburden samples containing siderite. *J. Envi. Qual.* 36(3) 673-681.

Suarez S, Nieto F, Velasco F, Martin FJ (2011) Serpentine and chlorite as effective Ni-Cu sinks during weathering of the Aguablanca sulphide deposit (SW Spain). TEM Evidence for metal-retention mechanisms in sheet silicates. *Eur. J. Mineral.* 23:179-196.

Timpano AJ, Schoenholtz SH, Soucek DJ, Zipper CE (2015) Salinity as a limiting factor for biological condition in mining-influenced Central Appalachian headwater streams. *J. Am. Water Resour. Assoc.* 51: 240-250.

Tuttle ML, Breit GN, Goldhaber MB (2009) Weathering of the New Albany Shale, Kentucky: II. Redistribution of minor and trace elements. *Appl. Geochem*. 24: 1565-1578.

US EPA (2017) “National Recommended Water Quality Criteria-Aquatic Life Criteria Table.” Accessed 14 Feb. 2017. https://www.epa.gov/wqc/national-recommended-water-quality-criteria-aquatic-life-criteria-table

US EPA (1996) The Metals Translator Guidance for Calculating a Total Recoverable Permit Limit from a Dissolved Criterion. EPA 823-B-96-007.

Veizer J (1983) Trace Elements and Isotopes in Sedimentary Carbonates. In: Reeder, RJ (Ed.) *Carbonates-Mineralogy and Chemistry: Mineralogical Society of America Reviews in Mineralogy,* vol. 11, pp. 265-299.

Xu CY, Schwartz FW, Traina SJ (1997) Treatment of acid-mine water with calcite and quartz. *Env. Eng. Sc.* 14(3): 141-152.

Yudovich YE, Ketris MP (2005) Arsenic in coal: A review. *Int. J. Coal Geol.* 61 (3-4): 141-196.

Yudovich YE, Ketris MP (2006) Selenium in coal: A review. *Int. J. Coal Geol.* 67: 112-126.

CHAPTER VI: Specific Conductance-Stage Relationships in Appalachian Valley Fill Streams

Elyse V. Clark, Breeyn M. Greer, Carl E. Zipper and Erich T. Hester

Citation: Clark EV, Greer BM, Zipper CE, Hester ET (2016) Specific conductance-stage relationships in Appalachian valley fill streams. *Environmental Earth Sciences* 75: 1222. DOI 10.1007/s12665-016-6026-2

ABSTRACT

Surface coal mining impacts on water resources in the Appalachian region, USA are widely studied. Total dissolved solids (TDS), which are estimated *in situ* by the proxy variable specific conductance (SC) are of interest due to potential aquatic macroinvertebrate effects. Prior studies have documented the hydrochemical impacts of surface mining on streams, but research on the relationships between SC and discharge is limited. SC-Stage relationships can help infer potential hydrologic flow paths, as well as source water TDS concentrations in mining-influenced watersheds. The objectives of this study were to compare baseflow and stormflow hydrochemistry and determine SC-Stage relationships in valley fill (VF) streams. Five VF streams of varying ages in Virginia were equipped with continuous SC and stage data loggers for up to 12 months (Dec. 2013-Nov. 2014). Data analyses included baseflow and stormflow hydrochemistry, and SC-Stage regressions and storm hysteresis patterns. Data were analyzed seasonally. Stages were generally highest in winter and lowest in summer, while SCs were generally highest in summer and lowest in winter. All SC-Stage regressions indicated SC dilution during stormflow, but significance differed seasonally. Storm SC-Stage hysteresis patterns varied with storm precipitation amounts, season, and vegetative period, implying climatic controls on VF stream storm responses. Counterclockwise storm hysteresis likely occurred in response to high rainfall amounts exceeding the mine soil infiltration

capacity. Clockwise storm hysteresis likely resulted from precipitation dissolving salts brought to the surface by evapotranspiration, but may have also resulted from rapid flow through pseudokarst features within the VF.

6.1 INTRODUCTION

Land disturbances by mining impact water resources globally by altering hydrologic flow pathways, discharge patterns, and water quality (Atanackovic et al. 2013; Evans et al. 2015; Huang et al. 2010; Younger and Wolkersdorfer 2004). Stream hydrologic and chemical impacts are especially of interest in the Appalachian coalfields of eastern USA, as the surface mining process has disturbed >6,000 km^2 of land in the region since the late 1970s (Zipper et al. 2011). Surface waters from mining-influenced watersheds often drain through valley fills (VF), which are landforms constructed of mining-disturbed rocks (mine spoils) that are placed in valleys adjacent to the mining excavations. Individual VFs often cover >10 ha (Evans et al. 2014) and thousands of VFs have been constructed in the Appalachian region (US EPA 2003, 2011).

Coal surface mines with VFs have numerous impacts on water resources and water quality in the Appalachian coalfields (Evans et al. 2014; Messinger and Paybins 2003; Negley and Eshleman 2006; Phillips 2004). During and after VF construction, environmental O_2 and water interact with the freshly mined spoils, initiating rapid spoil weathering. Rainwater leaches soluble ions from the mine spoils, resulting in water discharges with elevated concentrations of dissolved ions which are collectively termed total dissolved solids (TDS). The predominant components of TDS in Appalachian mined streams are SO_4^{2-}, HCO_3^-, Ca^{2+} and Mg^{2+} (Hartman et al. 2005; Pond et al. 2008; Timpano et al. 2015), and other ions at lower concentrations (Skousen et al. 2000). Total

dissolved solids of mine water discharges are typically estimated *in situ* by the proxy electrical conductivity (EC), and by specific conductance (SC), which is EC corrected to a standard 25º C and highly correlated to TDS (Timpano et al. 2010).

Typical SCs in discharges from Appalachian VFs range from < 500 to > 3,000 µS cm^{-1} (Evans et al. 2014; Hartman et al. 2005; Pond et al. 2008, 2014), whereas forested streams in unmined watersheds generally have SCs < 200 µS cm^{-1} (Boehme et al. 2016; Lindberg et al. 2011; Pond et al. 2008, 2014; Timpano et al. 2015). Elevated SCs in VF streams may alter aquatic macroinvertebrate community assemblages relative to unmined streams due to organism sensitivity to elevated ion concentrations (Boehme et al. 2016; Pond et al. 2008, 2014; Timpano et al. 2015), and these effects have been reported to occur at SCs > 300 µS cm^{-1} (Cormier et al. 2013) and ≥ 500 µS cm^{-1} (Pond et al. 2008).

Although some aspects of VF hydrology and chemistry are documented (Miller and Zegre 2014), few studies have used VF discharges to characterize potential source waters and their associated TDS contributions to streams. Thus, integrative approaches such as concentration-discharge (C-Q) analyses are needed to improve the understanding of the source waters responsible for TDS release to VF streams. C-Q relationships describe changes in streamwater chemistry as discharge varies in response to precipitation, and are useful tools for inferring hydrologic flow paths, source waters, basin characteristics, and surface disturbances (Bonta 2004; Evans and Davies 1998; House and Warwick 1998; Rice et al. 2004; Stump 2001). C-Q regressions assist in understanding the chemical- or ion-supply dynamics to streams (i.e. concentration increases or decreases during precipitation events), and have been used to assess watershed land disturbances (Bonta 2004; Lewis and Grant 1979) and temporal trends in

hydrochemistry (Murdoch and Shanley 2006). C-Q hysteresis is also used to understand streamwater ion-supply dynamics. During precipitation events, hydrologic systems with C-Q hysteresis generally have a loop pattern, indicating differential discharge timing of a water quality property (e.g. SC, temperature, pH) relative to the rise and fall of water level (Evans and Davies 1998; Walling and Webb 1980).

Hysteresis patterns have been interpreted in a two-component context (Figure 6.1a) in which hysteresis results from the differential discharge timing of pre-event and event water (Williams 1989), and in a three-component context (Figure 6.1b) in which hysteresis patterns are interpreted to indicate differential discharge timing of the three following hydrograph components: overland flow (*of*), baseflow (*bf*) and soil water (*so*) (Evans and Davies 1998). In the context of VF hydrology, the *so* component is termed spoil water (*sp*) (Murphy et al. 2014). Overland flow describes water that did not infiltrate into the mine spoil materials and flowed into a stream as runoff, *bf* describes groundwaters (both local and regional) that may have come into contact with spoil materials or may source from areas that have not been mined, and *sp* describes water that has infiltrated and flowed through local mine spoils as matrix and preferential flows in the near-surface zone (Clark and Zipper 2016) or through voids and macropores deeper in the subsurface (Greer 2015; Guebert and Gardner 2001; Hawkins 2004). As Evans and Davies (1998) described, these three storm hydrograph components have different concentrations and discharge timing, and each component influences overall stream chemistry. Therefore, C-Q relationships can be categorized into differing hysteresis patterns that are interpreted to infer relative source contributions of chemical constituents.

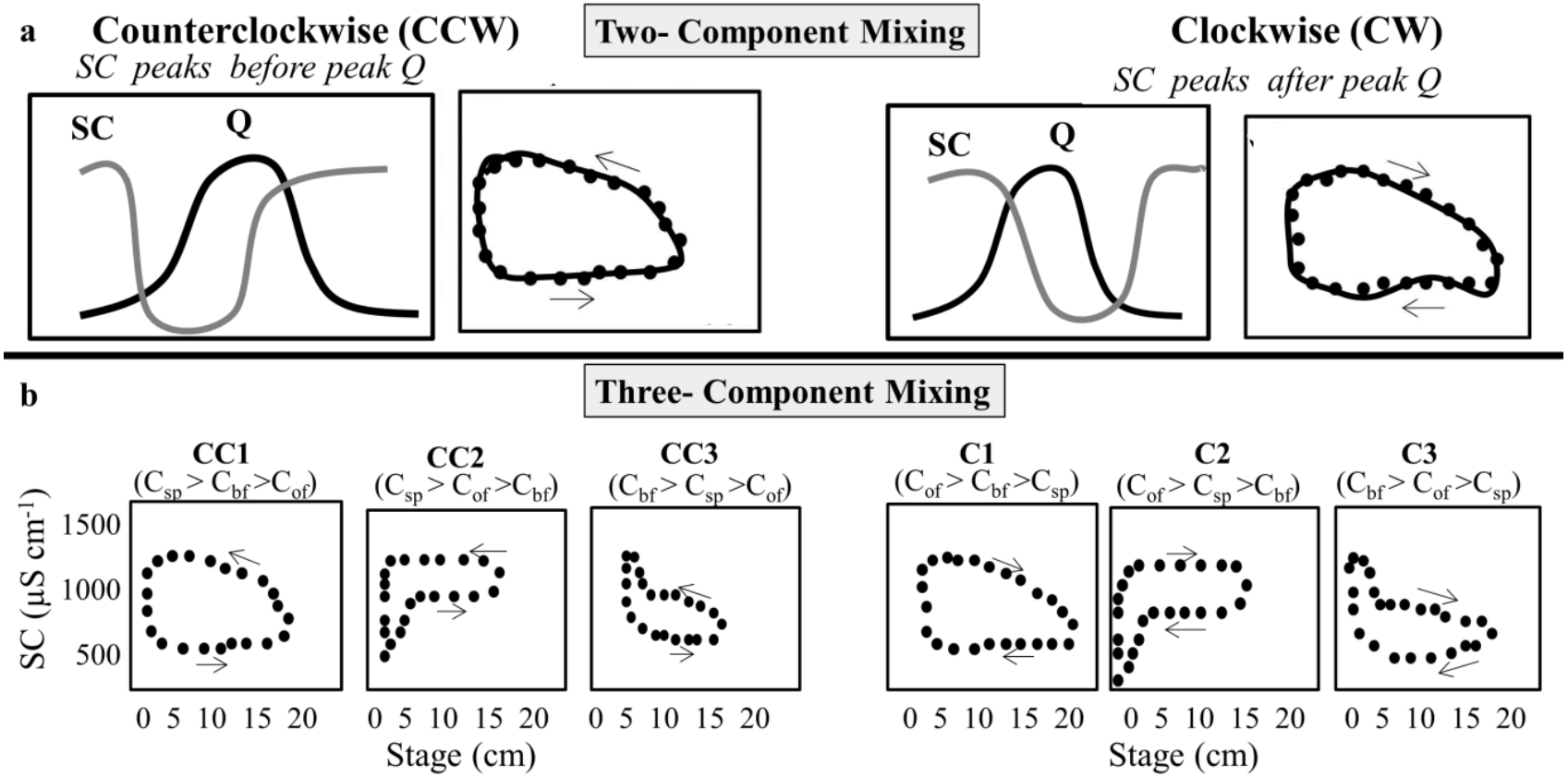

Figure 6.1 Two-component (a) and three-component (b) mixing models based on SC-Stage hysteresis. Loop classifications include counterclockwise (CCW) and clockwise (CW) rotation, which can be subdivided into types CC1, CC2, CC3, C1, C2, and C3 (Evans and Davies, 1998) based on relative SC concentrations of baseflow (*bf*), overland flow (*of*) and spoil water (*sp*).

Few studies have examined C-Q relationships in a surface mining context. Bonta (2004) used C-Q regressions to analyze three mining-influenced streams in Ohio, USA, and found significant relationships between streamwater chemical concentrations and discharge during the pre-disturbance and post-mining phases. Murphy et al. (2014) analyzed C-Q hysteresis in mining-influenced watersheds in Tennessee, USA for 40 storms (1975-2009), and concluded that a continuous supply of dissolved ions from mining areas was the source of elevated TDS in the New River. Murphy et al. (2014), however, documented one watershed and two sub-basins within that watershed, and sampled >1km downstream of mining activities where small fractions of upstream watersheds were disturbed by coal mining.

In order to improve understanding of TDS release from mining-influenced watersheds, more research is necessary. Using high temporal resolution (10-15 min. interval) sampling within 100m of VF streamflow emergence, we analyzed SC, stage, and SC-Stage relationships for five VFs of varying ages in Virginia over 12 months. Specific objectives were to examine the differences in hydrochemical discharge patterns among VF streams, and to compare relationships between SC and stage for VF streams on multiple time scales (i.e. storm event, seasonally). Results are intended to aid the understanding of stream discharge and TDS-generation pathways of mined landforms in watersheds with VFs.

6.2 MATERIALS AND METHODS

6.2.1 Site Description

Five valley fills were selected for analysis; all sites were in two clusters in the Appalachian coalfields of southwestern Virginia (Figure 6.2). Sites 1 and 4 were located

in Dickenson County, VA, and sites 2, 3, and 5 were clustered in Wise County, VA (Table 6.1). Site numbering is by ascending age, ranging from ~2.5 years old (Site 1, which was partially constructed during the analysis period) to 20 years old (Site 5) at the time of data collection. All VFs were constructed with Pennsylvanian-aged gray and brown sandstones of the Wise and Norton Formations (Meissner 1978; Nolde et al. 1986). Aerial imagery and geometric tools in ArcMap (v. 10.1, ESRI: Redlands, CA) were used to estimate VF surface areas. Site 3 had the largest surface area and Site 5 had the smallest surface area. The VFs at Sites 2-5 were constructed as V-shaped tiered structures using the loose-dump method which enables gravity-induced segregation of spoil materials such that larger rocks occur near the VF base where they form a rock drain that discharges water rapidly from the fill. At the time of data collection, Site 1 was being constructed of tiered lifts with the lower lifts of the VF completed and vegetated, but the upper lifts were still being constructed. Vegetative cover ranged from grass on the younger fills, to immature tree coverage without closed canopy on the medium-aged VFs, to closed canopy tree coverage on the oldest fills.

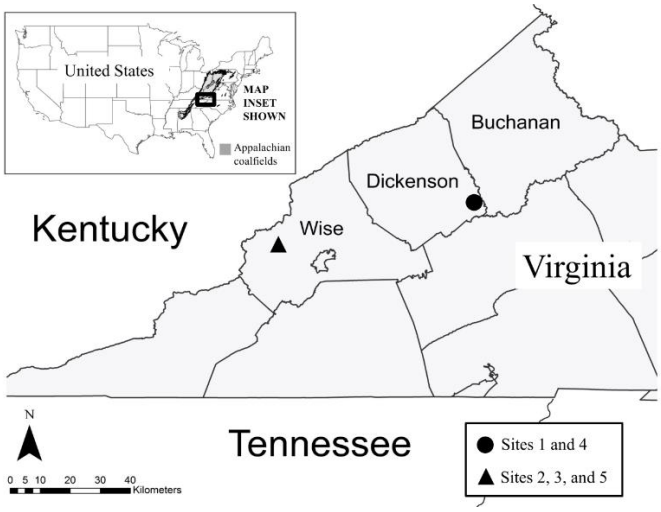

Figure 6.2 Location map for Sites 1-5. The Appalachian coalfields are indicated by gray coloration on the United States map.

Table 6.1 Descriptions of basic site conditions.

Site	Age (y)	County	VF Surface Area(m^2)	Vegetative Cover	Storm Event Threshold (mm)
1[†]	2.5	Dickenson	13,540	grassed	2.5
2	6	Wise	7,540	grassed	3.5
3	9	Wise	16,030	immature forest, open canopy	4.0
4	15	Dickenson	11,650	forested, closed canopy	1.5
5	20	Wise	7,040	immature forest, open canopy	2.5

[†] This valley fill had been under construction since mid-2012. At the time of data collection, the lower sections were complete and vegetated, but construction of upper sections was ongoing.

6.2.2 Data Collection

Data collection was initiated on all sites on 1 December 2013 and extended on all but one site to 30 November 2014; Site 2 data collection was terminated on 23 July 2014 due to channel reconstruction by the cooperating mining firm. Daily precipitation data (mm) were obtained from the nearest National Climatic Data Center (NOAA 2016) weather stations (Grundy, VA for Sites 1 and 4; Norton, VA for Sites 2, 3, and 5). Automated data loggers recorded SC and stage data every 15 minutes at Sites 1 and 4, and every 10 minutes at Sites 2, 3 and 5. Data collection occurred within ~100m of streamflow emergence from the VF toes and above sedimentation ponds. Streams flowed continuously from all VF toes during the study period. Onset HOBO conductivity (HOBO U24-001, Bourne, MA, USA), and barometric pressure (HOBO U20-001-01) data loggers collected SC and stage data at Sites 1 and 4. Data at sites 2, 3, and 5 were collected with Solinst Levelogger Junior 3001 (Toronto, Canada) and Onset HOBO barometric pressure transducers.

Data processing included converting raw instrument output files to stage and SC in accordance to manufacturers' instructions. For Sites 1 and 4, SC data were corrected using HOBO software and manual measurements made with a handheld conductivity meter (Thermo Scientific Orion Star A122) during data collection. For other sites, SC

was manually calibrated with standard solutions at three points (1,413, 5,000, and 12,880 µs cm^{-1}) then converted from the instrument reading via a linear regression line ($r^2 >$ 0.99). Stage was determined using HOBO software, which converted pressure to stage using both air and submerged absolute pressures recorded by the automated data loggers.

Hydrologic analyses typically utilize stream discharge data; however, discharge data were not collected at most of these sites due to stream bed and bank instability, differences in watershed disturbance levels, and personnel travel time constraints. Prior studies have used stage, rather than discharge, in multiple types of hydrologic analyses (e.g. Herman et al. 2008; Magnusson et al. 2014; McMahon et al. 2003; Shuster et al. 2008), including hydrochemical storm event analysis (Miller and Drever 1977); thus stage was used for all methods subsequently described.

6.2.3 Data Analyses

Two analyses were conducted: 1) analysis of general VF stage and SC patterns 2) analysis of SC-Stage relationships via regression and hysteresis loop analyses. Summaries of these analyses were done seasonally (Winter: December – February, Spring: March – May, Summer: June – August, and Fall: September – November), and all data collected over the entire study period were also summarized.

General Valley Fill Stage and Specific Conductance Patterns

In order to separate stormflow from baseflow periods, storm event discharge thresholds were determined for each site using a two stage process. First, cumulative distribution functions (CDFs) and histograms were created for all stage data collected at each site (Figure 6.3). The CDFs were visually inspected for abrupt changes in slope, and those change points were visually estimated. Second, storm event thresholds were then

verified using histograms of the stage data, and data analyses revealed that the visually identified CDF thresholds were approximately equivalent to the mean + one standard deviation. Thus, storm event thresholds were defined for each VF as equivalent to one standard deviation of that VFs dataset (Table 6.1). Stormflow and baseflow SC and stage values were used to calculate seasonal means of SC and stage for each flow type.

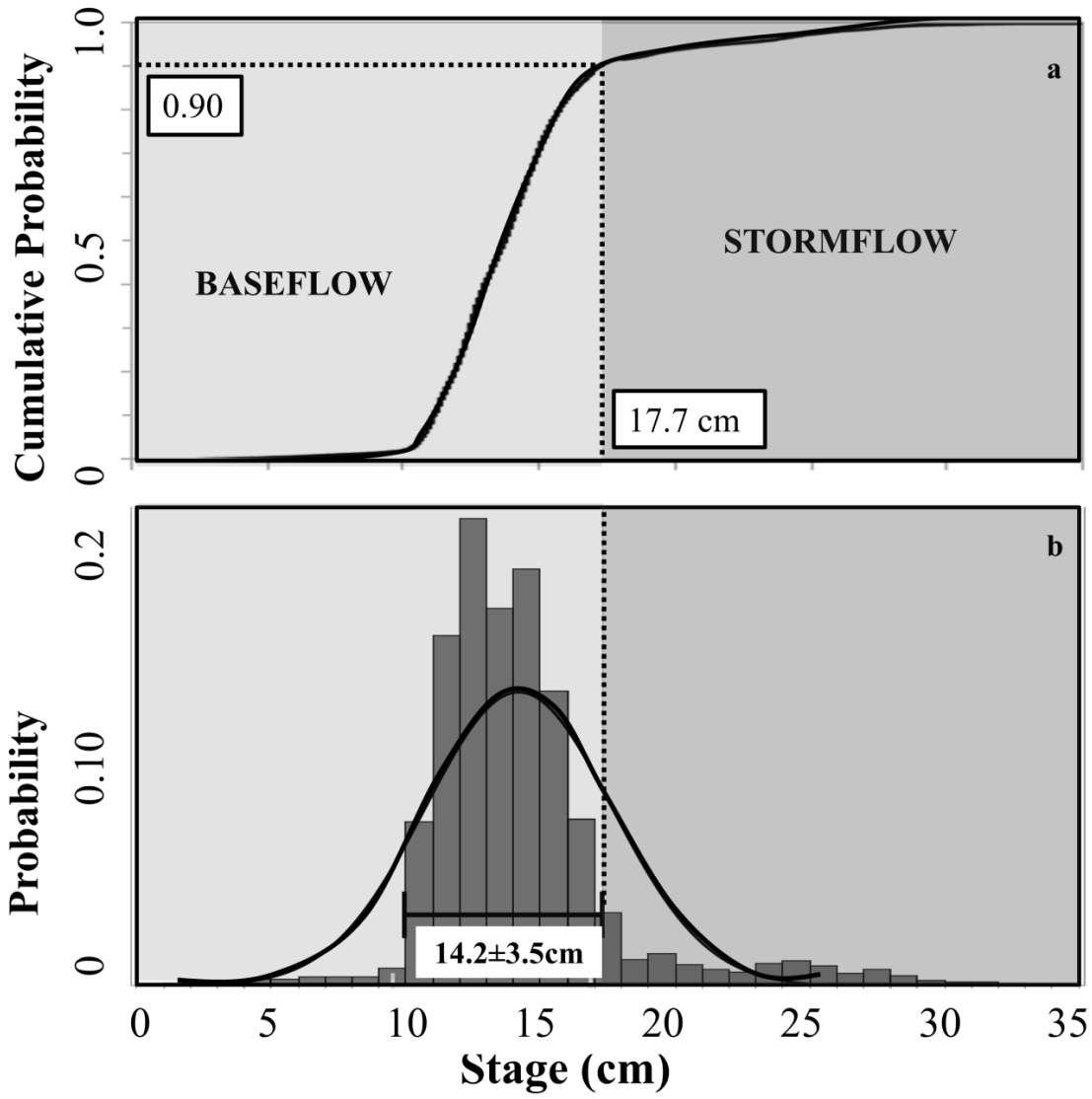

Figure 6.3 The baseflow and stormflow separation technique using (a) cumulative density frequency analysis and (b) histogram mean + standard deviation for Site 2.

Specific Conductance-Stage Regressions

Regression analyses were used to describe SC-Stage relationships. A power law regression, modified from Bonta (2004) to incorporate stage data, was defined as follows:

$$SC = a(Stage)^b \quad (6.1)$$

where *a* is the coefficient parameter and *b* is the exponent parameter. Both SC and stage were log- transformed and a linear regression was performed. The resulting slope of the transformed linear regression is equivalent to the *b* exponent parameter, whereas the intercept is equivalent to the log of *a*.

Specific Conductance-Stage Hysteresis

Individual storm events were separated from the stage data record by first identifying exceedances of the storm-event threshold for each VF (Table 6.1), separating storm sequences that exceeded the storm threshold, then adding observations recorded for 30 minutes prior to the initial exceedance. Such sequences were defined as a single storm event.

Bivariate plots of stage vs. SC were created for all storm events (hereafter "storms"). Storms without hysteresis were classified as not applicable (NA), storms with a downward slope but no discernible loop direction were classified as downward sloping (DS), and storms with clearly evident hysteresis were classified as clockwise (CW) or counterclockwise (CCW) using a two-component model (Figure 6.1a). For three-component hysteresis analysis based on the *bf, sp,* and *of* hydrograph components, CCW and CW loop types were classified as type 1, 2 or 3, thus the possible storm classifications were as follows: CC1, CC2, CC3, C1, C2, or C3 (Evans and Davies 1998;

Figure 6.1b). Both two- and three-component storm hysteresis patterns were summarized for all data and seasonally. Hysteresis patterns were also summarized by vegetative period as either growing season (April 15-October 15) or non-growing season (October 16-April 14) based on regional climate data (Southeast Regional Climate Center 2016a, b).

6.2.4 Statistical Analyses

Using JMP (v. 11.0, SAS Institute: Cary, N.C.), Kruskal-Wallis tests determined significant differences ($p \leq 0.05$) in baseflow and stormflow SC and stage seasonally, as well as significant differences in precipitation amounts associated with hysteresis loop classifications. Significant SC-Stage regressions were defined as those in which the slope was significantly different from zero ($p \leq 0.05$). Contingency tables and chi-squared (χ^2) analyses identified statistical differences ($p \leq 0.05$) between the number of SC-Stage hysteresis loops by site, season, and vegetative period.

6.3 RESULTS

6.3.1 General Valley Fill Stage and Specific Conductance Patterns

Stage

Mean stage values ranged from 2.2 cm (Site 4) to 25.4 cm (Site 3), and maximum stages ranged from 18.6 cm (Site 4) to 55.3 cm (Site 3). Stages at all sites had clear seasonal influences (Table 6.2), and four of five sites had significantly higher stages in winter than any other season. Site 5 had the strongest seasonal effect; all four seasons had significantly different stages.

Mean baseflow stages were highest in winter (Table 6.2) and lowest in summer for four of the five sites. All sites had seasonal baseflow stage effects with all seasons

having significantly different mean baseflow values. Mean stormflow stages ranged from 4.1 cm (Site 4) to 34.4 cm (Site 3), and seasonal effects were present at all five VFs. The largest stormflow stages occurred in winter for 4 of 5 sites.

Table 6.2 Valley fill daily mean stage and SC-Stage Regressions for Sites 1-5.

Site (Age)	Season	Stage (cm)	BF-Stage (cm)*	SF-Stage (cm)*	*a*	*b*	p (α =0.05)
1	Winter	7.0[a†]	6.3[a]	11.3[a]	1,140	-1.50	<0.0001
	Spring	6.2[b]	6.1[b]	8.8[d]			NS[‡]
(2.5 y)	Summer	5.2[c]	5.2[d]	10.0[b]			NS
	Fall	6.2[b]	5.9[c]	9.2[c]	1,450	-1.69	<0.0001
	ALL	*6.2*	*5.9*	*9.7*	*1,170*	*-1.48*	*<0.0001*
2	Winter	14.6[a]	14.0[a]	23.7[a]	1,750	-1.51	0.0144
	Spring	15.0[a]	13.5[b]	22.0[b]	1,090	-0.87	0.0048
(6 y)	Summer	12.1[b]	12.0[c]	17.7[c]	1,660	-1.63	<0.0001
	ALL	*14.2*	*13.3*	*22.7*	*1,350*	*-1.19*	*0.0021*
3	Winter	31.0[a]	31.0[a]	34.9[a]	1,320	-0.84	0.0349
	Spring	22.8[c]	22.8[d]	35.0[a]	1,600	-1.24	0.0002
(9 y)	Summer	23.6[b]	23.6[c]	28.2[c]	1,900	-1.36	<0.0001
	Fall	24.2[b]	24.1[b]	29.2[b]	1,910	-1.37	<0.0001
	ALL	*25.4*	*25.3*	*34.4*	*1,770*	*-1.31*	*<0.0001*
4	Winter	2.9[a]	1.9[b]	6.3[a]	1,630	-1.88	<0.0001
	Spring	2.3[b]	2.3[a]	2.8[d]	1,950	-2.06	<0.0001
(15 y)	Summer	1.5[c]	1.5[d]	4.4[c]	2,060	-2.19	<0.0001
	Fall	1.9[bc]	1.7[c]	5.8[b]	2,060	-2.23	<0.0001
	ALL	*2.2*	*2.0*	*4.1*	*1,930*	*-2.10*	*<0.0001*
5	Winter	15.8[a]	14.7[a]	20.4[b]	1,260	1.67	0.0003
	Spring	12.3[c]	12.1[c]	23.5[a]			NS
(20 y)	Summer	11.3[d]	11.3[d]	15.3[d]	2,750	-2.20	<0.0001
	Fall	14.6[b]	14.0[b]	18.1[c]	950	-1.23	0.0106
	ALL	*13.5*	*12.8*	*19.6*	*1,680*	*-1.83*	*<0.0001*

* BF= Baseflow, SF= Stormflow, SC= Specific Conductance

† Values followed by the same letter within each site are not significantly different from one another ($p \leq 0.05$).

‡NS= SC-Stage regression not statistically significant ($p > 0.05$).

Specific Conductance

Minimum SCs measured were ~200 µS cm^{-1}, maximum SCs measured were > 2000 µS cm^{-1}, and mean baseflow SCs ranged from 790 µS cm^{-1} (Site 5) to 1,660 µS cm^{-1} (Site 4) (Figure 6.4). Seasonal effects on baseflow SC were present at all sites. Summer had the largest mean baseflow SC and winter had the smallest mean baseflow SC at 3 of

5 sites. Site 5 had the largest season-to-season range of baseflow SCs (350 µS cm^{-1}) which occurred between summer and winter, whereas Site 3 had the smallest season-to-season range of baseflow SCs (160 µS cm^{-1}).

Mean stormflow SCs ranged from 490 µS cm^{-1} (Site 5) to 1,450 µS cm^{-1} (Site 4) and were generally lower than baseflow SCs (Figure 6.4). Seasonal effects on stormflow SC occurred at all sites; spring had significantly larger stormflow SCs at 3 of 5 sites. Site 4 had the largest season-to season range in stormflow SCs, with a range of > 450 µS cm^{-1} between spring (1,640 µS cm^{-1}) and winter (1,160 µS cm^{-1}), whereas Site 1 had the smallest season-to-season range (140 µS cm^{-1}).

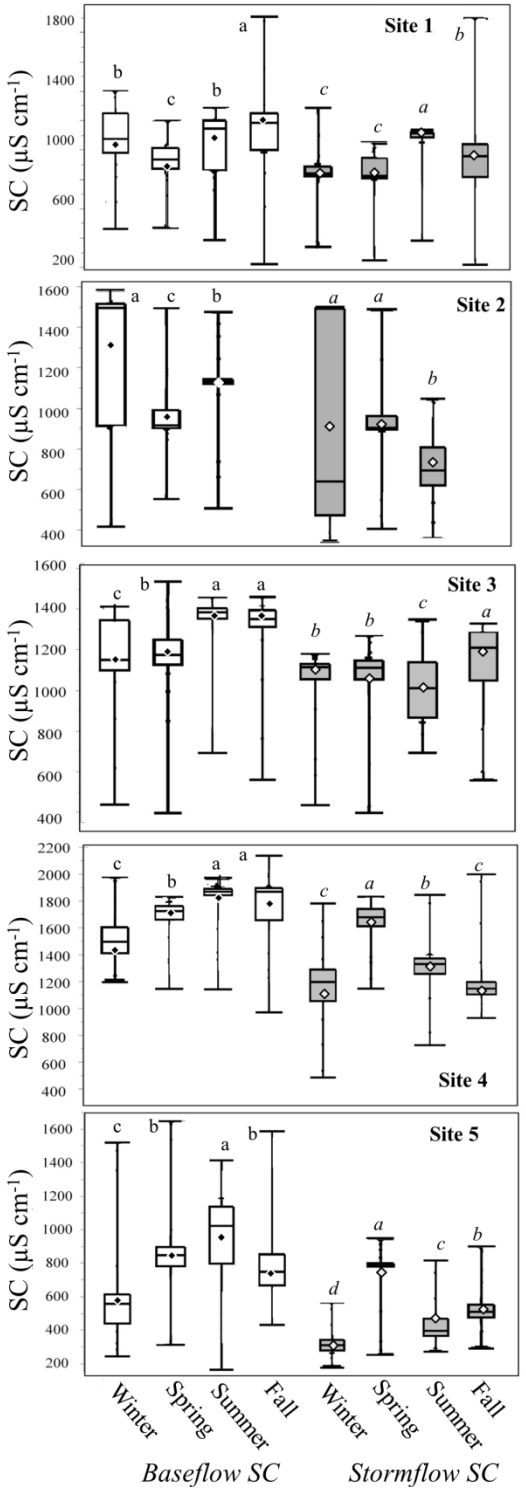

Figure 6.4 Boxplots illustrating the range of baseflow (white) and stormflow (gray) SCs in Sites 1-5. Wide bars represent the minimum, 25th percentile, median, 75th percentile, and maximum values, respectively. Diamonds represent means. Baseflow and stormflow SC is classified by season. For each flow type, boxplots with different letters indicate significant differences between seasons ($p \leq 0.05$). Note differences in y-axis scales.

6.3.2 Specific Conductance-Stage Relationships

Specific Conductance-Stage Regressions

All sites had significant regressions for the full study period (Figure 6.5). Site 4 had the most negative *b* constant (-2.10) and Site 2 had the least negative (-1.19), with more negative *b* constants (Eq. 6.1) indicating a greater dilution of SC during stormflow. The regression *a* parameter value (intercept, Eq. 6.1) was largest at Site 4 (1,930 μS cm^{-1}) and smallest at Site 1 (1,170 μS cm^{-1}), with larger *a* values implying greater potential SC during baseflow.

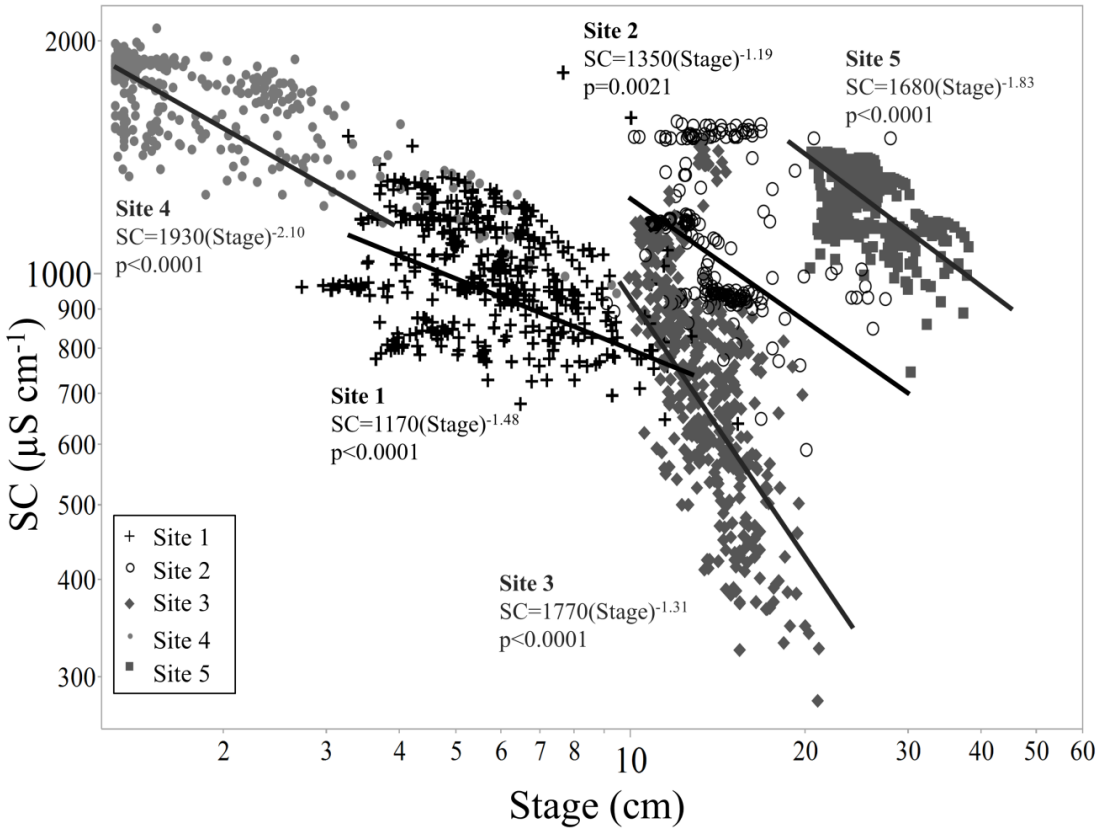

Figure 6.5 Full year regressions showing significant relationships between SC and stage in Sites 1- 5.

Sixteen of the 19 seasonal SC-Stage regressions were statistically significant (Table 6.2). Seasonal *b* parameter values ranged from -2.23 to -0.87, and seasonal *a*

parameter values ranged from 950 to 2,750 μS cm^{-1}. Seasonal regressions varied in significance by site. Site 1 had only two significant seasons and Site 5 had three significant seasons. Sites 2, 3 and 4 had significant SC-Stage regressions for all seasons. All five VFs had significant SC-Stage regressions for fall and winter, whereas spring flows had the fewest significant regressions (3 of 5).

Specific Conductance-Stage Hysteresis

A total of 97 storms were identified and analyzed across all VFs. Storm totals for individual VFs ranged from 14 (Site 4) to 30 storms (Site 5) (Table 6.3). Winter had the largest number (31 in Dec., Jan., and Feb.) and summer had the smallest number (17 in June, July, Aug.) of storms. Excluding Site 4, which only had storms of a single hysteresis type, more storms occurred during the growing season (43 storms) than in the non-growing season (40 storms). Larger precipitation events occurred in summer and winter (25 and 21 mm, respectively) than in fall (18 mm on average) and spring (12 mm on average), and seasonal rainfall averages were largest in summer and fall (12 mm on average for the entire season) and smaller in winter (10 mm) and spring (7 mm).

Precipitation events had clear signatures in the hydrographs and the patterns of SC during storms were generally the inverse of stage (Figure 6.6), with SC at high concentrations during baseflow, diluting to a minimum during stormflow, and gradually increasing in SC as the system returned to baseflow conditions.

Table 6.3 Summary of Specific Conductance-Stage hysteresis loop patterns by type (Figure 6.1) and season.

	Clockwise (n=C1, n=C3)	**Counterclockwise (n=CC1, n=CC3)**	**No Hysteresis (n=DS*, n=NA*)**	**Total**
Site (Age)	Numbers of storms			
1 (2.5 y)	11 (3,8)	6 (0,6)	1 (0,1)	**18**
2 (6 y)	2 (1,1)	6 (0,6)	8 (4,4)	**16**
3 (9 y)		11 (3,8)	8 (3,5)	**19**
4 (15 y)	14 (6,8)			**14**
5 (20 y)	6 (0,6)	11(4,7)	13 (11,2)	**30**
Total	**33(10, 23)**	**34 (7,27)**	**30 (18,12)**	**97**
Season	Numbers of Storms			
Winter	6 (1,5)	21 (4,17)	4 (1,3)	**31**
Spring	10 (5,5)	7 (3,4)	12 (4,8)	**29**
Summer	5 (0,5)	3 (0,3)	9 (9,0)	**17**
Fall	12 (4,8)	3 (0,3)	5 (4,1)	**20**
Vegetation Period	Numbers of Storms			
Growing Season†‡	17^{a}	7^{b}	19^{a}	**43**
Non-growing Season†‡	2^{b}	27^{a}	11^{b}	**40**
Mean Precipitation (mm)§	17^{b}	22^{a}	13^{b}	

* DS= Downward Sloping, NA=no trend/random

†Storm event counts followed by different letters are significantly different ($p \leq 0.05$).

‡ Growing and non-growing season storm counts exclude Site 4 storms.

§Precipitation values followed by different letters are significantly different ($p \leq 0.05$).

Of the 97 storms analyzed, 67 (70%) showed hysteresis effects and 30 (30%) did not (Table 6.3). Approximately one third of the storms had CW hysteresis patterns, one third had CCW hysteresis patterns, and the last third had no hysteresis effects (Figure 4.6). Of the 30 storms without hysteresis effects, 18 had DS patterns and 12 were classified as NA, thus only 12% of the total 97 storms analyzed had a random SC-Stage relationship. Storms without hysteresis occurred in response to smaller precipitation events (13 mm, on average) than CW and CCW storms.

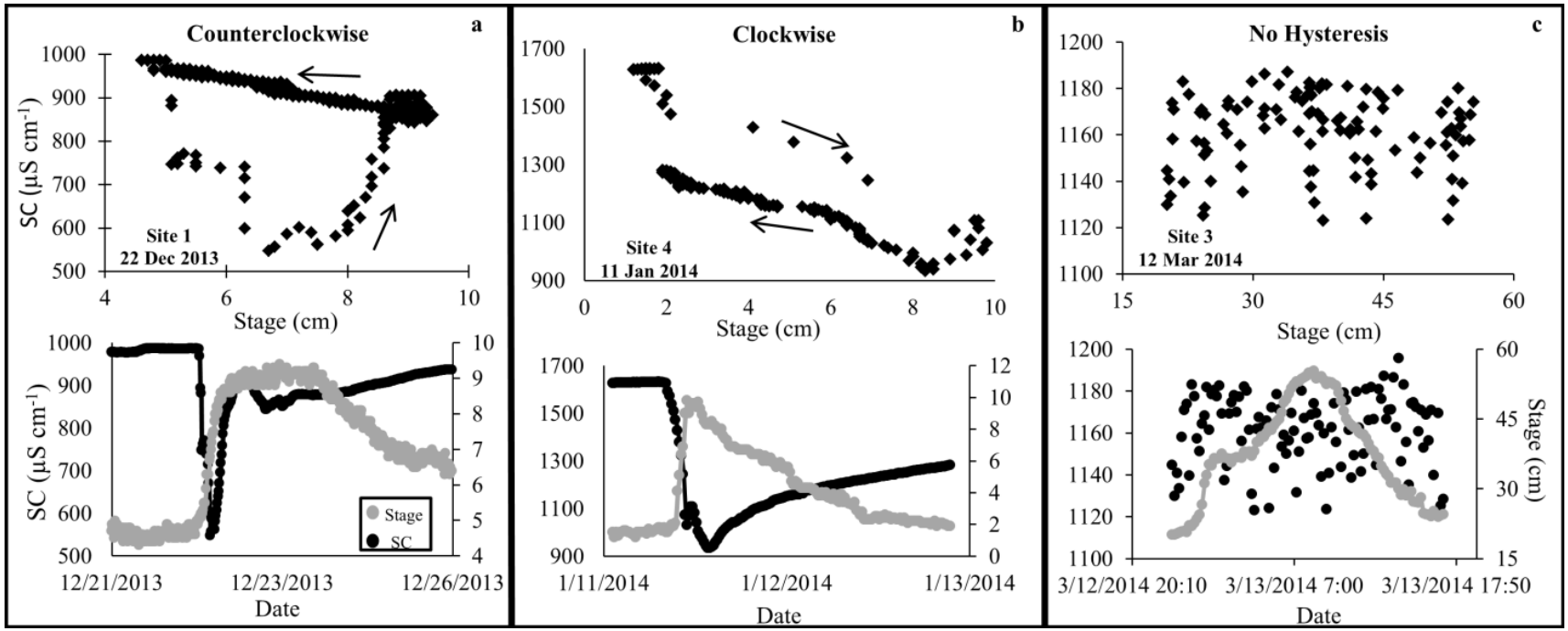

Figure 6.6 Examples of SC-Stage bivariate plots and associated hydrographs for individual precipitation events with (a) counterclockwise rotation (b) clockwise rotation and (c) no hysteresis.

For two-component model analysis, CCW rotation occurred for 34 storms, whereas CW rotation occurred for 33 of the 67 storms with hysteresis. Precipitation for CCW storms (22 mm, on average) was significantly greater ($p \leq 0.05$) than for CW storms (17 mm, on average). Site 4 only had CW storms, and Site 3 did not have any CW storms. All other sites had both CW and CCW storms. Site 1, the youngest, had the fewest storms without hysteresis, whereas Site 5, the oldest, had the most storms without hysteresis. Winter had more storms with CCW than with CW or no hysteresis. Significantly more CW storms occurred during the growing season ($p \leq 0.05$), whereas significantly more CCW storms occurred during the non-growing season ($p \leq 0.05$).

For three-component model analysis, no C2 or CC2 hysteresis patterns were identified for any storm analyzed (Figure 6.1). Types C1 and C3 patterns occurred in 10 and 23 storms, respectively, whereas CC1 and CC3 patterns occurred in 7 and 27 storms, respectively (Table 6.3). The most common hysteresis pattern of all storms was CC3, which occurred in 27 storms and was associated with significantly higher precipitation amounts (24 mm) than any other classification ($p \leq 0.05$). Type C3, CC3, and DS storms occurred in all seasons, C1 and NA occurred in all seasons except summer, and CC1 only occurred in winter and spring. Winter was the season most-dominated by a single loop type, as 21 of the 31 winter storms had CC3 patterns.

6.4 DISCUSSION

Analyses of VF stream stage, SC, and SC-Stage relationships revealed a pattern of relatively high SC during baseflow periods and dilution as a mechanism that reduced relative SC levels during stormflow periods. This general pattern was exhibited by all methods of analysis; mean stormflow SCs were lower than baseflow SCs in all sites and

seasons, negative SC-Stage regressions implied dilution of SCs at higher stage conditions, and most storm hysteresis loops displayed a decrease in SC relative to a rise in stage.

Baseflow SCs ranged from ~500 µS cm^{-1} to > 2,200 µS cm^{-1}, which is consistent with other studies on VF streams (Evans et al. 2014; Hartman et al. 2005; Pond et al. 2008, 2014). All seasonal baseflow and stormflow SC averages were > 500 µS cm^{-1} except for winter and summer stormflow in Site 5 (360 and 450 µS cm^{-1}, respectively), indicating that SCs were generally above the 500 µS cm^{-1} level described by Pond et al. (2008) as a threshold above which detrimental aquatic macroinvertebrate community effects occur, and well above the 300 µS cm^{-1} level described by Cormier et al. (2013) as a threshold above which 5% of aquatic genera are extirpated.

A prior study of 137 VFs in Virginia indicated that 19.6 ± 6.6 years after the initiation of VF construction may be required for SC in VF streams to decline to < 500 µS cm^{-1} (Evans et al. 2014). However, the number of years since initial disturbance was not a predictor of mean discharge SC (Evans et al. 2014), and no association between VF age and discharge SC was found in a study of four VFs in West Virginia (Merricks et al. 2007). In our study, no age effect on SC was apparent as Site 5, the oldest VF (20 y), had the lowest mean SC (790 µS cm^{-1}) and Site 4 (15 y) had the highest mean SC (1660 µS cm^{-1}). Collectively, these results indicate that VF-stream SCs are variable with age, thus other factors must also influence SC. A factor known to influence SC levels in discharge is mine spoil properties (i.e. rock type, weathering extent, mineralogy), as mine spoils have varying potentials to produce SC (Daniels et al. 2016; Orndorff et al. 2015); hence the types of mine spoils used to construct VFs may have a greater influence on SCs than

VF age. Internal VF structure and flow path configuration may also influence SCs, as VFs may differ in their capacity to store and transmit waters; however, such observations have been suggested but not documented by other studies (Miller and Zegre 2014; Evans et al. 2015; Greer 2015).

6.4.1 Specific Conductance-Stage Regressions

Significant SC-Stage regression parameters in all sites indicated that VFs and their contributing watersheds, which were predominantly mining influenced for all VFs studied, serve as sources of TDS to mining-influenced streams. Sites with more negative *b* parameters coupled with larger *a* values indicated higher SCs in baseflow that became more dilute during stormflow relative to other VFs. Such patterns are likely influenced by different geologic materials and spoil compositions used in VF construction, differences in VF construction methods, as well as differing channel configurations in the VF streams, hence the separation of individual VFs as shown in Figure 4.5. Seasonal SC-Stage relationships also differed among VFs, implying that in addition to spoil composition differences, streamwater SCs were influenced to an extent by seasonally-dependent factors, likely including vegetative cover and evapotranspiration (ET).

Prior studies on three streams in Ohio (Bonta 2004) and two streams in Tennessee (Murphy et al. 2014) also found significant SC-Q relationships in mining-influenced streams. Regression *a* parameters in this study (950 to 2,750 µS cm^{-1}) were larger than the Bonta (2004) parameter values (168 to 629 µS cm^{-1}) and Murphy et al. (2014) parameter values (89-378 µS cm^{-1}). Differences in parameter values are likely due to differing geologies and TDS production potentials, but could also be due to sampling locations being ≥ 1000 m downstream of streamflow emergence for both studies (Bonta

2004; Murphy et al. 2014). Differences could also be due to sampling locations occurring below sedimentation ponds (Bonta 2004), which increases the likelihood of SC dilution from other source waters or tributaries. Although Bonta (2004) and Murphy et al. (2014) analyzed discharge rather than stage, most SC-Q regressions had negative slopes like those documented in this study, suggesting that mining-influenced watersheds across the Appalachian region serve as sources of TDS to streamwater and that SC is diluted at relatively high stages.

6.4.2 Storm Event Hysteresis

Hysteresis occurred in a majority of storm events analyzed, with all sites exhibiting multiple storm classifications (CC1, CC3, C1, C3). Hysteresis patterns varied with precipitation amounts and season, as CCW storms tended to occur in association with higher precipitation amounts and during winter, whereas CW storms tended to occur in association with lower precipitation amounts and during the growing season.

Considering VF streams, we assumed that overland flow (*of)* waters generally had lower SCs than baseflow (*bf)* and spoil waters (*sp)* due to limited contact time with spoil materials, and due to the highly leached nature of surface spoils that have been subjected to repeated contact with precipitation waters. We also assumed that *bf* waters for most VFs had relatively constant SCs during a given storm event, although this assumption may not hold for Sites 1 and 4 where *bf* is known to include underground mine water discharges. On all VFs it was assumed that *sp* water flows occur in response to precipitation infiltration into the VF, which generates TDS via spoil-water interactions within the VF interior. These assumptions described above were used to interpret observed hysteresis patterns.

Counterclockwise hysteresis patterns (Figure 6.6a) are characterized by a greater influence of dilute waters during the hydrograph's rising limb and an increased influence of higher SC waters during the falling limb, suggesting that dilute *of* waters have a strong influence on SC during the initial storm response. The fact that CCW hysteresis occurred during significantly larger storm events (22 mm on average) supports this explanation, suggesting that CCW hysteresis occurred in response to rapid runoff of dilute *of* waters during the precipitation event. Large precipitation events are more likely to exceed VF-surface infiltration capacities than storms with smaller amounts of rainfall (Jorgensen and Gardner 1987), causing event water, which has limited contact with VF spoils to dominate the hydrograph's rising limb. After such dilution, the stormflow shifts to apparent dominance by higher SC waters, specifically *sp* and/or *bf* waters, during the hydrograph's falling limb. Also, CCW hysteresis occurred more often in winter relative to other seasons, implying a climatic influence. Colder winter temperatures and minimal vegetative cover cause reduced ET and enable increased soil moisture relative to summer months, perhaps reducing infiltration and increasing *of* waters. Frozen soil surfaces may also have contributed to increased *of* for some storms.

Clockwise hysteresis patterns (Figure 6.6b) are characterized by delayed SC dilution relative to the rise in stage during a storm, and their interpretation is not as direct. Significantly more CW storms occurred during the growing season, thus one possible interpretation is that CW storms may flush easily-soluble surface salts that were brought to the surface via ET processes. Prior studies have found high cation concentrations in the top 5cm of a mine soil (Nash et al. 2016), salt accumulation within spoil materials placed in field leaching lysimeters (Daniels et al. 2016; Ross 2015), as well as visible salt

accumulation on the surface of coal refuse piles (Daniels et al. 2010). Surficial salt accumulation may also occur on VF mine spoils, and is likely influenced by seasonal wetting and drying cycles and ET during drier periods. Accumulated surficial salts may be flushed as high SC *of* waters during the initial stages of precipitation events, resulting in relatively high SC in the initial *of* runoff during a storm. Subsequent *of* waters would be more dilute relative to the initial flush of surface salts, enabling the CW hysteresis pattern to occur.

More complex explanations for CW storms are also possible. Site 4 generated CW hysteresis for all storms, suggesting that the hydrology of this site is unique. As described above, *bf* waters in Site 4 include underground mine discharges, which appear to be responsive to surface hydrologic events. Although underground, the mining conduits are located above the VF and relatively close to the surface, and may discharge high-TDS waters that have been stored in the underground mine complex for a period of time, resulting in relatively high SCs during the hydrograph's rising limb of CW hysteresis.

Another possible explanation for CW rotation involves the rapid flushing of *sp* waters. A prior study demonstrated that mine spoil fill surfaces can be highly heterogeneous and can contain zones that are porous and promote rapid infiltration (Clark and Zipper 2016). Similarly, Greer (2015) found rapid rainwater infiltration into a VF, which was followed by rapid downward movement of the wetting front along preferential flowpaths within the VF. These studies suggest the presence of subsurface properties resembling "pseudokarst" features, i.e. highly permeable materials with inter-connected subsurface channels and voids that enable rapid throughflow (Caruccio and Geidel 1995;

Hawkins and Aljoe 1990). Miller and Zegre (2014) suggested that such pseudokarst features may occur within loose-dumped VFs such as those in this study. Pseudokarst features may enable infiltrated water to become *sp* water that travels rapidly through the VF, either mobilizing readily-soluble salts or displacing stored or pre-event water (McDonnell 1990) with relatively high SCs. If such *sp* waters were to dominate the initial phase of a given storm response, the result would be relatively high SC waters discharged during the hydrograph's rising limb and CW hysteresis.

Overall, hysteresis patterns in the five VF streams were influenced by storm event size, seasonal climate variation, and growing season. A prior study on mining-influenced streams in Tennessee, USA similarly concluded that storm event size influenced hysteresis patterns, as Murphy et al. (2014) found that CCW (CC2) patterns occurred when peak flow was < 25 $m^3 s^{-1}$ and CW (C3) patterns occurred when peak flow was > 25 $m^3 s^{-1}$. In contrast, our results suggested that storms with higher precipitation amounts tended to have CCW rotation, whereas smaller storms tended to have CW hysteresis. Furthermore, no CC2 patterns were identified for any of the 97 storms in this analysis. Discrepancies between our results and Murphy et al. (2014), as well as the Bonta (2004) C-Q regression analyses indicate that mining-influenced streams vary chemically and hydrologically between sites, but also by sampling location within the watershed (i.e. upstream vs. downstream) and seasonally. Results, therefore, highlight the importance of sampling directly at the emergence of VF streamflow to fully characterize the "mining signature" in discharges and water chemistry of VF streams.

6.5 CONCLUSION

The hydrochemistry of five streams emerging from Appalachian VFs varied by season, precipitation amounts during storm events, and among VFs. Stream stage and SC patterns, SC-Stage regressions, and storm hysteresis indicated high SCs during baseflow with dilution of SC during stormflow. Seasonal climatic factors such as antecedent moisture conditions, frozen soil surfaces, and evapotranspiration rates also appear to influence VF hydrologic responses and stream hydrochemistry. Future research should include chemical analysis of source waters (spoil water, overland flow, groundwater) in order to understand the specific chemistry of each source water component, as well as the interaction of all three source waters during baseflow and stormflow. Storm hysteresis analysis of specific ions may also help to more fully understand VF hydrochemistry and the sources of TDS in VF streams.

6.6 ACKNOWLEDGEMENTS

The authors would like to thank the cooperating mining firms, Dan Evans, and Dr. Trip Krenz for site access and data collection. This research was sponsored by the Appalachian Regional Initiative for the Environmental Sciences (ARIES), Virginia Tech Institute for Critical Technology and Applied Sciences, Powell River Project, Virginia Agricultural Experimental Station, Wells Fargo through the Clean Technology and Innovation Grant Program, and the USDA Hatch Program of the National Institute of Food and Agriculture. The opinions expressed herein are solely those of the authors and do not imply endorsement by ARIES or Wells Fargo employees.

6.7 REFERENCES

Atanackovic N, Dragisic V, Stojkovic J, Papic P, Zivanovic V (2013) Hydrochemical characteristics of mine waters from abandoned mining sites in Serbia and their impact on surface water quality. *Environ. Sci. Pollut. R.* 20: 7615-7626.

Boehme EA, Zipper CE, Schoenholtz SH, Soucek DJ, Timpano AJ (2016) Temporal dynamics of benthic macroinvertebrate communities and their response to elevated specific conductance in Appalachian coalfield headwater streams. *Ecol. Indic.* 64: 171-180.

Bonta JV (2004) Concentration-discharge regression parameters in watersheds of varying lithology subjected to surface coal mining and reclamation. *J. Soil. Water Conserv.* 59: 86–101.

Caruccio FT, Geidel G (1995) Status Report: Long-Term Effects of Alkaline Trenches and Funnels at the Mercer Site. West Virginia Surface Mine Drainage Task Force Symposium: Morgantown, WV, USA.

Clark EV, Zipper CE (2016) Vegetation influences near-surface hydrological characteristics on a surface coal mine in eastern USA. *Catena* 139: 241-249.

Cormier SM, Suter GW, Zheng L (2013) Derivation of a benchmark for freshwater ionic strength. *Environ. Toxicol. Chem.* 32: 263-271.

Daniels WL, Stewart B, Zipper CE (2010) Reclamation of coal refuse disposal areas. Virginia Cooperative Extension Publication 460-131.

Daniels WL, Zipper CE, Orndorff CW, Skousen JG, Barton CD, McDonald L, Beck M (2016) Predicting total dissolved solids release from central Appalachian coal mine spoils. *Environ. Pollut.* 216: 371-379.

ESRI (Environmental Systems Resource Institute) (2012) ArcMap 10.1. ESRI, Redlands, California.

Evans C, Davies C (1998) Causes of concentration/discharge hysteresis and its potential as a tool for analysis of episode hydrochemistry. *Water. Resour. Res.* 34: 129-137.

Evans DM, Zipper CE, Donovan P, Daniels WL (2014) Long-term trends of specific conductance in waters discharged by coal-mine valley fills in central Appalachia, USA. *J. Am. Water Resour. As.* 50: 1449-1460.

Evans DM, Zipper CE, Hester ET, Schoenholtz S (2015) Hydrologic effects of surface coal mining in Appalachia (USA). *J. Am. Wat. Resour. As.* 51(5):1436-1452.

Greer BM (2015) Electrical Resistivity Imaging of Preferential Flow Through Surface Mine Valley Fills with Comparisons to Other Land Forms. Thesis, Virginia Polytechnic Institute and State University.

Guebert MD, Gardner TW (2001) Macropore flow on reclaimed surface mines: infiltration and hillslope hydrology. *Geomorphology* 39: 151-169.

Hartman KJ, Kaller MD, Howell JW, Sweka JA (2005) How much do valley fills influence headwater streams? *Hydrobiologia* 532: 91–102.

Hawkins JW (2004) Predictability of surface mine spoil hydrologic properties in the Appalachian plateau. *Ground Water* 42: 119-125.

Hawkins JW, Aljoe JA (1990) Hydrologic characterization and modeling of a heterogeneous acid-producing surface coal mine spoil, Upshur County, WV. Proceedings of the National Symposium of Mining, University of Kentucky, pp 43-52.

Herman EK, Toran L, White WB (2008) Threshold events in spring discharge: Evidence from sediment and continuous water level measurement. *J. Hydrol.* 351: 98-106.

House WA, Warwick MS (1998) Hysteresis of the solute concentration/discharge relationship in rivers during storms. *Water. Resour.* 32: 2279–2290.

Huang X, Sillanpaa M, Gjessing E, Peraniemi S, Vogt R (2010) Environmental impacts of mining activities on the surface water quality in Tibet: Gyana Valley. *Sci. Total Environ.* 408: 4177-4184.

Jorgensen DW, Gardner TW (1987) Infiltration capacity of disturbed soils: temporal change and lithologic control. *Water Resour. Bull.* 23: 1161-1172.

Lewis WM, Grant MC (1979) Relations between stream discharge and yield of dissolved substances from a Colorado mountain watershed. *Soil Sci. Soc. Am. J.* 128: 353-363.

Lindberg TT, Bernhardt ES, Bier R, Helton AM, Merola RB, Vengosh A, DiGiulio RT (2011) Cumulative impacts of mountaintop mining on an Appalachian watershed. *P. Nat. Acad. Sci. USA* 108:20929-20934.

Magnusson J, Kobierska F, Huxol S, Hayashi M, Jonas T, Kirchner JW (2014) Melt water driven stream and groundwater stage fluctuations on a glacier forefield. *Hydrol. Process.* 28: 823-836.

McDonnell J (1990) A rationale for old water discharge through macropores in a steep, humid catchment. *Water Resour. Res.* 26: 2821-2832.

McMahon G, Bales JD, Coles JF, Giddings EM, Zappia H (2003) Use of stage data to characterize hydrologic conditions in an urbanizing environment. *J. Am. Water Resour. As.* 39: 1529-1546.

Meissner, CR (1978) Geologic map of the Duty quadrangle, Dickenson, Russell, and Buchanan Counties, Virginia. US Geological Survey, Geologic Quadrangle Map GQ-1458.

Merricks TC, Cherry DS, Zipper CE, Currie R, Valenti T (2007) Coal-mine hollow fill and settling pond influences on headwater streams in southern West Virginia, USA. *Environ. Monit. Assess.* 129:359–378.

Messinger T, Paybins KS (2003) Relations between precipitation and daily and monthly mean flows in gaged, unmined and valley-filled watersheds, Ballard Fork, West Virginia, 1999-2001 USGS Report WRi no.2003-4113.

Miller AJ, Zegre NP (2014) Mountaintop Removal Mining and Catchment Hydrology. *Water* 6:472-479.

Miller WR, Drever JI (1977) Water chemistry of a stream following a storm, Absaroka Mountains, Wyoming. *Geol. Soc. Am. Bull.* 88: 286-290.

Murdoch PS, Shanley JB (2006) Detection of water quality trends at high, median, and low flow in a Catskill Mountain stream, New York, through a new statistical method. *Water Resour. Res.* 42:W08407.

Murphy JC, Hornberger JM, Liddle RG (2014) Concentration-discharge relationships in the coal mined region of the New River basin and Indian Fork sub-basin, Tennessee, USA. *Hydrol. Process.* 28:718-728.

Nash WL, Daniels WL, Haering KC, Burger JA, Zipper CE (2016) Long-term effects of rock type on Appalachian coal mine spoil properties. *J. Environ. Qual.* doi:10.2134/jeq2015.10.0540.

National Oceanic and Atmospheric Administration (NOAA) (2016) National Centers for Environmental Information. Climate Data Online. http://www.ncdc.noaa.gov/cdo-web/

Negley T, Eshleman K (2006) Comparison of stormflow responses of surface-mined and forested watersheds in the Appalachian mountains, USA. *Hydrol. Process.* 20: 3467-3483.

Nolde JE, Lovett JA, Whitlock WW, Miller RL (1986) Geology of the Norton quadrangle, Virginia. Virginia Division of Mineral Resources, Publication 65.

Orndorff ZW, Daniels WL, Zipper CE, Eick M, Beck M (2015) A column evaluation of Appalachian coal mine spoils' temporal leaching behavior. *Environ. Pollut.* 204: 39-47.

Phillips JD (2004) Impacts of surface mine valley fills on headwater floods in eastern Kentucky. *Environ. Geol.* 45: 367–380.

Pond GJ, Passmore ME, Borsuk FA, Reynolds L, Rose CJ (2008) Downstream effects of mountaintop coal mining: comparing biological conditions using family- and genus-level macroinvertebrate bioassessment tools. *J. N. Am. Benthol. Soc.* 27: 717–737.

Pond GJ, Passmore ME, Pointon ND, Felbinger JK, Walker CA, Krock KJ, Fulton JB, Nash WL (2014) Long-term impacts on macroinvertebrates downstream of reclaimed mountaintop mining valley fills in central Appalachia. *Environ. Manag.* 54: 919–933.

Rice KC, Chanat JG, Hornberger GM, Webb JR (2004) Interpretation of concentration-discharge patterns in acid-neutralizing capacity during storm flow in three small, forested catchments in Shenandoah National Park, Virginia. *Water Resour. Res.* 40: W05301

Ross LC (2015) Effect of Leaching Scale on Prediction of Total Dissolved Solids Release from Coal Mine Spoils and Refuse. M.S. Thesis, Virginia Polytechnic Institute and State University.

Shuster WD, Zhang Y, Roy AH, Daniel FB, Troyer M (2008) Characterizing storm hydrograph rise and fall dynamics with stream stage data. *J. Am. Water Resour. As.* 44: 1431-1440.

Skousen JG, Sexstone A, Ziemkiewicz PF (2000) Acid mine drainage control and treatment. In: Barnhisel, R.I. et al. (Eds.), Reclamation of Drastically Disturbed Lands. Agronomy Monographs. #41. ASA, CSSA, and SSSA, Madison, WI, pp 131-168.

Southeast Regional Climate Center (2016a) Spring Freeze Possibilities (Jan. –Jul. 31): Wise, VA. http://www.sercc.com/cgi-bin/sercc/cliMAIN.pl?va9215.

Southeast Regional Climate Center (2016b) Fall Freeze Possibilities (Jul. 31-Dec. 31): Wise, VA. http://www.sercc.com/cgi-bin/sercc/cliMAIN.pl?va9215.

Stump DE (2001) Customized techniques for interpretation of suspended sediment data. Proceedings of the Seventh Federal Interagency Sedimentation Conference, Reno NV, pp 12–19.

Timpano AJ, Schoenholtz SH, Zipper CE, Soucek DJ (2010) Isolating Effects of Total Dissolved Solids on Aquatic Life in Central Appalachian Coalfield Streams. In: Proceedings, National Meeting of the American Society of Mining and Reclamation, Pittsburgh, PA, pp 1284-1302.

Timpano AJ, Schoenholtz SH, Soucek DJ, Zipper CE (2015) Salinity as a limiting factor for biological condition in mining-influenced Central Appalachian headwater streams. *J. Am. Water Resour. As.* 51: 240-250.

US EPA (2003) Mountaintop Mining/Valley Fills in Appalachia Draft Programmatic Environmental Impact Statement. EPA 9-03-R-00013.

US EPA (2011) The Effects of Mountaintop Mines and Valley Fills on Aquatic Ecosystems of the Central Appalachian Coalfields. EPA/600/R-09/138F.

Walling DE, Webb BW (1980) The spatial dimension in the interpretation of stream solute behavior. *J. Hydrol*. 47: 129–149.

Williams GP (1989) Sediment concentration versus water discharge during single hydrologic events in rivers. *J. Hydrol.* 111:89-106.

Younger PL, Wolkersdorfer C (2004) Mining impacts on the fresh water environment: technical and managerial guidelines for catchment scale management. *Mine Water and the Environment* 23: 2-80.

Zipper CE, Burger JA, McGrath JM, Rodrigue JA, Holtzman GI (2011) Forest restoration potentials of coal-mined lands in the eastern United States. *J. Environ. Qual.* 40:1567-1577.

CHAPTER VII: Summary and Conclusions

These four studies contribute to improved scientific understanding of hydrologic and hydrochemical processes occurring on mine spoils fills.

7.1 Research Summary

In Chapter III, the near-surface hydrologic properties of mine soils on two southwest Virginia mine spoil fills were characterized via infiltration tests and dye staining analyses. Both mine spoil fills were reclaimed fourteen years prior to analysis, were adjacent to one another on the same mine site, and had similar characteristics such as slope, aspect, and the materials used for soil construction. However, one site was reclaimed with trees and the other reclaimed with grasses. Results indicated that the reforested area had higher infiltration rates and hydraulic conductivities relative to the area reclaimed with grasses. This study also found that both matrix and preferential flows occurred in the near-surface zone of both mine soils, with apparent transitions between vegetation-controlled and abiotic-controlled flow pathways deeper in the subsurface.

In Chapter IV, a five-parameter nonlinear model consisting of an exponential decay function combined with a linear function was developed and applied to describe the SC leaching patterns of 39 non-acid-forming Appalachian mine spoil samples placed in laboratory leaching columns and subjected to 40 sequential leaching events. All tested mine spoils produced high SCs within the first few leaches, and all leachate SCs declined in an exponential decay pattern in subsequent leaches. After exponential decay, the leaching pattern became linear after ~5-7 pore volumes or Leach 16 on average. The linear slopes of most samples were significantly declining or had slopes that were not

significantly different from zero but nominally declining in the linear phase. Waters eluted during the linear phase of leaching were in the range of 250 to 300 µS cm^{-1} on average, which is higher than the SCs typically found in forested reference streams (25-200 µS cm^{-1}; Hartman et al. 2005; Pond et al. 2014), but similar to the lower range of aquatic effect thresholds such as the 300 µS cm^{-1} benchmark intended to prevent >5% of aquatic macrobenthic genera extirpation (Cormier et al. 2013). The measured total S and neutralization potentials of the mine spoil samples predicted four of the five SC leaching model parameters.

Using a subset (n = 26) of the mine spoil samples placed into leaching columns and modeled in Chapter IV, Chapter V extended the exponential decay and linear slope segmented regression model to describe the leaching patterns of major, mine water, and trace elements. All analytes except Fe and HCO_3^- conformed to the exponential decay and linear slope segmented regression model. Bicarbonate leaching patterns were the inverse of all other analytes and thus were modeled with a segmented growth and linear function model. The major elements (S, Ca, Mg, Na, and K) produced leaching patterns similar to one another, and those patterns resembled those of SC as described in Chapter IV. Comparatively, two of three mine water (Al, Mn) and all trace elements (As, Cd, Cu, Ni, Pb, and Se) stabilized (i.e. the linear slope was not significantly different from zero) earlier in the leaching period than the major elements. The leaching patterns were interpreted to infer the geochemical weathering mechanisms governing elemental release within mine spoils. Pyrite oxidation and carbonate dissolution appeared to be the two most influential geochemical drivers of leaching patterns. During the exponential decay phase of leaching, both of these weathering processes likely slowed due to Fe-precipitates

coating mineral surfaces and limiting the interaction of water and oxygen with minerals. These coatings can retain trace elements, which may explain the earlier stabilization of trace elements relative to major elements. Certain elements, especially Se, were leached at concentrations elevated above ecotoxicological thresholds for aquatic life during all phases of leaching, but most elements were at concentrations below those associated with aquatic macroinvertebrate impacts.

In Chapter VI, five Appalachian VFs were continuously monitored for SC and stage over a one-year period to determine SC-Stage relationships in VF streams. Results indicated that VF streams generally have the lowest stages in summer and highest stages in winter, which corresponds to the highest SC levels during summer and lowest SC values on average during winter. Of the 97 storm events analyzed, SC was diluted as stage increased in all storms, although the relative dilution of SC differed for all sites and seasons. The SC-Stage relationships were interpreted to suggest that infiltration-excess overland flow dominated storm discharge responses in some storm events, whereas other storm events promoted infiltration into the VF interior, resulting in delayed SC dilution in the discharge waters as water flowed through subsurface voids.

7.2 Hydrologic and Hydrochemical Processes of Mine Spoil Fills

Collectively, these four studies can be used to infer hydrologic and hydrochemical processes occurring on mine spoil fill surfaces, within mine spoil fills, and in mine spoil fill discharges.

7.2.1 Surficial Hydrologic Processes of Mine Spoil Fills

Mine spoil fill surfaces have been shown to be compact, and are often associated with very low initial infiltration rates (<1 cm hr^{-1}) that may increase over time as flow

paths that direct water into the subsurface develop (Jorgensen and Gardner 1987; Ritter and Gardner 1993; Guebert and Gardner 2001). Infiltration rates on 14-year-old mine soils were found to range from 1.4 to 38.2 cm hr^{-1} (Clark and Zipper 2016; Chapter III), and although infiltration rates were not measured initially after mining at those same sites, results suggest that mine soils can develop relatively high infiltration rates over time. Such increases in infiltration rates were attributed to vegetation establishment and the occurrence of both matrix and preferential flow paths that directed surficial waters into the subsurface (Clark and Zipper 2016; Chapter III).

7.2.2 Hydrologic and Hydrochemical Processes within Mine Spoil Fills

Dye staining experiments revealed the presence of both matrix and preferential flow paths in the shallow subsurface (< 30 cm) of mine spoil fills (Clark and Zipper 2016; Chapter III). Greer (2015) similarly identified preferential flow paths in a mine spoil fill, although these flow paths penetrated much deeper (~15 m) into the subsurface. Both of these studies concluded that subsurface flow likely occurred as flow through voids and cracks that were created during mine spoil placement, or by vegetative establishment in near-surface spoils.

Flow paths direct O_2 and H_2O into the subsurface, thus TDS generation within mine spoil fills likely occurs in conjunction with infiltrated water movement through the subsurface. Since the mine spoils that comprise mine spoil fills contain silicates, carbonates, and trace amounts of sulfide minerals (Johnson 2016), water-rock interaction in the subsurface initiates mineral weathering. Based on laboratory studies of Appalachian mine spoils, it appears that TDS generation is rapid initially, then slows over time as pyrite oxidation and carbonate dissolution reactions reach an equilibrium

(Orndorff et al. 2015; Daniels et al. 2016; Clark et al. 2017; Chapters IV and V). Appalachian mine spoil leaching patterns in laboratory studies resemble those of field-leached mine spoils (Daniels et al. 2016). The decline of TDS release in both laboratory and field-leaching studies is likely due to several factors, including Fe-coatings preventing weathering reactions from occurring in the internal portions of mineral grains (Chapters IV and V).

7.2.3 Mine Spoil Fill Discharge Hydrology and Hydrochemistry

It is well-established that VFs release waters with TDS concentrations elevated above those of undisturbed watersheds (Hartman et al. 2005; Pond et al. 2008, 2014). A study of five Appalachian VFs aged 2.5 to 20 years after construction found that SCs were generally $\geq$ 500 µS cm^{-1} during both baseflow and stormflow conditions (Clark et al. 2016; Chapter VI), indicating that SC levels discharged from these VFs were above the 300 and 500 µS cm^{-1} benchmarks for aquatic impacts (Pond et al. 2008; Cormier et al. 2013) during all flow conditions.

In 97 storm events analyzed from the same five Appalachian VFs, infiltration-excess overland flow was evident in the hydrographs of certain storm events, whereas internal storage and flow through the VF was interpreted to occur in other storm events (Clark et al. 2016). Such storage and transport of infiltrated waters through "pseudokarst features" within the VF was previously hypothesized by various studies (Caruccio and Geidel 1995; Hawkins 2004; Miller and Zegre 2014). Greer (2015) found that artificially-applied rainwater infiltrated up to 15 m deep within a VF and was stored in subsurface voids, indicating that it is likely that such internal transport and storage is occurring in VFs.

7.3 Implications

In order to detail specific recommendations for spoil management, the overall transport of water through a mine site must first be described. As rainwater falls onto a mine site, some of it directly runs off to a stream via overland flow, especially for large storm events. This overland flow has limited contact with mine spoils and thus in most cases will be unlikely to pose any issues for TDS management. When smaller storms occur on mine spoils with established vegetation, much of the rainfall will likely infiltrate into the mine spoil subsurface. Some of that rainwater will be retained in the near-surface and stored as soil moisture, whereas other water infiltrates deeper via preferential flow paths. Along those flowpaths, mineral weathering and soluble ion release and transport will typically occur and continue with subsequent storm events. Eventually, these infiltrated waters, as well as any groundwater entering the VF from adjacent areas, will discharge to a stream as baseflows, often with high TDS concentrations in the initial phase after mine spoil placement. As storm events occur, the TDS will be temporarily diluted by runoff and/or rapid throughflow (if enabled by the internal VF structure) until flow levels return to baseflow conditions.

Collectively, these results and detailed flow processes can inform mining companies about TDS management strategies. Since TDS treatment options after release are limited, it is essential to minimize TDS generation during and following the mining process. Pre-testing of spoils prior to mining will assist mine operators with deciding where to place particular geologic strata during reclamation. Testing the spoils by determining paste SC and total S, which are relatively easy tests that can be completed

quickly in a laboratory, will result in values that can be interpreted to infer potential TDS releases (Chapter IV).

Samples with low paste SC values (< 500 µS cm^{-1}) and total S (< 0.05%) corresponded to peak SC values of < 700 µS cm^{-1} and asymptote SC values < 200 µS cm^{-1} in the leaching column experiment (Chapter IV). Given these relationships, samples within those paste SC and total S guidelines may be placed on the surface with the highest water-rock contact potential. Generally, brown weathered sandstones originating from geologic strata closest to the surface prior to mining are the best materials to use for high water-rock interaction zones such as the surface of the reconstructed landform and in VFs if mining operations allow. When the post-mining land use is to be reforested, a blend of weathered spoils and salvaged soils (if available) is ideal for promoting tree growth. Spoils that originate from deeper geologic strata could potentially have lower paste SCs and total S values and may also be viable materials for high water-rock interaction areas such as VFs.

For spoil samples with paste SC values > 1,500 µS cm^{-1} and total S > 0.10%, the corresponding leaching column experiment results were peak SCs of ~2,000 – 4,500 µS cm^{-1} and asymptote SCs of ~500 – 600 µS cm^{-1}. Such results corresponded to unweathered mudstones and finer-grained spoils originating from deeper in the geologic strata. Thus, those samples originating from closer to the coal seam have greater potentials to release high TDS and should not be placed in high water-rock contact areas. These spoils should be either isolated away from hydrologic flows or highly compacted with multiple bulldozer passes to prevent water infiltration into the materials.

It is advised that mining firms test all rock materials prior to mining. Although specific paste SC and total S values are described above, those values should not be considered as fixed guidelines for spoil testing. A general guideline is as follows: Mine rock samples with the lowest TDS-generation potentials (i.e. relatively low Paste SC and total S values) may be placed in high water-rock contact areas, whereas it is advised to place rock samples with the highest TDS-generation potentials isolated away from hydrologic flows to the greatest extent possible.

The leaching column experiment values for peak and asymptote SC values should be used as general guidelines for TDS-generation potentials and not as estimates of actual TDS concentrations that would occur after mining in the field. Preliminary field studies indicate that actual TDS concentrations released are often higher than the concentrations generated by column leaching for the same materials (unpublished data). Actual TDS discharges may be higher in the field than in laboratory results due to larger volumes of materials, variable climate (i.e. precipitation amounts, drought, etc.), and longer flow paths and water-rock contact times for infiltrated waters.

Runoff control on mine sites is also essential, and planting trees in suitable soils or topsoil amendments on mined areas on mined areas is typically recommended for promoting forest ecosystem re-establishment, controlling runoff, and reduction of peak flows in downstream areas. Trees, however, promote rainwater infiltration to the subsurface, enabling TDS generation in the fractured mine spoils. Thus, it is advised to highly compact higher-TDS materials with multiple dozer passes, then loose-dump the lowest TDS-generation potential spoils on top of the compacted layer in a thickness adequate for tree growth. Such construction is intended to promote infiltration into the

soils and prevent runoff, but will only enable subsurface flow through rocks with the lowest TDS-production potentials. Although this type of treatment is intended to restore hydrologic functions similar to natural landforms on mine sites, field-scale trials to test such restoration have not been implemented.

7.4 Conclusions

This research was intended to improve scientific understanding of the hydrologic and hydrochemical processes occurring on mine spoil fills in Appalachia. It was found that the surficial and near-surface hydrologic properties and processes on 14-year-old reclaimed landforms significantly differed by vegetation type. The SC release patterns of 39 mine spoil samples were modeled with a five-parameter exponential decay and linear function segmented regression model, and model parameter values had predictive relationships with total S and neutralization potential. Major, mine water, and trace element release patterns were also modeled with the same five-parameter segmented regression model, and the bulk chemistry, model parameters and depletion percentages differed among elements. Lastly, the baseflow and stormflow hydrochemistries and SC-Stage relationships in VFs differed by site, precipitation amounts, vegetative cover and season. Overall, research findings have contributed to improving the scientific understanding of the hydrologic and hydrochemical processes occurring on Appalachian mine spoil fills.

7.5 Areas for Future Research

There are many potential areas for future research on the hydrology and hydrochemistry of mine spoil fills. Mine soils of varying ages should be compared to undisturbed soils to determine if the hydrologic properties of mine soils begin to

resemble those of natural landforms over time, and how long it takes for those properties to develop in mine soils. More research is needed to determine water flow paths deeper in valley fills, as those flow paths ultimately influence SCs and discharge patterns from VFs. Such research could be accomplished with tracers, isotopes, and geochemical characterizations of groundwater, spoil waters that have been stored in the VF for a long period of time (i.e. "old waters"), and recently-infiltrated waters (i.e. "new waters") that travel through the VF.

It is still unknown how and if TDS levels in mining-influenced streams will decline to natural background levels over time. Thus, future research should incorporate more field studies that characterize hydrogeochemical changes occurring in VFs over time. Such studies should be long-term efforts that enable characterization of temporal changes in TDS release from mine spoils in order to determine (a) how long it will take for TDS release to decline in streams, (b) what factors influence the decline in TDS release, (c) how stream chemistry changes over time, and (d) how all of these factors influence ecosystem recovery in mining-influenced streams.

7.6 REFERENCES

Caruccio FT, Geidel G (1995) Status Report: Long-Term Effects of Alkaline Trenches and Funnels at the Mercer Site. West Virginia Surface Mine Drainage Task Force Symposium: Morgantown, WV, USA.

Clark EV, Greer BM, Zipper CE, Hester ET (2016) Specific conductance-stage relationships in Appalachian valley fill streams. *Envi. Earth Sci.* 75: 1222.

Clark EV, Zipper CE (2016) Vegetation influences near-surface hydrological characteristics on a surface coal mine in eastern USA. *Catena* 139: 241-249.

Clark EV, Zipper CE, Daniels WL, Orndorff ZW, Keefe MJ (2017) Modeling patterns of total dissolved solids release from Central Appalachia, USA mine spoils. *J. Envi. Qual.* 46:55-63.

Cormier SM, Suter GW, Zheng L (2013) Derivation of a benchmark for freshwater ionic strength. *Environ. Toxicol. Chem*. 32:263-271.

Daniels WL, Zipper CE, Orndorff ZW, Skousen JG, Barton CD, McDonald L, Beck M (2016) Predicting total dissolved solids release from central Appalachian coal mine spoils. *Environ. Pollut.* 216:371-379.

Greer BM (2015) Electrical Resistivity Imaging of Preferential Flow through Surface Mine Valley Fills with Comparison to Other Land Forms. M.S. Thesis, Virginia Tech.

Guebert MD, Gardner TW (2001) Macropore flow on reclaimed surface mines: infiltration and hillslope hydrology. *Geomorphology* 39: 151-169.

Hartman KJ, Kaller MD, Howell JW, Sweka JA (2005) How much do valley fills influence headwater streams? *Hydrobiologia* 532: 91–102.

Hawkins JW (2004) Predictability of surface mine spoil hydrologic properties in the Appalachian plateau. *Ground Water* 42: 119-125.

Johnson D (2016) Geochemical Properties of Soils and Associated Overburden of the Pottsville Group in Central Appalachia. Virginia Polytechnic Institute and State University. Ph.D. Dissertation.

Jorgensen DW, Gardner TW (1987) Infiltration capacity of disturbed soils: temporal change and lithologic control. *Water Resour. Bull.* 23: 1161-1172.

Miller AJ, Zegre NP (2014) Mountaintop Removal Mining and Catchment Hydrology. *Water* 6:472-479.

Orndorff ZW, Daniels WL, Zipper CE, Eick M, Beck M (2015) A column evaluation of Appalachian coal mine spoils' temporal leaching behavior. *Environ. Pollut.* 204: 39-47.

Pond GJ, Passmore ME, Borsuk FA, Reynolds L, Rose CJ (2008) Downstream effects of mountaintop coal mining: comparing biological conditions using family- and genus-level macroinvertebrate bioassessment tools. *J. N. Am. Benthol. Soc.* 27: 717–737.

Pond GJ, Passmore ME, Pointon ND, Felbinger JK, Walker CA, Krock KJ, Fulton JB, Nash WL (2014) Long-term impacts on macroinvertebrates downstream of reclaimed mountaintop mining valley fills in central Appalachia. *Environ. Manag.* 54: 919-933.

Ritter JB, Gardner TW (1993) Hydrologic evolution of drainage basins disturbed by surface mining, Central Pennsylvania. *Geol. Soc. Am. Bull.* 105: 101-115.

APPENDIX A. Mine Soil Infiltration Rates and Hydraulic Conductivities

Vegetation Type	Transect Location*	Infil. Rate (cm h^{-1})	Hydr. Cond. (k; cm s^{-1})
Reforested	150T1	9.0	0.0014
	150T2	3.2	0.00052
	150T3	2.5	0.00041
Reforested	150M1	13.0	0.00050
	150M2	14.4	0.00055
	150M3	9.7	0.00037
Reforested	150L1	17.3	0.0028
	150L2	29.9	0.0048
	150L3	10.8	0.0017
Reforested	100T1	27.0	0.0019
	100T2	38.2	0.0027
	100T3	36.0	0.0026
Reforested	100M1	22.7	0.0036
	100M2	14.4	0.0023
	100M3	11.9	0.0019
Reforested	100L1	28.8	0.0014
	100L2	18.7	0.00093
	100L3	32.8	0.0016
Reforested	50T1	19.1	0.0014
	50T2	7.6	0.00054
	50T3	1.4	0.00010
Reforested	50M1	5.8	0.00022
	50M2	12.6	0.00048
	50M3	9.0	0.00034
Reforested	50L1	78.1	0.0039
	50L2	68.8	0.0034
	50L3	57.6	0.0029

Vegetation Type	Transect Location*	Infil. Rate (cm h^{-1})	Hydr. Cond. (k; cm s^{-1})
Grassed	175L1	5.0	0.00025
	175L2	9.0	0.00045
	175L3	13.3	0.00066
Grassed	175M1	14.4	0.00071
	175M2	11.2	0.00055
	175M3	45.0	0.0022
Grassed	175T1	11.9	0.00085
	175T2	24.5	0.0017
	175T3	3.6	0.00026
Grassed	100L1	4.0	0.00015
	100L2	10.4	0.00040
	100L3	15.1	0.00058
Grassed	100M1	52.2	0.0037
	100M2	96.5	0.0069
	100M3	144.0	0.010
Grassed	100T1	4.7	0.00033
	100T2	3.6	0.00026
	100T3	7.6	0.00054
Grassed	25L1	2.5	0.00012
	25L2	5.0	0.00025
	25L3	27.4	0.0014
Grassed	25M1	17.6	0.00087
	25M2	28.1	0.0014
	25M3	8.6	0.00043
Grassed	25T1	3.6	0.00026
	25T2	3.6	0.00026
	25T3	5.8	0.00041

* Mine spoil fill surfaces were divided into grid patterns with vertical and horizontal transects (lower=L, middle=M, top=T). Three infiltration measurements were taken at each transect location

APPENDIX B. Nonlinear Segmented Exponential Decay and Linear Regression R Code

```
#Model for SC, Ca, Mg, S, Na, K, Mn, Al, As, Cu, Ni, Se ;  Iron and Bicarbonate do not conform to this model
#read in data
>dat <- read.csv("C:/Users/Elyse/Google
Drive/VTFiles/x_SC_LeachateModeling/RawData/EXP_Clark_ConductivityData.csv")

#write function for three parameter exponential then linear component
>exp3breakpoint<-function(x,theta1,theta2,theta3,b1,BP){
  (x<BP)*(theta1+theta2*exp(-theta3*x)) + (x>=BP)*(theta1+theta2*exp(-theta3*BP) - b1*BP + b1*x)}

#WV 1 Model
>plot(dat$LEACH..,dat$WV1)
>points(seq(0,40,.01),exp3breakpoint(seq(0,40,.01),theta1=328,theta2=1100,theta3=0.5,b1=4,BP=10),type='l',
          col="blue")

>model.wv1<nls(WV1~exp3breakpoint(LEACH..,theta1,theta2,theta3,b1,BP),start=c(theta1=328,theta2=1100
          ,theta3=0.5,b1=4,BP=10),dat=dat,trace=T)
>summary(model.wv1)
>plot(dat$LEACH..,dat$WV1,xlab="Leach",ylab="WV1",title(main="WV1 Model"))
>newdat = data.frame(LEACH.. = seq(min(dat$LEACH..),max(dat$LEACH..),len=200))
>lines(newdat$LEACH..,predict(model.wv1,newdata=newdat),col="black",lwd=2)
>lines(newdat$LEACH..,coef(model.wv1)[1]+coef(model.wv1)[2]*exp(coef(model.wv1)[3]*newdat$LEACH
          ..),col="orange")
>lines(newdat$LEACH..,(coef(model.wv1)[1]+coef(model.wv1)[2]*exp(-
          coef(model.wv1)[3]*coef(model.wv1)[5]) - coef(model.wv1)[4]*coef(model.wv1)[5] +
          coef(model.wv1)[4]*newdat$LEACH..),col="green")
>plot(fitted.values(model.wv1),residuals(model.wv1))
```

APPENDIX C. Specific Conductance Nonlinear Segmented Regression Model Results

ID	ROCK*	WX Type*	Θ2-Peak SC (µS cm^{-1})	Θ3- Decay Constant	BP	β1-Linear Slope (Sig.) †	Θ1-Asymptote SC (µS cm^{-1})
WV1	SS	UW	1,094	0.54	13	2.7 (I)	351
WV2	SS	UW	1,092	0.34	23	7.1 (I)	314
WV3	MUD	UW	609	0.18	17	3.1 (I)	294
WV4	SS	UW	462	0.29	8	3.8 (I)	211
WV5	SS	UW	1,278	1.21	20	8.8 (I)	542
WV6	MXR	UW	539	0.29	17	-1.4 (D)	152
WV8	SS	MXW	1,009	0.26	34	-4.3 (D)	261
WV9	SS	UW	1,215	0.87	38	16 (I)	160
WV10	SS	UW	590	0.25	20	4.1 (I)	259
WV11	SS	UW	604	0.46	13	-0.9 (C)	165
WV14	MXR	UW	712	0.40	27	2.8 (I)	233
VA1	SS	UW	1,818	0.43	12	-5.4 (D)	346
VA3	MXR	MXW	1,323	0.31	16	-5.4 (D)	215
VA4	MUD	WX	285	0.52	22	-4.6 (D)	196
VA5	SS	MXW	1,219	0.24	20	-2.6 (D)	143
VA6	SS	UW	1,955	0.15	19	-11.7 (D)	612
VA7	MUD	WX	215	0.06	24	-1.7 (D)	50
VA8	MUD	UW	2,015	0.23	16	-1.5 (C)	450
VA9	MXR	MXW	575	0.21	14	-0.5 (C)	223
VA10	MUD	UW	921	0.23	13	4.9 (D)	488
VA11	SS	WX	789	0.19	13	-1.9 (D)	86
VA12	SS	UW	678	0.12	12	-3.6 (D)	317
VA13	SS	MXW	563	0.18	12	-1.4 (D)	139
VA14	SS	WX	626	0.20	25	-3.5 (D)	205
VA15	MUD	UW	496	0.07	26	0.3 (C)	200
KY1	SS	WX	1,333	0.91	7	-2.2 (D)	102
KY2	SS	UW	661	0.66	8	1.8 (D)	339
KY3	MXR	MXW	2,121	0.55	11	-4.9 (D)	412
KY4	MUD	UW	2,964	0.24	9	-12.8 (D)	332
KY5	MUD	WX	1,133	1.61	2	-4.4 (D)	164
KY6	MUD	WX	34	0.17	31	0.9 (I)	34
KY8	MUD	UW	2,326	0.24	18	-3.8 (D)	500
KY9	MXR	UW	3,702	0.13	20	-11.1 (D)	650
KY10	SS	MXW	4,480	0.21	19	-1.2 (C)	300
KY11	MXR	UW	783	0.17	17	1.8 (D)	300

* Abbreviations: SS = sandstone, MUD = mudstone, MXR = mixed rock; UW = unweathered, WX = weathered, MXW = mixed weathering.

†I=significantly increasing slope ($p \leq 0.05$), D=significantly decreasing slope ($p \leq 0.05$), C= constant slope (i.e. slope not significantly different from zero, $p > 0.05$).

APPENDIX D. Nonlinear Segmented Growth and Linear Regression R Code

```
# Bicarbonate and pH Leaching Pattern Modeling
#read in data
>dat <- read.csv("C:/Users/Elyse/Google Drive/VT
Files/Leachateproject/NEW_LeachateandDepletionAnalyses/CSVs/HCO3_mg.csv")

#write function for three parameter exponential then linear component
>growth.breakpoint<-function(x,theta1,theta2,theta3,b1,BP){(x<BP)*(theta1*(1-theta2*exp(-
        theta3*x))) + (x>=BP)*(theta1*(1-theta2*exp(-theta3*BP)) - b1*BP + b1*x)}

#NO DATA FOR VA1-4,6-7,10-12,14

#WV 1 Model
>plot(dat$LEACH..,dat$WV1)
>points(seq(0,40,.01),exp3breakpoint(seq(0,40,.01),theta1=328,theta2=1100,theta3=0.5,b1=4,BP
        =10),type='l',col="blue")

>model.WV1<-nls(WV1~growth.breakpoint(LEACH..,theta1,theta2,theta3,b1,BP),
>start=c(theta1=5,theta2=1,theta3=0.5,b1=0.04,BP=8),dat=dat,trace=T)
>summary(model.WV1)
>plot(dat$LEACH..,dat$WV1)
>newdat = data.frame(LEACH.. = seq(min(dat$LEACH..),max(dat$LEACH..),len=200))
>lines(newdat$LEACH..,predict(model.WV1,newdata=newdat),col="black",lwd=3)
>lines(newdat$LEACH..,(coef(model.WV1)[1]*(1-coef(model.WV1)[2]*exp(-
        coef(model.WV1)[3]*newdat$LEACH..))),col="orange")
>lines(newdat$LEACH..,(coef(model.WV1)[1]*(1-coef(model.WV1)[2]*exp(-
        coef(model.WV1)[3]*coef(model.WV1)[5])) -
        coef(model.WV1)[4]*coef(model.WV1)[5] +
        coef(model.WV1)[4]*newdat$LEACH..),col="green")
```

APPENDIX E. Major, Mine Water and Trace Element Depletion Percent Results

ID	S	Ca	Mg	K	Na	Al	Mn	As	Cu	Ni	Se
WV1	30	102	23.2	1.2	2.8	0.010	30.4	0.2	2.2	8.3	7.1
WV2	60	57	22.2	1.0	2.1	0.0083	9.4	0.2	2.2	1.9	
WV3	150	26	4.5	2.2	6.1	0.0033	0.1	0.4	0.6	0.4	
WV4	133	42	12.3	1.1	3.2	0.0075	1.4	0.4	2.2	0.7	5.2
WV5	96	13	8.7	1.8	2.0	0.0018	0.2	0.5	0.4	0.3	
WV6	117	23	3.8	0.2	1.4	0.0087	0.3	0.2	0.5	0.2	
WV8	68	34	5.9	0.7	1.4	0.0063	2.3	0.4	0.9	0.6	4.7
WV9	97	45	8.9	1.2	4.1	0.019	7.4		2.6	1.3	6.0
WV10	44	24	6.4	1.5	2.4	0.0078	0.4		0.8	0.2	8.4
WV11	124	124	3.9	1.1	3.1	0.016			2.5	1.3	9.5
WV14	89	22	4.6	0.7	1.7	0.0017	3.2		0.2	1.0	1.8
VA5	177	26	6.7	0.3	1.1	0.0009	8.2		0.2	2.0	
VA8	434	116	16.3	2.6	6.9	0.0062	8.9		3.0	26.3	58.1
VA9	76	14	4.3	0.6	0.8		0.3		0.4	0.3	
VA13	73	19	5.6	0.5	0.6		0.2		0.8	0.5	
VA15	66	6	--	1.0	11.8	0.0052			0.4	0.3	19.5
KY1	205	41	8.2	0.1	1.9	0.033	2.0		1.2	1.0	1.0
KY2	120	13	16.7	0.9	1.6	0.0032	0.1		0.5	0.3	3.4
KY3	128	18	20.1	1.3	2.1	0.0044	0.2		0.3	0.7	8.9
KY4	629	91	23.7	3.5	10.8	0.025	4.5	1.1	3.7	40.0	233.0
KY5	28	19	1.7	0.2	0.2	0.0010	0.4		0.1	0.2	
KY6	99	5	0.6	0.1	0.6	0.0065	0.1		0.1	0.3	
KY8	143	102	10.6	1.5	3.9	0.0044	2.0		0.1	1.1	
KY9	232	146	37.3	1.5	1.2	0.0015	20.7		0.1	7.9	
KY10	614	147	33.0	0.5	0.9	0.0095	56.0		0.3	28.7	
KY11	103	50	8.0	0.9	2.4		0.2	0.6	0.2	0.6	

APPENDIX F. Specific Conductance-Stage Storm Event Hysteresis Results

Storm	Mo.	Day	Year	Type*	Rain (mm)	Site	Season†	Δ Level (cm)	Max SC (µS cm^{-1})	Min SC (µS cm^{-1})
1	12	8	2013	CC3	17	BH	W	12.2	927	571
2	12	16	2013	CC3	5	BH	W	2.9	968	596
3	12	28	2013	CC3	25	BH	W	4.6	987	844
4	2	8	2014	CC3	25	BH	W	15.2	1,001	297
5	2	28	2014	CC3		BH	W	7.3	1,013	608
6	3	5	2014	CC3	20	BH	SP	6.6	947	625
7	4	30	2014	C1	9	BH	SP	7.6	961	625
8	5	13	2014	C3	12	BH	SP	7.3	879	306
9	5	17	2014	C3	31	BH	SP	6.3	793	302
10	6	12	2014	C3	19	BH	SU	4.5	776	341
11	8	11	2014	C3	16	BH	SU	4.2	1,133	791
12	9	6	2014	C1	5	BH	F	15.1	1,188	186
13	9	12	2014	NA	10	BH	F	6.6	1,193	190
14	9	14	2014	C3	3	BH	F	8.5	1,004	263
15	10	7	2014	C3	37	BH	F	13.2	1,580	523
16	10	8	2014	C3	6	BH	F	5.3	1,728	786
17	10	14	2014	C3	27	BH	F	8.8	1,882	285
18	12	22	2013	CC3	31	CT	W	12.8	1,556	155
19	12	29	2013	CC3	31	CT	W	7.5	473	112
20	1	6	2014	CC3	9	CT	W	6.3	1,492	472
21	1	11	2014	CC3	21	CT	W	6.3	1,492	379
22	1	29	2014	NA	1	CT	W	6.2	1,496	1,489
23	2	3	2014	CC3	40	CT	W	15.9	1,487	380
24	2	19	2014	DS	12	CT	W	11.4	920	440
25	3	2	2014	DS	23	CT	SP	8.9	1,495	526
26	3	12	2014	NA	4	CT	SP	6.4	989	986
27	3	25	2014	C1	1	CT	SP	6.0	921	909
28	4	16	2014	NA	5	CT	SP	9.0	921	919
29	4	28	2014	C3	19	CT	SP	7.7	932	496
30	5	10	2014	NA	4	CT	SP	9.8	1,006	490
31	6	12	2014	DS	20	CT	SU	12.2	1,177	497
32	7	14	2014	CC3	18	CT	SU	8.8	1,161	550
33	12	6	2013	CC3	37	GF	W	11.1	1,337	587
34	12	22	2013	CC3	31	GF	W	5.4	1,187	671
35	12	29	2013	CC3	31	GF	W	4.8	1,162	697
36	1	6	2014	CC1	9	GF	W	8.3	1,115	963
37	1	11	2014	CC3	21	GF	W	8.3	1,115	686
38	1	24	2014	NA		GF	W	4.3	1,130	1,109
39	1	29	2014	NA	1	GF	W	8.7	1,137	1,073

Storm	Mo.	Day	Year	Type*	Rain (mm)	Site	Season†	Δ Level (cm)	Max SC (µS cm^{-1})	Min SC (µS cm^{-1})
40	2	2	2014	CC3	40	GF	W	7.0	1,164	487
41	3	5	2014	CC1	23	GF	SP	18.8	999	1,069
42	3	13	2014	NA	4	GF	SP	35.2	1,145	1,097
43	3	26	2014	CC1	1	GF	SP	36.7	1,124	1,105
44	4	4	2014	NA	16	GF	SP	5.0	1,239	1,091
45	4	16	2014	NA	5	GF	SP	8.7	1,241	1,040
46	5	29	2014	CC3	13	GF	SP	10.9	1,428	292
47	7	15	2014	DS	18	GF	SU	6.7	1,116	720
48	7	19	2014	CC3	24	GF	SU	6.5	1,356	832
49	7	28	2014	DS	15	GF	SU	5.6	1,398	868
50	9	11	2014	DS	10	GF	F	5.1	1,404	1,019
51	10	10	2014	CC3	27	GF	F	6.5	1,313	814
52	12	8	2013	C3	39	HP	W	11.9	840	288
53	12	22	2013	CC3	31	HP	W	9.0	1,088	304
54	12	29	2013	CC1	31	HP	W	6.2	351	270
55	12	3	2014	DS	11	HP	W	5.2	717	434
56	1	4	2015	DS	11	HP	W	3.1	690	471
57	1	23	2015	DS	16	HP	W	3.3	638	453
58	1	11	2014	CC1	21	HP	W	7.7	486	248
59	2	2	2014	CC3	40	HP	W	9.6	422	215
60	2	21	2014	CC1	12	HP	W	5.4	458	315
61	3	4	2014	NA	23	HP	SP	19.1	520	547
62	3	13	2014	CC3	4	HP	SP	32.9	795	584
63	3	25	2014	CC1	1	HP	SP	34.7	820	786
64	4	4	2014	CC3	16	HP	SP	5.6	884	540
65	4	7	2014	NA	5	HP	SP	3.7	878	528
66	4	29	2014	C3	19	HP	SP	4.6	860	405
67	5	10	2014	DS	7	HP	SP	9.4	914	312
68	5	21	2014	DS	14	HP	SP	4.5	1,033	434
69	5	29	2014	DS	13	HP	SP	11.0	1,011	313
70	6	12	2014	DS	20	HP	SU	4.9	1,170	418
71	7	14	2014	DS	18	HP	SU	6.1	1,082	328
72	7	19	2014	CC3	24	HP	SU	6.1	569	363
73	7	27	2014	C3	15	HP	SU	6.9	1,080	378
74	8	8	2014	C3	36	HP	SU	3.9	897	481
75	8	12	2014	C3	4	HP	SU	5.4	919	385
76	8	23	2014	DS	31	HP	SU	10.9	772	321
77	8	31	2014	DS	4	HP	SU	3.8	941	551
78	9	5	2014	DS	9	HP	F	7.7	1,265	344
79	9	11	2014	C3	10	HP	F	4.8	733	457
80	10	7	2014	DS	39	HP	F	5.8	906	543

Storm	Mo.	Day	Year	Type*	Rain (mm)	Site	Season†	Δ Level (cm)	Max SC (µS cm^{-1})	Min SC (µS cm^{-1})
81	10	10	2014	CC3	27	HP	F	8.1	911	387
82	10	14	2014	CC3	15	HP	F	9.1	888	338
83	11	5	2014	DS	10	HP	F	4.7	758	434
84	12	8	2013	C3	18	EF	W	8.7	1,821	930
85	12	16	2013	C3	6	EF	W	3.7	1,408	1,235
86	12	28	2013	C1	25	EF	W	6.6	1,624	1,082
87	1	12	2014	C3	11	EF	W	8.3	1,632	934
88	2	8	2014	C3	26	EF	W	18.1	1,796	508
89	3	5	2014	C3	20	EF	SP	6.0	1,530	1,213
90	5	17	2014	C1	32	EF	SP	1.5	1,767	1,410
91	5	24	2014	C1	6	EF	SP	2.9	1,746	1,157
92	9	12	2014	C1	11	EF	F	3.5	1,991	1,004
93	9	14	2014	C3	3	EF	F	1.5	1,728	1,251
94	10	7	2014	C1	37	EF	F	2.3	2,132	1,382
95	10	8	2014	C3	6	EF	F	3.7	1,853	1,312
96	10	14	2014	C1	27	EF	F	7.1	1,720	1,004
97	11	18	2014	C3	14	EF	F	1.9	2,001	1,796

* Type CC storms = counterclockwise rotation, Type C storms = clockwise rotation, numerical descriptors based off loop shape as shown in Figure 3.1.

† Season abbreviations: W = winter, SP = spring, SU = summer, F = fall.